National Technical University of Athens

School of Naval Architecture and Marine Engineering

Division of Marine Engineering

Diploma Thesis:

"Technical feasibility study on the retrofit of a conventional harbor tugboat into a battery powered one by simulation in MATLAB Simulink"

Theocharis Konstantinos

Supervisor: Prousalidis Ioannis

Associate Professor N.T.U.A. of Marine Electrical Engineering

July 2021

Acknowledgments

I would like to express my sincere appreciation to my supervisor, Professor I. M Prousalidis for this guidance and assistance during the implementation of the present dissertation and his willingness to clarify thoroughly all my questions.

Also, I would like to express my gratitude to Mr. Chilitidis and Spanopoulos Group for providing all the necessary information concerning the tugboat “CHRISTOS XL”.

Finally, I would like to thank my family for their support and patience during my studies.

Abstract

Living in the era of decarbonization, the regulations concerning emissions are becoming more and more strict. Walking towards the goal of IMO for 50% reduction to GHGs by 2050, compared to the values of 2008, maritime industry is looking for viable alternatives to the fuel oil. Electric propulsion is becoming a more and more sustainable solution due to the lower battery prices, the zero emissions and its high efficiency. Even if there are still certain technical boundaries imposed for its adoption to large – scale applications such as tankers, containerships or bulkers, due to the low specific energy of the battery systems compared to fuel oil, electric propulsion can be applied to vessels with moderate energy needs operating close to the coastline.

One of them are tugboats and the purpose of this dissertation is to investigate the technical viability of retrofitting an existing conventional harbor tugboat into a battery powered one, utilizing the high efficiency of the induction motor along with the reliability of Lithium-Ion battery technology.

The tugboat in question will be "CHRISTOS XL" which will be operating inside and near the port of Piraeus in a very narrow and tight environment with a range from 5-10 nautical miles outside the port. The operational profile of the tugboat is based on a 12-hour daily operation, 360 days per year.

In order to be able to estimate the battery sizing, the electric motor, which is selected based on the power and speed characteristics of the fitted diesel engine, will be simulated in the environment of MATLAB Simulink. Using certain torque and speed profiles, estimations of the tugboat's power needs based on its daily operation as references for the electric motor, its energy needs and consequently the required battery capacity is calculated.

Key Words: battery ship, all-electric ship, electric motor, induction motor, field-oriented control (FOC), Li-Ion batteries, inverter, retrofit methodology, IMO, Clarke, Park, equivalent circuit, tugboat.

This page is intentionally left blank

Table of Contents

List of Figures:

List of Tables:

1.0 Introduction

1.1 Background of the Study

The purpose of the present dissertation is to evaluate the technical viability of retrofitting a conventional harbor tug into an all-electric one, powered by two battery systems.

A tugboat is a special type vessel characterized from its high propulsive power compared to size. Most of the times they are utilized for towing bigger vessels that cannot be self manoeuvered effectively due to either their low speed or being in narrow areas such as ports but they can also be used as fire fighters, ice breakers or for salvage operations. Their main propulsion system had always been the conventional diesel engine due to its simplicity, low maintenance costs and the relatively high efficiency operating close to the maximum load. However, tugboats operate around 10-15 % of their total lifetime at their design point with the expense of high fuel consumption and increased emissions. Even if the economic impact of tugboats on the marine industry is negligible, this cannot be assumed for their environmental repercussions at their operating areas.

Harbor tugboats are excellent candidates for the all-electric alternative because unlike the internal combustion engines, electric motors can run efficiently at a wide range. Furthermore, all-electric tugs produce zero emissions. This is a great benefit compared to IC engines because tugboats operating in a narrow environment, close the coastline and into the ports, burden the local atmosphere at a great extent.

Over the following years stricter regulations are expected with the goal of GHGs reduction. Energy Efficiency Design Index (EEDI) and Energy Efficiency Existing Ship Index (EEXI) will push for novel designs such us hybrid propulsion systems or the very promising air propulsion (Flettner Rotors) along with the cost effective and safe battery systems.

The maritime industry is very reluctant to new designs and the transformation to electric/hybrid vessels will not take overnight. Even if the battery powered ship can offer a solution in terms of the reaching the required emissions standards, it faces one main drawback. The energy density of a typical battery is around 1-1.5% that of an ordinary fuel oil. This implies that it cannot be applied to large scale applications. The development of All – Electric Vehicles (EVs) can pave the way for a similar implementation at the maritime industry.

Several implementations have shown that ship electrification can offer considerable potential to reduce both energy consumption and emissions of CO_2, particulate matter (PM), NO_x and SO_x along with lower maintenance costs. Nowadays, the all – electric propulsion finds more and more applications mainly in ferries, offshore vessels, passenger boats and tugboats. All these applications share certain distinct characteristics. Vessels with moderate energy and power needs, with short trip operating profiles.

1.2 Problem statement and objectives

The purpose of the current thesis is the implementation of an all-electric battery powered propulsive system in a preexisting diesel-powered conventional tugboat. The main goal is to examine whether the selected electric motor, the induction motor, can cover the energy needs of the diverse operating profile of a harbor tugboat.

The current dissertation will focus on the operating principle of the induction motor and one of the ways for the control of its delivered torque. The theoretical background of the Field Oriented Control (FOC) will be analyzed along with the implementation in the case of the induction motor.

The main objective is to examine the responsiveness of the electric motor based on certain reference torque and speed signals that will be derived based on the operational profile of the tugboat. These simulations will be implemented in the environment of MATLAB Simulink.

Finally, the battery sizing will be calculated based on the energy needs of the electric motors which will be derived from the simulation. Thus, the goal is apart from examining the broad operational window of the induction motor, the calculation of the energy needs by simulating a typical operational scenario.

1.3 Structure of study

This study is structured as follows:

Chapter 2: Environmental impact of shipping

In the second chapter, the environmental effects of conventionally powered ships are analyzed. In particular, the most common and harmful types of pollutants found on the emissions of diesel engines on ships are listed and their impact on the climate change, the eco-system and the human health are described. A quantitative analysis of shipping caused air pollution with respect to other industrial sectors is presented followed by the international regulations, mainly the ECAs and Tier I-III standards that are implemented to reduce the negative effects of the emissions.

Chapter 3: Electric motor theoretical background and control

In the third chapter the operating principle of the induction motor is described along with the derivation of its equivalent circuit. The equivalent circuit is necessary in order to be able to simulate the operation of induction motor. Subsequently the Field Oriented Control (FOC) algorithm is analyzed for the case of the induction machine which has the target of calculating the reference currents based on speed and torque references. Finally, the operational principle

of the inverters and the theoretical background of its components, the IGBTs, is analyzed along with their control algorithm for a closed loop control of the induction motor.

Chapter 4: Batteries

In the fourth chapter, the main battery chemistries are analyzed, the Lead Acid, the Nickel-based and the Lithium-based, along with their characteristics, their pros and cons in order to evaluate the appropriate battery technology for the current thesis. Furthermore, necessary technical terminology is explained concerning the battery properties along with a summary of the main types of battery cells. Lastly, future promising battery technologies are mentioned.

Chapter 5: Tugboats

In the chapter five of the current thesis, the different types of tugboats and their propulsion arrangements as well as their operational role are listed. Moreover, different power systems, such as diesel, diesel-electric and hybrid, already implemented in tugboats are mentioned. Finally, the alternative of the all-electric tugboat is examined along with the presentation of already existing implementations for the case of a tugboat, a ferry and a cargo ship are mentioned.

Chapter 6: Design Methodology

Beginning in the sixth chapter, the electric motor is selected and the parameters of its equivalent circuit are calculated. Consequently, the simulation model is presented along with the calculation of the rated flux of the motor following with the presentation of the investigated operational profile and the battery system sizing. Finally, measurements of the average discharge current of the battery system and the calculation of Total Harmonic Distortion (THD%) took place in order to assess the performance of the system.

Chapter 7: Discussion

Final conclusions on vessel's retrofit, the performance of the Field Oriented Control with hysteresis band algorithm and comments on the battery system are presented along with suggestions for future investigation.

2.0 Environmental impact of shipping

Shipping is the most energy-efficient way of transportation, both for goods and people. The international shipping industry covers around 90% of total world trade. Seaborne trade continues to expand, bringing benefits for consumers across the world through competitive freight costs. However, this expansion comes along with increased pollution which can be categorized in two main categories, the discharges to the sea that impact the marine environment and fuel emissions to the air that impact the atmosphere.

International Maritime Organization (IMO) is a special agency under the United Nations intended to regulate the international shipping and among other things, has the responsibility to develop a comprehensive framework about the environmental impact of shipping. While IMO had issued regulations concerning the release of oil, sewage and liquid harmful substances with the Annexes I-VI of MARPOL 73/78 since 1973, the regulation of air pollution was adopted much later, at 1997 and was put into force at 2005.

Lately IMO has shifted its focus on the energy efficiency. Since 2013, with the Energy Efficiency Design Index (EEDI) a technical measure that requires a minimum energy efficiency level per tonne mile, IMO is pushing the shipping companies to operate their vessels in a more well-regulated way. Also, EEDI's minimum level will be tightened incrementally every five years, in order to stimulate continued innovation and technical development of all the components influencing the fuel efficiency of a ship from its design phase. EEDI is applicable to newbuilt ships whereas for the existing ships the Energy Efficiency Existing Ship Index (EEXI) will be adopted in June 2021 and will enter into force in 2023.

2.1 Ship emissions

Maritime sector has been built upon the diesel engines. They are based on a mature technology with more than a century of experience thus, they are reliable, relatively efficient, with low operating costs and with high maintainability. Also, they can be operated at a wide range of loads with an acceptable efficiency. For many decades these engines dominated the maritime industry due to their ability to operate with low quality fuels, mainly heavy fuel oil (HFO) and marine diesel oil (MDO). These fuels were inexpensive however, they were containing in high concentrations substances that were not only harmful for the engine itself but also for the environment.

These substances with the process of fuel combustion are being converted into exhaust gases which are released into the atmosphere. These emissions can be grouped into two major categories:

1. Greenhouse Gases (GHGs), emissions contributing in the greenhouse effect,
2. Other emissions.

The first group consists mainly of Carbon Dioxide (CO_2), Methane (CH_4) and Hydrochlorofluorocarbons (HCFCs) whereas the second group consists of emissions such as Sulphur Oxides (SO_x), Nitrogen Oxides (NO_x), Particular Matters (PM_s), Volatile Organic Compounds (VOCs) and Carbon Monoxide (CO). The above pollutants can also be categorized in another two categories, primary and secondary pollutants. The first come directly from the source (engine) while the later come from the primary that react with the atmosphere, mainly photochemical reactions, in a radius approximately 50 km from the source. These pollutants are mainly SO_x, NO_x and O_3. Subsequently, the main pollutants will be briefly analyzed:

- CO_2 is the product of the complete combustion of the carbon that the fuel contains. It is found naturally in the Earth's atmosphere, where it regulates the temperature but over the last decades due to its elevated concentrations, the average earth temperature has been increased. It is estimated that the total CO_2 emissions from the maritime sector for 2007 were equal to 1046 million tonnes, which was equal to 3.3% the total worldwide emissions.
- CO, contrary to CO_2, is the product of incomplete combustion. This is due to insufficient amount of O_2 during the combustion. CO has a lifespan of three months while it slowly oxidizes into CO_2 forming O_3 in the process.
- O_3 is a secondary pollutant that results from the reactions of hydrocarbons or nitrogen oxides with the sunlight, called photochemical reaction. Ozone can affect sensitive vegetation and ecosystems with effects such as loss of species diversity, changes to habit quality and changes to water and nutrient cycles.
- SO_x result from the reaction of the high sulphur content with the oxygen during combustion which forms mainly SO_2 and SO_3, with a ratio of 15:1 according to MAN B&W Diesel, 2004. Subsequently SO_3 can react with moisture (H_2O) and create sulphuric acid particles (H_2SO_4). SO_x are being regulated with either the use of low sulphur fuel (mainly LSHFO and MDO) and with the use of scrubbers.
- NO_x are created from the N_2 reaction with the O_2 under high temperature and pressure during the combustion. Under ambient temperature N_2 is chemically inert and does not react with the O_2. The byproduct is most of the times NO which is rapidly oxidized in the atmosphere to NO_2. NO_x are regulated with improvements at the combustion phase mainly with the Tier II and Tier III standards.
- PMs, consist of a mixture of organic and non-organic substances, which can be soot, metal oxides and sulfates and small fuel particles that were not burned completely during the combustion phase. They include a wide range of particles with diameters of less than 10 and 2.5 μm, the PM10 and PM2.5 respectively.

- VOCs or Volatile Organic Compounds are organic compounds that have high vapor pressure and low solubility in water. In the maritime industry, VOCs are mainly generated in oil and chemical tankers where cargo splashes in the piping system of the ships from the source to the cargo tanks and from evaporation from the surface of oil and chemicals stored in the tanks.

2.2 Impact of greenhouse gases on climate change

As mentioned, the main gases that contribute to the greenhouse effect are CO_2, CH_4 and HCFCs. HCFCs were regulated mainly with the Montreal protocol and ever since are on a declining course. On the other hand, CO_2 is the main greenhouse gas and its regulation is a difficult task because, it is a product of the perfect combustion of fuels that contain carbon. Therefore, the main alternatives are either to use alternative fuels that contain less carbon content (such as natural gas) compared to oil or reduce the consumption of oil fuel by a practice called slow steaming. Slow steaming is the practice of operating transoceanic cargo ships, especially container ships, at significantly less than their maximum speed, which reduces fuel consumption and offers cost reductions at shipowners.

The global average atmospheric CO_2 in 2019 was 409.8 parts per million (ppm), a level which is higher than at any point in at least the past 800000 years. Based on the following figure it is clear that the previous highest concentration of CO_2 was 300 ppm and in that scale the increase at today's level is instantaneous.

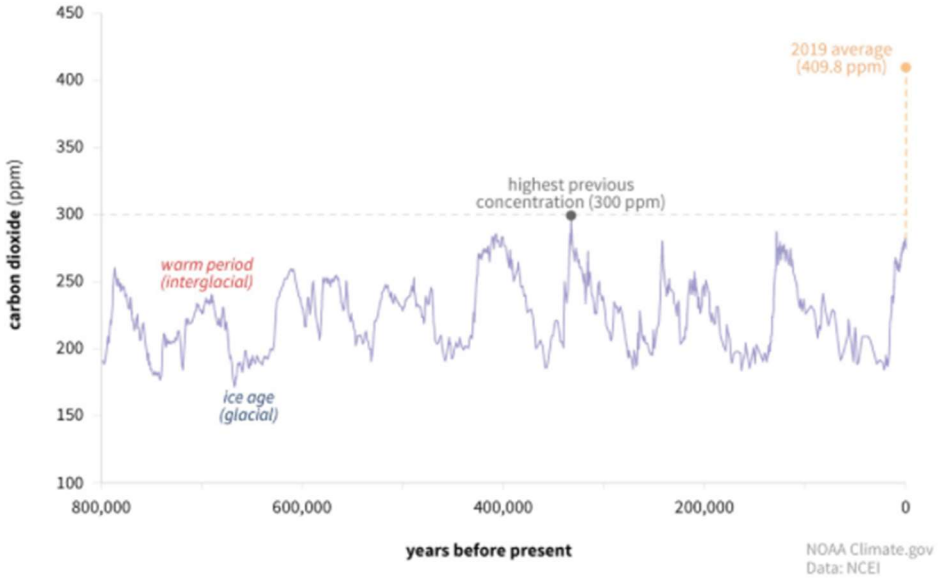

Figure 1: Carbon dioxide (CO_2) levels over the past 800000 years.

The self-regulation of CO_2 levels is a very complicated process not well understood but there is a clear correlation between the industrial growth, based on fossil fuels and the average increase in temperature. The annual increase of global atmospheric CO_2 from 2018 to 2019 was 2.5 ± 0.1 ppm whereas for comparison reasons in the 60s this rate was equal to 0.6 ± 0.1 ppm.

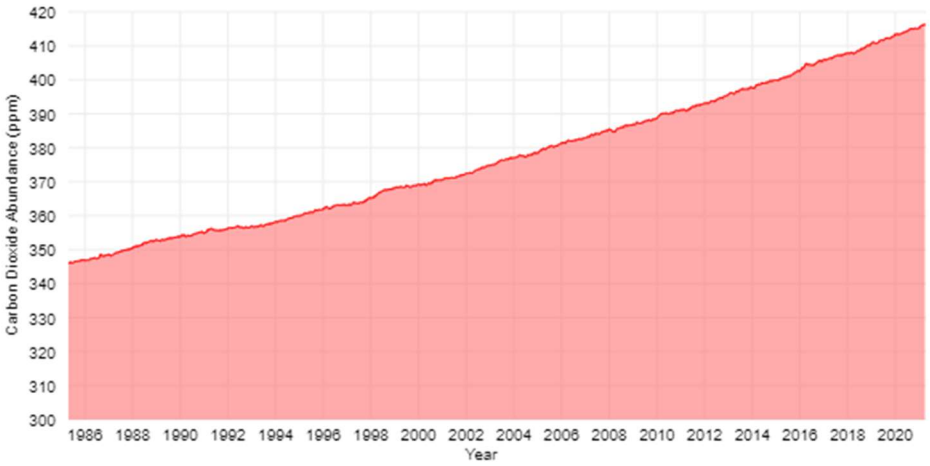

Figure 2: Increase of CO_2 concentrations from 1986.

CO_2 is the most important of Earth's long-lived greenhouse gases and whereas it absorbs less heat per molecule compared to CH_4 or N_2O it is more abundant and stays in the atmosphere much longer. Furthermore, compared to water vapor CO_2 is less abundant but it absorbs wavelengths of thermal energy that water vapor does not, adding to the greenhouse effect in a unique way. Increases in atmospheric CO_2 are responsible for about two-thirds of the total energy imbalance that is causing Earth's temperature to rise.

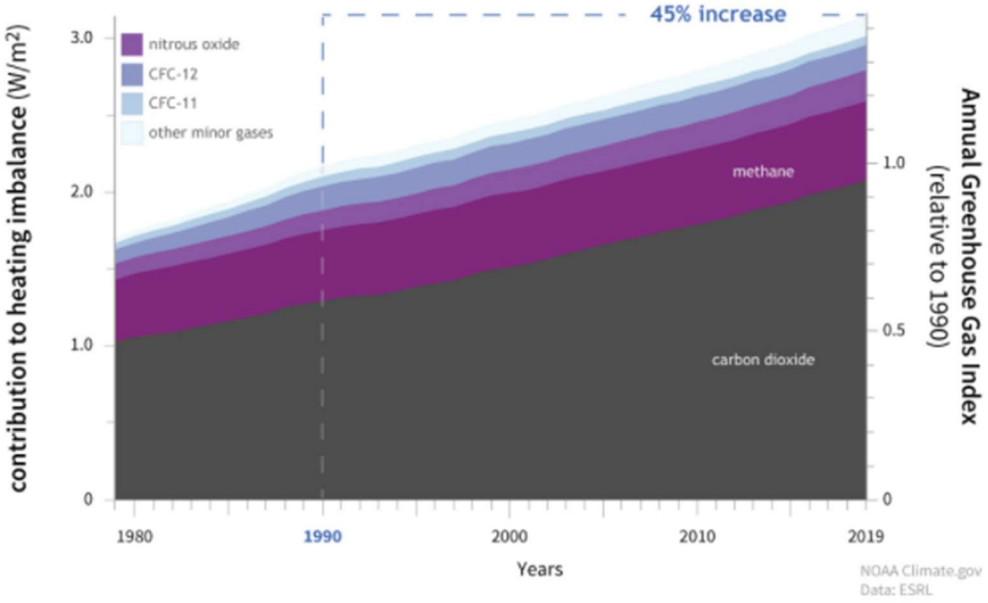

Figure 3: Combined heating influence of greenhouse gases.

CO_2 concentrations increase do not only affect the average earth temperature but also the ecosystems. It dissolves into the ocean, reacting with molecules producing carbonic acid which lowers the ocean's pH. Since the start of the Industrial Revolution, the pH of the ocean's surface waters has dropped from 8.21 to 8.10, this drop is called ocean acidification. A drop of 0.1 might seem small but pH scale is logarithmic therefore a change of 0.1 means a roughly 30% increase in acidity. This acidity interferes with the ability of marine life to extract calcium from the water to build their shells and skeletons.

The forecasts concerning CO_2 are ominous. Observing the past 270 years there is a correlation between the atmospheric CO_2 and the CO_2 human emissions. The increase in atmospheric CO_2 came along with a rapid increase of manmade emissions. If global energy demand continues to grow and to be met mostly with fossil fuels, CO_2 is projected to exceed 900 ppm by the end of this century.

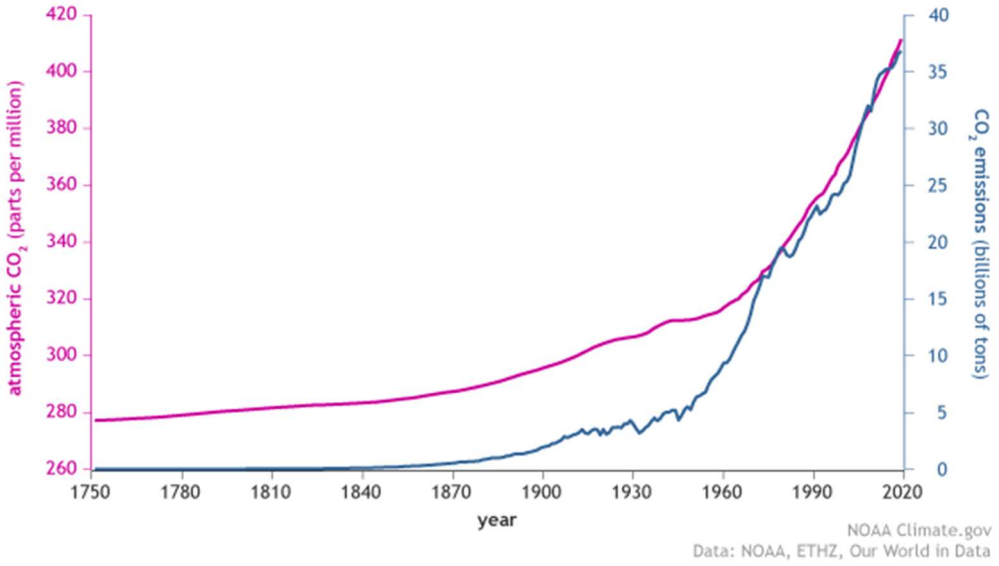

Figure 4: CO_2 in the atmosphere and annual emissions.

2.3 Impact of air pollution at eco-system and biodiversity

Pollutants like NO_x and SO_x are very harmful to the environment. SO_2 is converted to sulphuric acid (H_2SO_4), which reduces the pH of the rain, creating acid rain. Acid rain depending on the pH and the exposure time, can cause damage on flora (burning of plant leaves), corrode metals and affect building materials. For instance, marble ($CaCO_3$) absorbs SO_2 and is converted to gypsum $CaSO_4$. $CaSO_4$ is more water soluble than marble and as a result it is drifted by the rain. Also, the molecular volume of $CaSO_4$ is bigger than $CaCO_3$ which results in cracks on the marble. Those phenomena had been observed in archeological sites such as Acropolis and for this reason not only certain statues had been removed but also regulations were imposed for the reduction of sulphuric content in heating and motor oil in the area of Athens by the 80s.

The most important nitrogen oxides which are being produced during combustion are NO and NO_2. Their main characteristic is that they contribute to the formulation of photochemical smog. Nitrogen oxides are introduced into the atmosphere, which may combine with water to form nitric acid or react with sunlight to produce singular oxygen atoms, which they combine with molecular oxygen to produce ozone. The nitric acid may precipitate to the earth resulting in acid rain as with the case of SO_x. This phenomenon is mostly observed above dense cities mainly the morning hours and is more intense during days of high sunlight. Furthermore, eutrophication, the process of accumulation of nutrients, including nitrogen in water bodies is due to excess NO_x pollutants. Nutrient overloads in aquatic ecosystems can cause algae blooms and ultimately a loss of oxygen. This impacts eco-systems along with the biological diversity.

2.4 Impact of air pollution on human health

Humans come in contact with many different air pollutants primarily via inhalation and ingestion, whereas dermal contact comes as secondary exposure. The contamination of food and water, due to air pollutants as stated previously, makes the ingestion the major route of pollutant intake.

Air pollution contributes to increased mortality and hospital admissions with recent studies stating that this is the largest environmental health risk in developed countries. Human health effects can range from nausea and breathing difficulty to heart diseases and cancer while they can also affect children with birth defects and serious development delays. There are certain groups of people that are more affected than the general population mainly those who live close to Europe's coasts, areas with intense shipping activity.

The most typical health effects of certain pollutants are:

- SO_x: Aggravating asthma and reduced lung function, which can lead also to cough, irritation and headache.
- PM: Particulate Matters with diameter higher than 10μm are trapped into nose and consequently are being removed from the body without any adverse effect. However, smaller particles and mainly those with 2.5 μm diameter are trapped inside the lungs and can cause aggravating cardiovascular and lung diseases, heart attacks and arrythmias and may lead to some forms of cancer. According to a study (Corbett et al., 2007), PM from shipping activity are responsible for 60000 premature deaths every year from cardiovascular problems and lung cancer.
- NO_x: Can cause breathing problems, headaches, chronically reduced lung function and eye irritation.

- CO: Can cause heart disease and damage to nervous system along with dizziness and loss of consciousness.

Summarizing the main effects of air pollutants on environment and human health are:

Table 1: Air pollution and effects on human health and environment.

	SO_2, NO_x, PM, VOCs	CO_2
Spatial impact scale	Local, regional	Worldwide
Time impact scale	Short and long term	Mainly long term
Environmental impact	Acid rain, smog, photochemical smog	Greenhouse effect and average temperature rise, sea level rise, extreme weather conditions, impact on agriculture
Human health impact	Direct: respiratory diseases, eye irritation, asthma, chronic bronchitis, cardiovascular diseases	Indirect: rise of average temperature, extreme weather conditions, problem with water resources and agriculture

2.5 Quantitative analysis of shipping caused air pollution

It is estimated that the total CO_2 emissions from the shipping factor for the year of 2007 reached 1046 million tonnes, which represents the 3.3% of the worldwide emissions. From this quantity 870 million (2.7%) are attributed to the international shipping, where the rest is attributed to the domestic sector. CO_2 is the most important greenhouse gas emitted both in terms of quantity and on its effect on global warming. Long-term estimations state that in the absence of reduction policies the ship emissions will increase from 150-250% due to the development of maritime sector. However, shipping is the most efficient mean of goods transportation and its CO_2 emissions per unit of energy consumption can only be compared with railway sector.

Apart from CO_2, it is estimated that shipping emitted around 25 million tonnes NO_x, 15 million tonnes SO_x and 1.8 million tonnes PM. The impact of the NO_x on the global warming is debatable because these are neutral with respect to global warming as they neither absorb nor reflect the solar radiation. However, they contribute to chemical reactions in the lower atmosphere creating O_3 which is a greenhouse gas. On the other hand, they also contribute to

chemical decomposition reactions of methane (CH_4), which also is a greenhouse gas. Therefore, their contribution to the global warming effect is negligible.

SO_x in the atmosphere form sulphate particles that have the tendency to reflect the incoming solar radiation, reducing the percentage that reaches earth's surface. Furthermore, they have an indirect effect which also cools down the atmosphere. Floating particles in the atmosphere of a polluted area, become condensation cores of water vapor and contribute to the formation of clouds. In these clouds, moisture droplets have a smaller diameter than an unpolluted area. In this way the solar radiation reflected by the clouds increases, the reflectivity of clouds increases. This indirect effect of SO_x has not been quantified but it is estimated that is important.

Moreover, shipping emits soot as a percentage of particulate matter. Soot when located at the atmosphere, due to its black color, amplifies the greenhouse effect, increasing the absorption of solar radiation. This is very important for areas such as the Arctic cycle because this soot is decreasing the reflectivity of the ice, thus contributing in the local warming.

Nowadays, there are views supporting that there is no need for regulations focusing on the reduction of CO_2 and the other pollutants or at least these measures should not be stringent. However, they should take into consideration the fact that CO_2 and for instance SO_2, operate at different time scales. The sulphur particles remain in the atmosphere for only a few days whereas the CO_2 particles have a lifespan of 5 to 200 years. Therefore, the effects of CO_2 on the climate will continue to exist for a much longer period compared to the negating effects of SO_2.

2.6 Regulations for the prevention of air pollution from ships

IMO ship pollution rules are contained in the MARPOL 73/78. This international convention initially contained 5 annexes:

i. Regulation for the prevention of pollution by oil,
ii. Regulation for the control of pollution by noxious liquid substances,
iii. Regulation for the prevention of pollution by harmful substances carried by sea in packaged form,
iv. Regulation for the prevention of pollution by sewage from ships,
v. Regulation for the prevention of pollution by garbage from ships

None of these annexes concerned the regulation of air pollution. For this reason, in 1997 the Annex IV was introduced which sets limits on NO_x and SO_x emissions from ship exhausts and prohibits deliberate emissions of ozone depleting substances from ships of 400 GT and above engages in voyages to ports or offshore terminals under the jurisdiction of countries that have ratified it. The states that have ratified the MARPOL 73/78 are obligated to accept Annexes I

and II. Annexes III-VI are optional and require different ratification. Each one of those Annexes enters into force 12 months later, from the moment 15 countries that represent the 50% of world merchant shipping tonnage ratify it. On 18 May 2004, Samoa ratified Annex VI as the 15th country (along with Bahamas, Bangladesh, Barbados, Denmark, Germany, Greece, Liberia, Marshal Islands, Norway, Panama, Singapore, Spain, Sweden and Vanuatu). Therefore, Annex VI entered into force on 19 May 2005.

The NO_x emission standards are defined in the Annex VI as Tier I-III standards. The Tier I standards were defined in the 1997 version of Annex VI, while the Tier II/II standards were introduced by Annex VI amendments adopted in 2008, as follows:

- 1997 Protocol (Tier I): It applies retroactively to new engines greater than 130kW installed on vessels constructed on or after 1 January 2000, or engines which undergo a major conversion after 1 January 2000. The regulation also applies to fixed and floating rigs and to drilling platforms (except for emissions associated directly with exploration and/or handling of sea-bed minerals).
- 2008 Amendments (Tier II/III): Adopted in October 2008 introduced new fuel quality requirements beginning from July 2010, Tier II and III NO_x emission standards for new engines, and Tier I NO_x requirements for existing pre-2000 engines.

The revised Annex VI entered into force on 1 July 2010. Annex VI introduced the emission control areas (ECAs). An ECA can be designated for SO_x, NO_x, PM or all of them. These areas include:

- Baltic Sea (SO_x: adopted 1997 / entered into force 2005; NO_x: 2016/2021)
- North Sea (SO_x: 2005/2006; NO_x: 2016/2021)
- North American ECA, most of US and Canadian coast (NO_x & SO_x: 2010/2012).
- US Caribbean ECA, including Puerto Rico and the US Virgin Island (NO_x & SO_x: 2011/2014).

The NO_x emission limits apply to each marine diesel engine with a power output of more than 130kW installed on a ship. These limits are set for diesel engines depending on the engine maximum operating speed (n, RPM) as shown in the table below. Tier I and Tier II limits are global whereas the Tier III limits apply only in NO_x Emission Control Areas:

Table 2: NO_x emission limits.

Tier	Date	NO_x limit, g/kWh		
		n < 130	130 ≤ n < 2000	n ≥ 2000
Tier I	2000	17.0	$45 \cdot n^{-0.2}$	9.8
Tier II	2011	14.4	$44 \cdot n^{-0.23}$	7.7
Tier III	2016	3.4	$9 \cdot n^{-0.2}$	1.96

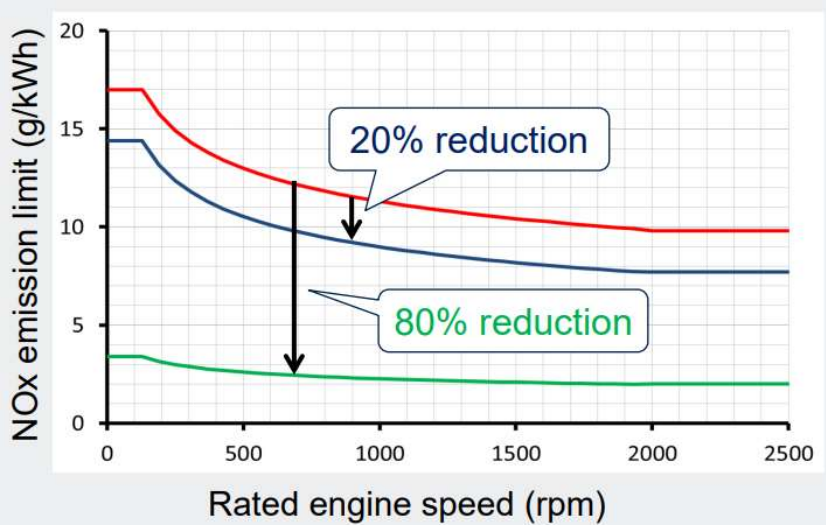

Figure 5: NOx emission limits with respect to engine speed n (RPM).

Annex VI regulations include caps on sulphur content of fuel oil as a measure to control SO_x emissions and indirectly PM (without having explicit PM emission limits). Special fuel quality provisions exist for SO_x Emission Control Areas (SECAs).

Table 3: MARPOL Annex VI fuel sulphur limits.

Date	Sulphur limit in fuel (% m/m)	
	SO_x ECA	Global
2000	1.5%	4.5%
2010.07	1.0%	
2012		3.5%
2015	0.1%	
2020		0.5%

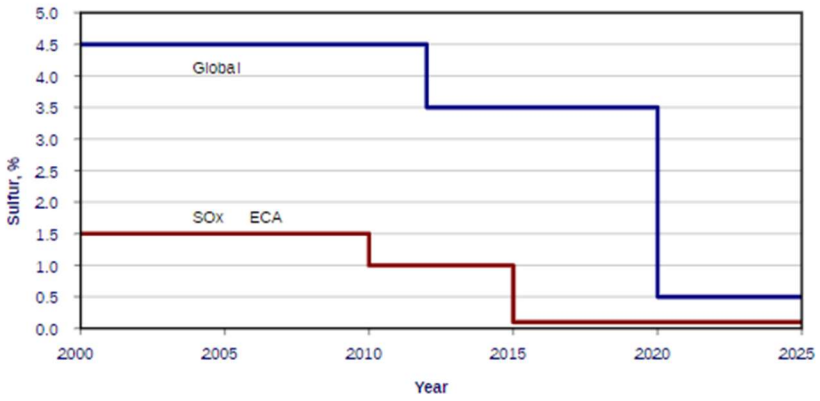

Figure 6: Sulphur emissions limits with respect to years

IMO has an ambition to halve GHG emissions by 2050 and a vision to decarbonize shipping as soon as possible within this century. In that order IMO has implemented certain measures. The existing measures are:

- The Energy Efficiency Design Index (EEDI) is applied to new ship designs after 1 Jan 2013 and it is a performance-based mechanism that requires a certain minimum energy efficiency in new ships. The level is to be tightened incrementally every five years in order to stimulate continued innovation and technical development of all the components influencing the fuel efficiency of a ship from its design phase. Ship designers and builders are free to choose the technologies to satisfy the EEDI requirements in a specific ship design.
- The Ship Energy Efficiency Management Plan (SEEMP) for all ships above 400 GT in operation – although it contains no explicit and mandatory requirements to content and implementation.
- The Fuel Oil Consumption Data Collection System (DCS) mandating annual reporting of CO_2 emissions and other activity data and ship particulars for all ships above 5000 GT.

As mentioned EEDI is applied to new ship designs after 2013, however there is the need for an energy efficiency measurement for existed ships. In that order IMO will adopt in June 2021 and put into force on 1 January 2023 the three following measures:

- The retroactive application of the EEDI to all existing cargo ships above a certain size, known as the Energy Efficiency Design Index for Existing Ships (EEXI). This will impose a requirement equivalent to EEDI Phase 2 or 3 (Phase 2 – ships built between 2021-2025 and Phase 3 2025 – onwards), with some adjustments to all existing ships regardless of year of build and is intended as a one-off certification.

- A mandatory Carbon Intensity Indicator (CII – e.g. Annual Efficiency Ratio [AER – grams of CO_2 per dwt-mile]) and rating scheme where all cargo and cruise ships above 5000 GT are given a rating of A to E every year. The rating thresholds will become increasingly stringent towards 2030. For ships that achieve a D rating for three consecutive years or an E rating a corrective action plan needs to be developed as part of the SEEMP and approved.
- A strengthening of the SEEMP (Enhanced SEEMP) to include mandatory content, such as an implementation plan on how to achieve the CII targets and making it subject to approval.

From all the prementioned measures the most important one is the EEDI. The EEDI is a coefficient that expresses the ratio of the environmental cost to the benefits for society that comes from the transportation goods. The environmental cost is expressed in the CO_2 emissions whereas the benefit is the transportation energy that the ship consumed. The calculated EEDI of a new ship must be compared to a database of EEDIs of existing ships which have been decreased by a percentage. In order to create the reference EEDI curve, the Lloyds' Register Fairplay database was used for ships that were delivered between 1/1/1999 and 1/1/2009 with gross tonnage above 400 GT. A typical reference EEDI curve for tankers is being displayed below:

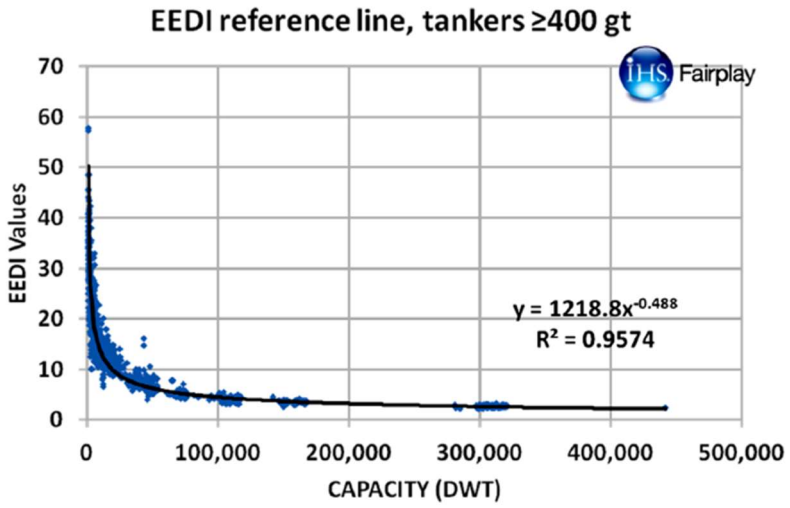

Figure 7: EEDI reference curve for tankers.

EEDI can be expressed with the following simple formula:

$$\text{EEDI} = \frac{\text{P} \cdot \text{SFC} \cdot \text{C}_\text{F}}{\text{Capacity} \cdot \text{V}_\text{ref}}$$

where:

- P (kW) is the main engine and auxiliary engines power,
- SFC (g/kWh) is the specific fuel consumption,
- C_F is a nondimensional coefficient factor, depended on the fuel's carbon content,
- Capacity is the 70% of DWT for containerships and 100% DWT for tankers, LNGs, bulk carriers, ROROs, and the Gross Tonnage for passenger and cruise ferries.
- V_{ref} is the reference speed in knots, for the maximum loading condition.

There are 3 simple ways to achieve an improved EEDI:

1. Speed reduction. The necessary engine power is proportional to the speed's velocity raised on the third degree ($P = a \cdot V^3$). Thus, a speed reduction can decrease the required power by a lot and consequently the EEDI value.
2. DWT increase. For an increased DWT the required increase in power is not proportional but raised to 2/3. Therefore, the increase in the denominator in the above formula is bigger than the increase in nominator. Also, it must be noted that a vessel with higher capacity might be imposed to a reduced reference EEDI.
3. Application of new technologies which do not affect or impose restrictions in functional or design parameters.

While EEDI is a very useful tool as it is the first attempt to create a measurement that focuses on the CO_2 emissions from a certain mean of transportation it has certain disadvantages. First of all, it is debatable in what extend the reference curves are valid, since it is not mandatory for the shipowners to provide data concerning the operation of their vessels. There is the possibility that a new database might be created with valid data from the shipowners, the classification societies and the shipyards. Furthermore, the initial EEDI (phase 0) was not stringent enough and the vessels that were created during that phase will approximately operate until 2040, assuming a mean lifespan of 25 years. Therefore, the real benefit from the EEDI might require one to two decades to be observable. Finally, the third problem is that the developing countries (mainly China, Brazil, India, South Africa and Saudi Arabia) have expressed their objections concerning the universal adoption of a common index. They express that the developed countries are responsible for the higher percentage of CO_2 emissions and thus they require to be excluded from the developing EEDI framework, or adopt it with more favorable terms. However, an emission reduction strategy with different criteria per country is ineffective for shipping, as ships can easily change flag.

It is clear that IMO is trying to decarbonize the maritime sector the sooner possible. In the following decades, the regulations will become more and more stringent and alternative ways of ship propulsion will emerge. Electric propulsion seems to be a very promising alternative as it offers a complete decarbonization and independence of fossil fuels.

3.0 Electric motor theoretical background and control

3.1 Induction motor's operating principle

The electric motor that will be investigated in the current thesis is the induction motor, therefore its operational principle will be analyzed. First of all, the induction motor can be of two types, the squirrel cage rotor and the wound one. The squirrel cage rotor consists of thin bars that are connected with end caps, circular in shape, at their opposite ends. The wound rotor, also known as slip ring-rotor has windings that are connected through slip rings to external resistance. By controlling these resistances, the speed/torque characteristics of the motor can be modified. Since in the current thesis the squirrel-cage motor will be used, it is the one to be analyzed.

As mentioned above every induction motor consists of two main parts, the stator and the rotor. The stator consists of a steel frame that supports a hollow, cylindrical core made up of stacked laminations. A number of evenly spaced slots, punched out of the internal circumference of the laminations, provide the space for the stator winding. These windings carry the three-phase alternating current and are evenly distributed in space by 120º. The working principle of the induction motor is based upon the application of Faraday's Law and the Lorentz force on a conductor. The AC current these windings carry, creates a rotating magnetic field, B_S, inside the stator. This magnetic field rotates at a synchronous speed depending on the current frequency of the windings and the number of poles the field has. Due to Faraday's law a voltage E is induced in each conductor (the thin bars) while it is being cut by the flux. Because of the rotor being short-circuited, current circulates inside the bars. Because of this current there is another magnetic field that is being created by the rotor, called B_R, that opposes its creator, the field B_S. The interaction between these two fields is called the magnetization field B_M. This field exists in the air gap between the stator and the rotor. This magnetic field B_M applies force on each conductor that is being circulated by current, this force always acts in a direction to drag the conductor along with the magnetic field. It should be noted that the magnetic field of the rotor doesn't have the same frequency of the stator's one. It has a different one that will be analyzed below, but it rotates in a synchronous speed because the rotor rotates also by himself at a speed called n_{mech}. We can get a qualitative understanding of the torque produced below.

By assuming a simplified figure below with a sinusoidal stator flux distribution that peaks in the upward direction and a single coil of wire mounted on the rotor. The stator flux distribution in this machine is $\mathbf{B_s(\alpha) = B_s \sin\alpha}$. B_s is the magnitude of the peak flux density and $B_s(\alpha)$ is positive when the flux density vector points radially outward from the rotor surface to the stator surface.

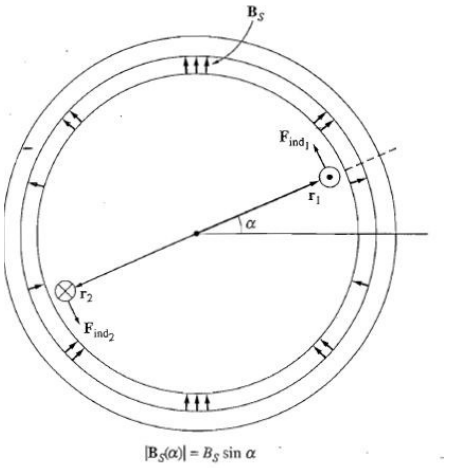

Figure 8: Simplified AC machine with a sinusoidal stator flux distribution and a single coil of wire mounted in the rotor.

The induced force on conductor 1 is: $\mathbf{F_{ind1} = i(l \times B) = ilB_s \sin \alpha}$ with direction as shown. The torque on the conductor is: $\boldsymbol{\tau_{ind1} = (r \times F_{ind1}) = rilB_s \sin \alpha}$ counterclockwise. The induced force on conductor 2 is: $\mathbf{F_{ind2} = i(l \times B) = ilB_s \sin \alpha}$ with direction as shown. The torque on the conductor 2 is: $\boldsymbol{\tau_{ind2} = (r \times F_{ind2}) = rilB_s \sin \alpha}$ counterclockwise. Therefore, the torque on the rotor loop is: $\boldsymbol{\tau_{ind} = 2rilB_s \sin \alpha}$.

The above equation can be written in a more convenient form by examining the figure below and noting two facts:

1. The current i flowing in the rotor coil produces a magnetic field of its own, B_R. The direction of the peak of this magnetic field is given by the right-hand rule and the magnitude of its magnetizing intensity H_R is directly proportional to the current flowing in the rotor, $H_R = C\ I$, where C is a constant of proportionality.
2. The angle between the peak of the stator flux density B_s and the peak of the rotor flux density B_R is γ. Furthermore, $\gamma = 180^o - \alpha$.

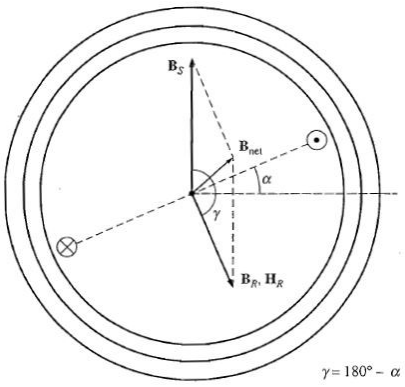

Figure 9: The components magnetic flux density inside the machine of Figure 5.

$$\mathbf{\sin \gamma = \sin(180^o - a) = \sin \alpha}$$

By combining the above two observations, the torque on the loop can be expressed as:

$$\boldsymbol{\tau_{ind} = KH_R B_S \sin \alpha}$$

Where K is a constant dependent on the construction of the machine. Note that both the magnitude and the direction of the torque can be expressed by the equation:

$$\boldsymbol{\tau_{ind} = KH_R x B_S}$$

Finally, since $B_R = \mu H_R$, this equation can be expressed as:

$$\boldsymbol{\tau_{ind} = kB_R x B_S}$$

Where $k = K/\mu$.

The net magnetic field in the machine is the vector sum of the rotor and stator fields (assuming no saturation):

$$\boldsymbol{B_{net} = B_R + B_S}$$

This fact can be used to produce an equivalent and sometimes more useful expression for the induced torque in the machine. From the above equation $\boldsymbol{B_S = B_{net} - B_R}$ and from equation:

$$\boldsymbol{\tau_{ind} = kB_R x(B_{net} - B_R) = kB_R x B_{net}}$$

It is important to be explained that the rotor doesn't rotate at the synchronous speed, n_{sync}, that the magnetic field B_M rotates, because if it did there would not be variation of the magnetic flux that cuts the rotor bars thus there would be no voltage induced and with no current the rotor would stop. As a result, the rotor always rotates at $n_{mech} < n_{sync}$. This difference is usually called slip and it is expressed as a percent of synchronous speed:

$$\boldsymbol{s = \frac{n_{sync} - n_{mech}}{n_{sync}} \cdot 100} \qquad 3.1.1$$

The synchronous speed n_{sync} is depended on the electrical frequency of stator's currents f_e and the stator's number of pole pairs p.

$$\boldsymbol{n_{sync} = \frac{60 \cdot f_e}{p}} \qquad 3.1.2$$

When the rotor works under normal loads, slip rarely exceeds 0.5% of synchronous speed. The frequency of the induced voltage and current of the rotor, also called as slip frequency, is proportional to the relative speed of the rotor to the magnetic field B_M:

$$\boldsymbol{f_{sl} = s \cdot f_e} \qquad 3.1.3$$

where f_e is the frequency of the voltage applied to the stator windings.

3.2 Induction's motor equivalent circuit

The working principle of the induction motor is very close to the transformer's one thus its equivalent circuit can be approached like a transformer's.

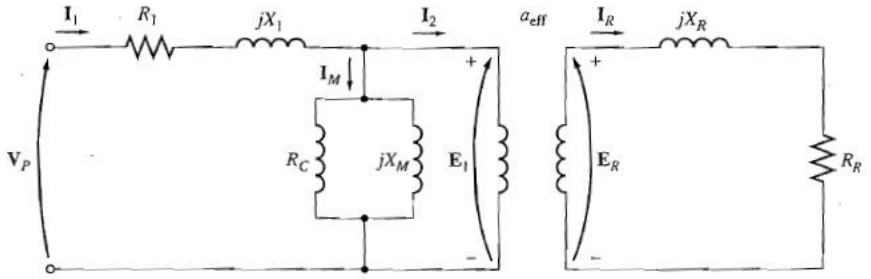

Figure 10: The transformer model of an induction motor.

The above circuit for one phase is as already said very similar to the circuit diagram of a transformer. For simplicity the part that consists of iron, windage and friction losses, R_M has not been included. First of all, the applied voltage V_P between one phase and neutral produces a stator current I_1. This current consists of two parts I_m and I_2. Current I_m is the magnetizing current that produces the flux Φ_M in the gap between the stator and the rotor. I_2 is a reflection of the current that actually flows in the rotor. E_1 is the induced voltage of the flux Φ_M at the stator's windings, which has the synchronous frequency f_e. On the rotor side the induced voltage E_R equals the slip by E_{ag}, because the induced voltage is dependent by the rotor's rotational speed with respect to the magnetic flux Φ_M. In fact, voltage and current in the rotor's side has the slip frequency f_{sl}, mentioned above. The working principle can be understood by examining the two following cases.

Firstly, let's examine the case of the rotor being locked, unable to rotate. Magnetizing current I_m creates the magnetic flux that links both the stator and the rotor. Because the rotor is locked, s equals to 1, magnetic flux Φ_M induces the maximum voltage E_R to the rotor and consequently the current I_R of the rotor has a big value. This current creates a rotating magnetic field that opposes field Φ_M thus it reduces the voltage E_1 of the stator. Because V_P is bigger now than E_1 it means that more current I_2 can leak into the stator, which in turn creates a magnetic field which opposes the magnetic field of the rotor and the system reaches an equilibrium. By the rotor being locked, the currents that circulate into the stator and the rotor are having high values, thus there are big copper losses in the form of heat. When the rotor is locked or when is begins to rotate, high currents are being created and it's a situation that must be avoided.

Now let's examine the second scenario, the normal operation of the motor. When the motor works at its nominal point, rotor's mechanical speed is close to the synchronous thus slip is small (in fact it's around 0.5%). Because of that the induced voltage E_R equals slip by the induced voltage when the rotor is locked and because slip has a small value, this voltage is

small. So, E_R has a small value and in consequence the current I_R that circulates in the rotor is small. Because of this, the copper losses are a small amount considering themselves when the rotor is locked thus the motor works in a high efficiency. This is the main reason that the induction motor has a high degree of efficiency.

In order to find the relation between the electrical power that is delivered to the motor and the mechanical that it produces, first of all the current voltage relations of the motor must be derived. Above the equivalent circuit that looks alike the transformer's one has been mentioned. It is much easier if the side of the rotor is converted with respect to the stator thus creating a unified circuit. But there is the difficulty that the current and the voltage on the rotor side have a different frequency than that of the stator. This issue can be overcome with a simple trick. The current that runs in the rotor $I_{r(r)}$ can be found by the following equation:

$$\mathbf{I_R = \frac{sE_1}{js\omega_e X_R + R_R}}$$

Dividing numerator and denominator by s:

$$\mathbf{I_R = \frac{E_1}{j\omega_e X_R + \frac{R_R}{s}}} \qquad 3.2.1$$

So, in this the equivalent circuit of the rotor is created, that has the same frequency like the stator and the only difference is a variable resistance R_r that is affected by the slip.

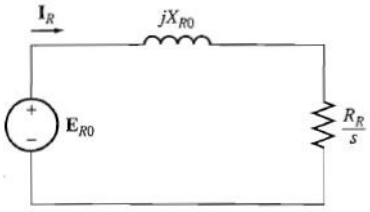

Figure 11: The rotor circuit model of an induction motor with all frequency effects concentrated in resistor R_r.

Now the equivalent circuit with respect to the stator can be derived:

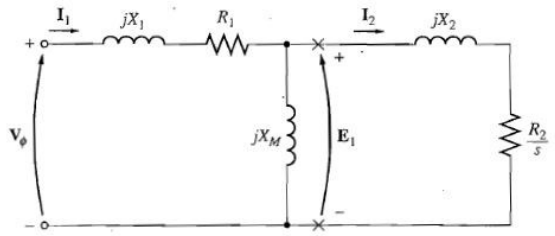

Figure 12: The per-phase equivalent circuit of an induction motor.

$$\mathbf{V_\Phi = I_1(R_1 + jX_1) + E_1} \quad 3.2.2$$

$$\mathbf{E_1 = I_2\left(\frac{R_2}{s} + jX_2\right)} \quad 3.2.3$$

$$\mathbf{I_1 = I_2 + \frac{E_1}{jX_m}} \quad 3.2.4$$

3.3 Torque-speed characteristic curve of the induction motor

The asynchronous induction motor converts the electrical input power to mechanical one. This electrical power is equal to:

$$\mathbf{P_{in} = 3V_P I_1 \cos\varphi} \quad 3.3.1$$

Where V_p is the phase voltage, I_1 is the stator current and φ is the phase difference between the input's voltage and current.

The power that is being transmitted to the rotor via the air gap (air gap power) is equal to the electrical input power minus the power that is being lost to the stator's copper winding $P_{cu,s}$ (ignoring the magnetic iron losses).

$$\mathbf{P_{cu,s} = 3R_1 I_1^2} \quad 3.3.2$$

From the equivalent circuit the air gap power can be found, that is being transmitted to the rotor and is being consumed by the resistance R_r/s.

$$\mathbf{P_{ag} = 3I_2^2 \frac{R_2}{s}} \quad 3.3.3$$

A part of the air gap power is lost as copper losses at the rotor side. These losses are equal to:

$$\mathbf{P_{cu,r} = 3R_2 I_2^2} \quad 3.3.4$$

The remaining power is being converted to mechanical power at the rotor's shaft. This power is called as mechanical or electromechanical power of the motor P_{em} and is equal to:

$$\mathbf{P_{em} = P_{ag} - P_{cu,r} = 3I_2^2 \frac{R_2}{s} - 3R_2 I_2^2 = 3\frac{1-s}{s} R_2 I_2^2} \quad 3.3.5$$

Thus, sometimes it is better to replace the fictious resistance R_2/s with a static one R_2 and a variable resistance $(1\text{-}s)\cdot R_2/s$, in series, which reflects the electromechanical power of the motor. It is noticeable that the mechanical power is depended on slip s and it is being maximized when slip tends to 0, or in other words, when the motor operates near its nominal condition.

Calculating now the electromagnetic torque T_{em}:

$$\mathbf{T_{em} = \frac{P_{em}}{\omega_m} = \frac{(1-s)P_{ag}}{(1-s)\omega_{sync}} = \frac{P_{ag}}{\omega_{sync}}} \qquad 3.3.6$$

The above equation is especially useful, since the synchronous speed is constant for a given frequency and a number of poles. Since ω_{sync} is constant, the knowledge of the air – gap power gives the induced torque of the motor. In order to find this, the current I_2 must be determined. In order to find it, the circuit of the figure 12 must be solved, and the easiest way is to determine the Thevenin equivalent for the portion of the circuit to the left of X's in the figure.

To calculate the Thevenin equivalent of the input side of the induction motor equivalent circuit, first open-circuit the terminals at the X's and find the resulting open-circuit voltage present there.

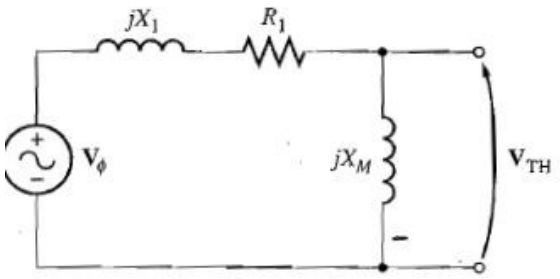

Figure 13.1: The Thevenin equivalent voltage of an induction motor input circuit.

$$\mathbf{V_{TH} = \frac{jX_M}{R_1 + jX_1 + jX_M} V_\Phi} \qquad 3.3.7$$

Then, the Thevenin impedance can be found, by short-circuiting the phase voltage and finding the Z_{eq} seen "looking" into the terminals.

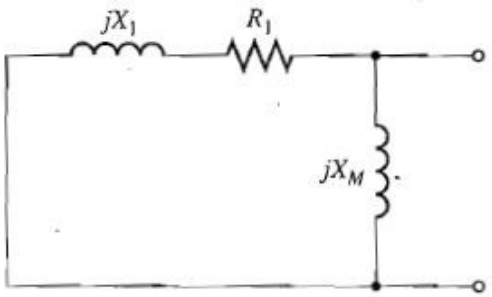

Figure 13.2: The Thevenin equivalent impedance of the input circuit.

$$\mathbf{Z_{TH} = \frac{jX_M(R_1 + jX_1)}{R_1 + j(X_1 + X_M)}} \qquad 3.3.8$$

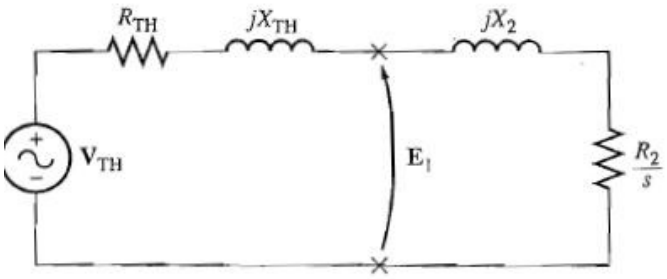

Figure 13.3: The resulting simplified equivalent circuit of an induction motor.

The magnitude of the Thevenin voltage V_{TH} is:

$$\mathbf{V_{TH}} = \mathbf{V_{\Phi}} \frac{\mathbf{X_M}}{\sqrt{\mathbf{R_1^2} + (\mathbf{X_1} + \mathbf{X_M})^2}} \tag{3.3.9}$$

The magnetization reactance $X_M >> X_1$ and $X_M >> R_1$ because of the low magnetic permeability of the air gap. Thus, the Thevenin voltage is approximately:

$$\mathbf{V_{TH}} = \mathbf{V_{\Phi}} \frac{\mathbf{X_M}}{\mathbf{X_1} + \mathbf{X_M}} \tag{3.3.10}$$

to quite good accuracy.

Because $X_M + X_1 >> R_1$ the Thevenin resistance and reactance are approximately given by:

$$\mathbf{R_{TH}} = \mathbf{R_1} \left(\frac{\mathbf{X_M}}{\mathbf{X_1} + \mathbf{X_M}} \right)^2 \tag{3.3.11}$$

$$\mathbf{X_{TH}} = \mathbf{X_1} \tag{3.3.12}$$

Therefore, the current I_2 according to Figure 6.3 is given by:

$$\mathbf{I_2} = \frac{\mathbf{V_{TH}}}{\mathbf{R_{TH}} + \frac{\mathbf{R_2}}{\mathbf{s}} + \mathbf{jX_{TH}} + \mathbf{jX_2}} \tag{3.3.13}$$

The magnitude of the current is:

$$\mathbf{I_2} = \frac{\mathbf{V_{TH}}}{\sqrt{\left(\mathbf{R_{TH}} + \frac{\mathbf{R_2}}{\mathbf{s}}\right)^2 + (\mathbf{X_{TH}} + \mathbf{X_2})^2}} \tag{3.3.14}$$

The air-gap power is therefore:

$$\mathbf{P_{ag}} = 3\mathbf{I_2^2} \frac{\mathbf{R_2}}{\mathbf{s}} = \frac{3\mathbf{V_{TH}^2}\mathbf{R_2}/\mathbf{s}}{\left(\mathbf{R_{TH}} + \frac{\mathbf{R_2}}{\mathbf{s}}\right)^2 + (\mathbf{X_{TH}} + \mathbf{X_2})^2} \tag{3.3.15}$$

and the rotor induced torque is given by:

$$T_{em} = \frac{P_{ag}}{\omega_{sync}} \tag{3.3.16}$$

$$T_{em} = \frac{3V_{TH}^2 R_2/s}{\omega_{sync}\left(R_{TH} + \frac{R_2}{s}\right)^2 + (X_{TH} + X_2)^2} \tag{3.3.17}$$

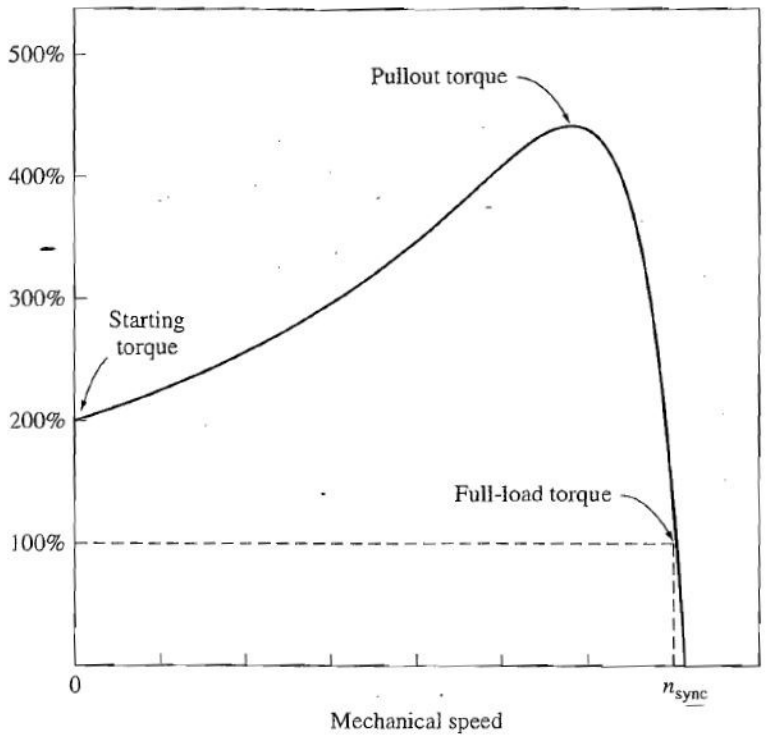

Figure 14: A typical induction motor torque-speed characteristic curve.

The induction motor torque-speed characteristics in Figure 14 provide several important pieces of information about the operation of the induction motors:

1. The induced torque of the motor is zero at synchronous speed, as discussed previously.
2. The torque-speed curve is nearly linear between no load and full load since the rotor resistance is much higher than its reactance therefore the rotor current, magnetic field and the torque increase linearly with increasing slip.
3. There is a maximum torque that cannot be exceeded, called pullout or breakdown torque which is 2 to 3 times higher than rated full load torque of the motor.
4. The starting torque is slightly higher than the full load one, therefore the motor will start carrying any load that it can supply at full power.

By a physical aspect, how the breakdown torque occurs? With the increasing slip and therefore the more relative motion between the rotor and the stator magnetic field, the induced voltage E_R to the rotor is higher which in turn produces a larger rotor current I_R. With a larger rotor current the rotor's magnetic field B_R is also increased. However, with the increased slip the

frequency of the rotor rises also ($f_{sl} = s \cdot f_e$) which in turn increases the rotor's reactance. Therefore, the rotor current lags further behind the rotor voltage and by consequence the angle γ (recall at Figure 9) is increased. The breakdown torque occurs when the increase of B_R is less than the decrease of sinγ term. The maximum torque is given by:

$$\tau_{max} = \frac{3V_{TH}^2}{2\omega_{sync}(R_{TH} + \sqrt{R_{TH}^2 + (X_{TH} + X_2)^2})} \qquad 3.3.18$$

Therefore, the main way to control the torque of the induction motor is mainly the input voltage and on the other hand the synchronous rotating speed which is affected by the three phase AC frequency. On the other hand, its rotating speed is mainly affected by also the three phase AC frequency.

3.4 Induction's motor torque-speed control

The torque-speed control of the induction motor is not an easy task. In order to be able to understand the working principle behind the Field Oriented Control (FOC) which will be analyzed below, the speed-torque control of the DC motor will be briefly explained since its principle of decoupled speed and torque control is also applied to the FOC.

3.4.1 DC's motor speed-torque control

DC's motor main advantage is the easy speed and torque regulation. A typical schematic of the DC motor is shown below:

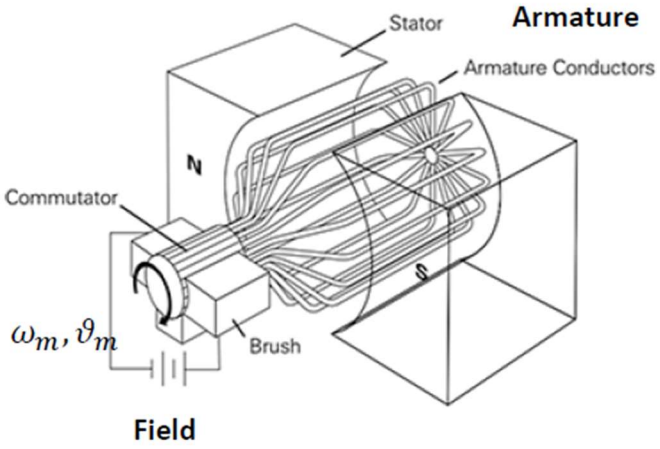

Figure 15: Typical DC motor schematic.

The stator can either be a typical magnet or coils as in the case of induction motor, an electromagnet. Most of the time the stator consists of windings in order to be able to control the power of the stator's electromagnetic field by regulating the input voltage v_f and consequently the stator's current i_f. The rotor, composed of armature conductors, either bars or windings, is connected to an externally controlled circuit, which voltage e_a is being regulated.

Therefore, there is a current i_a flowing into the windings of the rotor as a result of the voltage e_a.

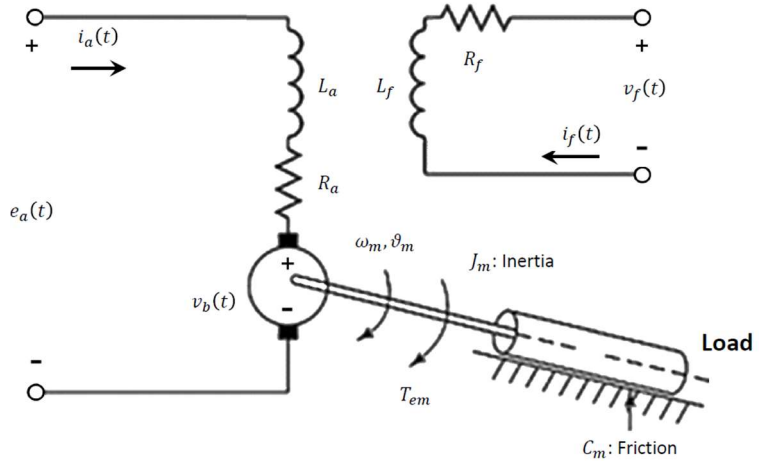

Figure 16: DC motor equivalent circuit.

Since the current-carrying armature is rotating in a magnetic field, its voltage is proportional to the angular speed ω_m by a constant of proportionality K_b:

$$\mathbf{v_b(t) = K_b \cdot \frac{d}{dt}\theta_m(t)}$$

A voltage source e_a is applied to the motor's armature, considered the input of the system, whereas the rotational speed $d\theta_m/dt$, is the output. In general, the torque generated by a DC motor is proportional to the armature current i_a and the strength of the magnetic field φ_s. The magnetic field φ_s is proportional to the current flowing in the stator windings multiplied with a constant k_f.

$$\boldsymbol{\varphi_s = k_f \cdot i_f}$$

Therefore, it is clear that by increasing the current i_f the strength of the magnetic field φ_s is also increased. Under the assumption that the magnetic field is constant, the motor torque is proportional to only the armature current i_a by a constant K_t.

$$\mathbf{T_{em} = k_t \cdot \varphi_s \cdot i_a = K_t \cdot i_a}$$

Thus, by controlling the input voltage e_a it is possible to control the speed ω_m and by controlling the voltage of the stator and consequently the current at the stator's windings it is possible to control the power of the magnetic field thus, the produced torque.

In the case of the induction motor, at first sight there is not the possibility to decouple the speed and the torque control because the rotor's current is not directly controlled, the rotor's current is short-circuited and therefore its voltage cannot be regulated. However, after certain mathematical transformations the speed-torque decouple is achievable.

3.4.2 Field Oriented Control (FOC)

3.4.2.1 Clarke's transformation (a,b,c)→(α,β)

In a three-phase reference frame the 3 windings are spatially distributed by 120°. The result of these three windings distributed both spatially and in time by 120° is a constant magnetomotive force MMF which can be found at a random angle φ based in the following formulas. Assuming that the currents flowing in each one of the three windings are i_a, i_b and i_c. At a random angle φ the total MMF that results from each one of the MMFs of the three windings is:

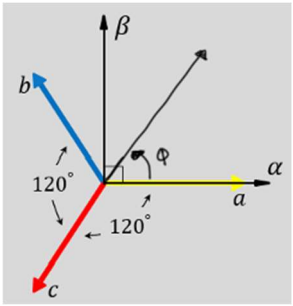

Figure 17: MMF at a random angle φ.

$$\mathbf{MMF(\varphi) = N_s \cdot i_a \cdot cos\varphi + N_s \cdot i_b \cdot cos\left(\frac{2\pi}{3} - \varphi\right) + N_s \cdot i_c \cdot cos\left(\frac{4\pi}{3} - \varphi\right)}$$

After a number of arithmetic operations, the MMF(φ) can be presented by the following formula:

$$\mathbf{MMF(\varphi) = N_s \cdot \left[(i_a - 0.5 \cdot i_b - 0.5 \cdot i_c) \cdot cos\varphi + \left(\frac{\sqrt{3}}{2} \cdot i_b - \frac{\sqrt{3}}{2} \cdot i_c\right)\right]} \qquad 3.4.1$$

Therefore, the MMF can be expressed as a fictitious current $i_a - 0.5 \cdot i_b - 0.5 \cdot i_c$ acting along axis α and another one $\frac{\sqrt{3}}{2} \cdot i_b - \frac{\sqrt{3}}{2} \cdot i_c$ acting along axis β. Therefore, the three currents i_a, i_b and i_c acting along axes a, b, c can be expressed as two currents i_α and i_β acting along axes α, β, by the following transformation.

$$\begin{bmatrix} i_\alpha \\ i_\beta \\ 0 \end{bmatrix} = \frac{2}{3} \begin{bmatrix} 1 & -0.5 & -0.5 \\ 0 & \frac{\sqrt{3}}{2} & -\frac{\sqrt{3}}{2} \\ \sqrt{\frac{1}{2}} & \sqrt{\frac{1}{2}} & \sqrt{\frac{1}{2}} \end{bmatrix} \cdot \begin{bmatrix} i_a \\ i_b \\ i_c \end{bmatrix} \qquad 3.4.2$$

The third row in the transformation matrix was added in order to make it square and thus invertible and the $\frac{2}{3}$ to keep the magnitude invariancy. Therefore, the transformation matrix

carries out the Clarke's transformation from the three-phase a, b, c reference frame to an orthogonal reference frame α, β.

3.4.2.2 Park's transformation

The Clarke's transformation is very useful because the MMF can be expressed in an orthogonal reference frame therefore, the 3 components are reduced to 2. However, still it is not an analogous of the DC motor because these fictitious currents are not time invariant, the MMF rotates at an angular speed depended on the supply frequency. It is necessary to transform these quantities with respect to a rotating reference frame, rotating with the stator's angular speed $\omega_{sync.}$

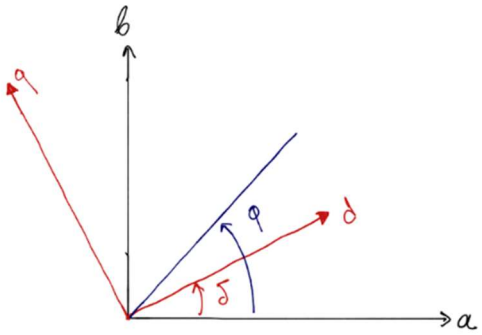

Figure 18: Projecting the α, β components to a rotating reference frame d, q.

The MMF at a random angle φ can be expressed with respect to the currents i_α and i_β in the following formula:

$$\mathbf{MMF(\varphi) = N_{\alpha\beta} \cdot i_\alpha \cdot \cos\varphi + N_{\alpha\beta} \cdot i_\beta \cdot \sin\varphi}$$

By substituting φ with δ + (φ-δ) and by using trigonometric functions formulas the above formula can be expressed as:

$$\mathbf{MMF(\varphi) = N_{\alpha\beta} \cdot \left[i_d \cdot \cos(\varphi - \delta) + i_q \cdot \sin(\varphi - \delta)\right]}$$

where the currents i_d and i_q are equal to:

$$\mathbf{i_d = i_\alpha \cdot \cos\delta + i_\beta \cdot \sin\delta}$$

$$\mathbf{i_q = -i_\alpha \cdot \sin\delta + i_\beta \cdot \cos\delta}$$

Therefore, the currents i_d and i_q can be expressed in the following matrix form:

$$\begin{bmatrix} i_d \\ i_q \end{bmatrix} = \begin{bmatrix} \cos\delta & \sin\delta \\ -\sin\delta & \cos\delta \end{bmatrix} \cdot \begin{bmatrix} i_\alpha \\ i_\beta \end{bmatrix} \qquad 3.4.3$$

The currents i_a and i_b can be expressed as proportional to an amplitude I_m multiplied by sinusoidal of the synchronous frequency ω_{sync}.

$$\begin{bmatrix} \mathbf{i_\alpha} \\ \mathbf{i_\beta} \end{bmatrix} = \mathbf{I_m} \cdot \begin{bmatrix} \mathbf{\cos(\omega_{sync} \cdot t)} \\ \mathbf{\sin(\omega_{sync} \cdot t)} \end{bmatrix}$$

Therefore, by performing the above transformation on the currents i_α and i_β as expressed above the following expressions will be derived:

$$\begin{bmatrix} \mathbf{i_d} \\ \mathbf{i_q} \end{bmatrix} = \mathbf{I_m} \cdot \begin{bmatrix} \mathbf{\cos(\omega_{sync} \cdot t - \delta)} \\ \mathbf{\sin(\omega_{sync} \cdot t - \delta)} \end{bmatrix}$$

The selection of δ is arbitrary, it can be expressed with respect to the angular velocity of synchronous stator's angular speed ω_{sync} or with respect to the rotor's angular speed ω_r. However, it is useful to express it with respect to ω_{sync} because the currents i_d and i_q will become constants. Thus, the angle δ is equal to:

$$\boldsymbol{\delta = \omega_{sync} \cdot t + \delta_0}$$

And the currents i_d and i_q are equal to:

$$\begin{bmatrix} \mathbf{i_d} \\ \mathbf{i_q} \end{bmatrix} = \mathbf{I_m} \cdot \begin{bmatrix} \mathbf{\cos(\delta_0)} \\ \mathbf{-\sin(\delta_0)} \end{bmatrix}$$

3.4.2.3 Transformation of stator and rotor's quantities at the dq reference frame

Having analyzed the Clarke's and Park's transformations it is time to use them in order to transform the stator's and rotor's quantities at the dq reference frame. To transform the stator's quantities at the dq reference frame the angle θ_s will be equal to $\boldsymbol{\theta_s = \omega_{se} \cdot t + \theta_0}$ where θ_0 can be selected equal to 0, thus $\boldsymbol{\theta_s = \omega_{se} \cdot t}$. To transform the rotor's quantities the angle δ_R will be equal to $\boldsymbol{\theta_R = (\omega_{se} - \omega_{me}) \cdot t}$. The ω_{se} and ω_{me} are expressed with respect to the synchronous angular velocity ω_{sync} and the rotor's mechanical velocity ω_m based on the following formulas, where p is the number of pole pairs.

$$\boldsymbol{\omega_{se} = \omega_{sync} \cdot p} \qquad 3.4.4$$

$$\boldsymbol{\omega_{me} = \omega_m \cdot p} \qquad 3.4.5$$

The self-inductances with respect to the self-inductances of the equivalent circuit of the induction motor can be expressed as:

$$\mathbf{L_m = \frac{X_m}{\omega_{sync}}} \qquad 3.4.6$$

$$\mathbf{L_s = L_m + \frac{X_{ls}}{\omega_{sync}} = L_m + L_{ls}} \qquad 3.4.7$$

$$\mathbf{L_R = L_m + \frac{X_{lr}}{\omega_{sync}} + L_m + L_{lr}} \qquad 3.4.8$$

where X_m, X_{ls}, X_{lr} are the magnetizing reactance, the leakage reactance at the stator and the leakage reactance at the rotor for the synchronous frequency ω_{sync}.

The magnetic fluxes can therefore be written as:

- $\mathbf{\lambda_{ds} = L_s \cdot i_{ds} + L_m \cdot i_{dr}}$ 3.4.9
- $\mathbf{\lambda_{qs} = L_s \cdot i_{qs} + L_m \cdot i_{qr}}$ 3.4.10
- $\mathbf{\lambda_{dr} = L_r \cdot i_{dr} + L_m \cdot i_{ds}}$ 3.4.11
- $\mathbf{\lambda_{qr} = L_r \cdot i_{qr} + L_m \cdot i_{qs}}$ 3.4.12

The above four expressions have a very interesting property. Each magnetic flux consists of the current components belonging in the same axis, there is not coupling between d and q axis because these are perpendicular to each other. Also, it is useful align the d axis of the rotating frame with the direction of the rotor's magnetic flux in order to simplify the problem since then the λ_{qr} flux will be set to 0. In order to do that the initial angle θ_R must be known.

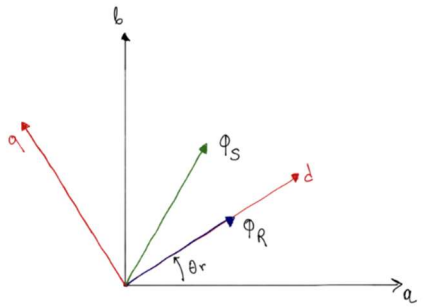

Figure 19: Alignment of d axis of reference frame with the rotor's magnetic flux.

The voltages can also be expressed in the dq reference frame, whereas for the rotor case these will be equal to 0 since the rotor is short-circuited. Thus:

- $\mathbf{v_{ds} = R_s \cdot i_{ds} + \frac{d\lambda_{ds}}{dt} - \omega_{sync} \cdot \lambda_{qs}}$ 3.4.13
- $\mathbf{v_{qs} = R_s \cdot i_{qs} + \frac{d\lambda_{qs}}{dt} + \omega_{sync} \cdot \lambda_{ds}}$ 3.4.14
- $\mathbf{0 = R_r \cdot i_{dr} + \frac{d\lambda_{dr}}{dt} - (\omega_{sync} - \omega_m) \cdot \lambda_{qr}}$ 3.4.15
- $\mathbf{0 = R_r \cdot i_{qr} + \frac{d\lambda_{qr}}{dt} + (\omega_{sync} - \omega_m) \cdot \lambda_{dr}}$ 3.4.16

But since $\lambda_{qr} = 0$ then also $R_r \cdot i_{dr} = -\frac{d\lambda_{dr}}{dt}$. For this reason, the magnetic fluxes equations can be written as:

- $\mathbf{\lambda_{ds} = L_s \cdot i_{ds} - \frac{L_m}{R_r} \cdot \frac{d\lambda_{dr}}{dt}}$ 3.4.17
- $\mathbf{\lambda_{qs} = L_s \cdot i_{qs} + L_m \cdot i_{qr}}$ 3.4.18
- $\mathbf{\lambda_{dr} = L_m \cdot i_{ds} - \frac{L_r}{R_r} \cdot \frac{d\lambda_{dr}}{dt}}$ 3.4.19
- $\mathbf{0 = L_r \cdot i_{qr} + L_m \cdot i_{qs}}$ 3.4.20

For the steady state, $\frac{d\lambda_{dr}}{dt} = 0$, therefore $i_{dr} = 0$. For this reason, the 3.4.17-3.4.20 equations can be written as:

- $\mathbf{\lambda_{ds} = L_s \cdot i_{ds}}$ 3.4.21
- $\mathbf{\lambda_{qs} = L_s \cdot i_{qs} + L_m \cdot i_{qr}}$ 3.4.22
- $\mathbf{\lambda_{dr} = L_m \cdot i_{ds}}$ 3.4.23
- $\mathbf{0 = L_r \cdot i_{qr} + L_m \cdot i_{qs}}$ 3.4.24

The above equations show that the fluxes in the d axis are defined only from the stator's current i_{ds}.

3.4.2.4 Torque expression and dq currents calculation

The torque T_{mech} can be expressed based on the previous current and magnetic fluxes as also the number of pole pairs p, as:

$$\mathbf{T_{mech}} = \frac{\mathbf{3}}{\mathbf{2}} \cdot \mathbf{p} \cdot \left(\frac{\mathbf{L_m}}{\mathbf{L_r}}\right) \cdot \boldsymbol{\lambda}_{\mathbf{dr}} \cdot \mathbf{i_{qs}} \qquad 3.4.25$$

From the above formula, it is obvious that there is an analogy between the torque of the induction motor and the torque generated by the DC motor, since it is an expression of the rotor's magnetic flux in the d-axis direction multiplied by the stator's current along the q-axis direction. The purpose of the FOC is the calculation of the i_{ds}, i_{qs} and i_{qr} currents in order to find the reference currents i_a, i_b, i_c by performing the inverse Clarke and Park transformation.

The calculation of these currents takes into consideration not only the reference torque and speed but also the proper operating conditions of the induction motor. The main condition is the magnitude of the magnetic flux λ_{dr}. It is advisable to operate the induction motor with a constant magnetic flux λ_{dr} close to the rated one. Therefore, by knowing that quantity, which is a characteristic of every motor, the current i_{ds} can be calculated since:

$$\mathbf{i_{ds}} = \frac{\boldsymbol{\lambda}_{\mathbf{dr}}}{\mathbf{L_m}} \qquad 3.4.26$$

By knowing the rated flux λ_{dr} and with a reference mechanical torque T_{mech} the i_{qs} current can be calculated since:

$$\mathbf{i_{qs}} = \frac{\mathbf{2}}{\mathbf{3}} \cdot \frac{\mathbf{1}}{\mathbf{p}} \cdot \left(\frac{\mathbf{L_r}}{\mathbf{L_m}}\right) \cdot \left(\frac{\mathbf{T_{mech}}}{\boldsymbol{\lambda}_{\mathbf{dr}}}\right) \qquad 3.4.27$$

Till this point, the currents i_{ds}, i_{qs} and i_{dr} have been calculated. In order to find also the i_{qr}, it is useful to utilize the formula that $\lambda_{qr} = 0$.

$$\mathbf{i_{qr}} = -\frac{\mathbf{L_m}}{\mathbf{L_r}} \cdot \mathbf{i_{qs}} \qquad 3.4.28$$

Having calculated the reference i_d and i_q currents to it is time to perform the inverse Clarke and Park transformation to define the reference i_a, i_b and i_c currents.

3.4.2.5 Inverse Clarke and Park transformation and reference voltages calculation

To calculate the reference currents from the dq ones, it is necessary to perform firstly the inverse Park transformation to calculate the currents at the αβ stationary reference frame. To do that the calculation of the angle θ_e between the d axis of the dq rotating reference frame and the α axis of the stationary reference frame is mandatory. This angle is equal to:

$$\boldsymbol{\theta}_{\mathbf{e}} = \boldsymbol{\omega}_{\mathbf{e}} \cdot \mathbf{t} + \boldsymbol{\theta}_{\mathbf{0}} \qquad 3.4.29$$

The θ_0 angle is usually not known and for this reason it is assumed equal to 0 with a small initial error which disappears quickly. From the voltage equations expressed above ω_e is equal to:

$$\boldsymbol{\omega_e = \omega_{me} - R_r \cdot (\frac{i_{qr}}{\lambda_{dr}})} \quad 3.4.30$$

which is equal to:

$$\boldsymbol{\omega_e = \omega_{me} + \frac{L_m \cdot R_r}{L_r} \cdot \frac{i_{qs}}{\lambda_{dr}}} \quad 3.4.31$$

The angular electrical velocity ω_{me} can be calculated based on the following formula, where ω_m is the rotor angular velocity that can be calculated with an angular velocity meter and p is the number of pole pairs.

$$\boldsymbol{\omega_{me} = p \cdot \omega_m} \quad 3.4.32$$

In the 3.4.31 formula the $\frac{R_r}{L_r}$ can be expressed as a rotor time constant τ_r.

$$\boldsymbol{\tau_r = \frac{L_r}{R_r}} \quad 3.4.33$$

And by using that notation the 3.4.31 formula can be expresseδ as:

$$\boldsymbol{\omega_e = \omega_{me} + \frac{L_m}{\tau_r} \cdot \frac{i_{qs}}{\lambda_{dr}}} \quad 3.4.34$$

The second term in the above equation is called slip electrical angular velocity and it is expressed as:

$$\boldsymbol{\omega_{sle} = \frac{L_m}{\tau_r} \cdot \frac{i_{qs}}{\lambda_{dr}}} \quad 3.4.35$$

Therefore, by calculating ω_{me} and ω_{sle} the electrical angle θ_e can be estimated:

$$\boldsymbol{\theta_e = \int_0^t \left[\omega_{me} + \frac{L_m}{\tau_r} \cdot \frac{i_{qs}}{\lambda_{dr}}\right] \cdot dt + \theta_0} \quad 3.4.36$$

The only problem with the above formula is that the τ_r constant must be accurately known, which is generally a tough problem, since the rotor's parameters are known with uncertainty and the resistance R_r is changing with the temperature. These uncertainties can lead to a wrong calculation of θ_e and consequently the $i_{d,ref}$ and $i_{q,ref}$ will not be aligned with the d, q axes, although the torque controller will still work with a certain error. The inverse Clarke transformation of the currents can be found based on the following formula:

$$\begin{bmatrix} \mathbf{i_\alpha} \\ \mathbf{i_\beta} \end{bmatrix} = \begin{bmatrix} \mathbf{\cos\theta_e} & \mathbf{-\sin\theta_e} \\ \mathbf{\cos\theta_e} & \mathbf{\sin\theta_e} \end{bmatrix} \cdot \begin{bmatrix} \mathbf{i_{ds}} \\ \mathbf{i_{qs}} \end{bmatrix} \quad 3.4.37$$

Having calculated the i_α and i_β currents at the stationary orthogonal a, β reference frame it is easy to calculate the three-phase reference currents i_a, i_b and i_c with the inverse magnitude invariant Clarke transformation.

$$\begin{bmatrix} \mathbf{i_a} \\ \mathbf{i_b} \\ \mathbf{i_c} \end{bmatrix} = \frac{\mathbf{2}}{\mathbf{3}} \cdot \begin{bmatrix} \mathbf{1} & \mathbf{0} & \sqrt{\frac{\mathbf{1}}{\mathbf{2}}} \\ \mathbf{-0.5} & \frac{\sqrt{\mathbf{3}}}{\mathbf{2}} & \sqrt{\frac{\mathbf{1}}{\mathbf{2}}} \\ \mathbf{-0.5} & -\frac{\sqrt{\mathbf{3}}}{\mathbf{2}} & \sqrt{\frac{\mathbf{1}}{\mathbf{2}}} \end{bmatrix} \cdot \begin{bmatrix} \mathbf{i_\alpha} \\ \mathbf{i_\beta} \\ \mathbf{0} \end{bmatrix} \quad 3.4.38$$

With the above formula the calculation of the reference currents i_a, i_b and i_c is complete. As mentioned, the difficulty of the FOC is the accurate calculation of θ_e and in fact the requirement that the motor parameters in the FOC must coincide with the actual parameters of the motor.

3.5 DC to AC voltage conversion – Inverters

An induction motor must be fed with AC voltage since it is necessary to create the rotating magnetic field. In the case of the battery powered AC electric motor this is not possible because the batteries deliver DC voltage. Thus, there is the necessity to somehow convert this constant voltage source to an approximate AC voltage. The word approximate was used because in fact the converted voltage is not a clear AC but a sequence of variable width steps. The principle of this conversion is based on the use of power electronics and specially semiconductors. This principle will be briefly discussed in the below.

3.5.1 Semiconductors

Semiconductors are the heart of the modern technology. Without them today there would be no computers, no TV's no electronic devices. The developments in semiconductor technology over the past 50 years have made electronic devices smaller, faster and more reliable. In order to understand how these work in general first of all the physics behind conductors must be explained.

Conductors are materials that allow the flow of charge (electrical current) in one or more directions. For instance, copper is a good conductor. This can be explained by its atomic structure, which is displayed in the figure below. The nucleus of the atom contains 29 protons and when a copper atom has a neutral charge, 29 electrons circle the nucleus. These electrons travel in distinct orbits, called shells and in the case of copper 2 electrons are in the first orbit, 8 electrons in the second orbit, 18 in the third orbit and 1 in the outer orbit.

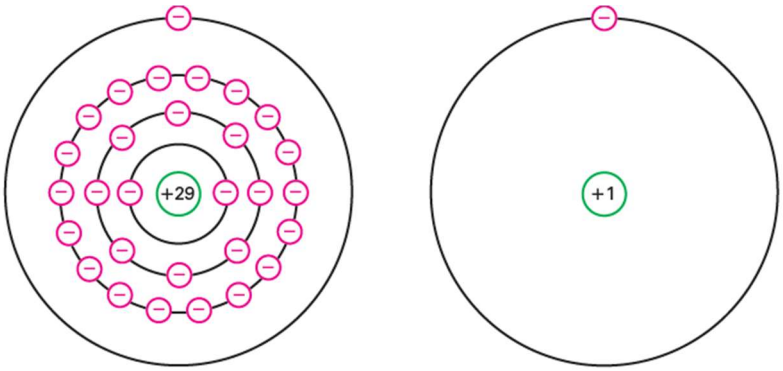

Figure 20: Copper atom and its valence orbit.

In electronics, all that matters is the outer orbit, called valence orbit. The valence electron feels the least inward pull by the core, because the net charge of the core, in the case of atom is +1, therefore by the slightest voltage the electron will flow from one atom to the next. The best insulators in the other hand have eight valence electrons, therefore their core's net charge is +8 therefore the inward pull is much stronger. The semiconductors have four valence electrons and its electrical properties are between those of a conductor and those of an insulator. One of the most famous semiconductors that shaped the modern era is silicon (Si) with four (4) valence electrons.

The first semiconductors were made based on germanium because it was easier to manipulate however once the manufacturing techniques improved, silicon replaced germanium due to its advantages. When silicon atoms combine to create a solid, they arrange themselves into an orderly pattern called a crystal. Each silicon atom shares its electrons with four neighboring atoms in such a way to have eight electrons in its valence orbit. Thus, each neighboring atom shares an electron with the central atom and each atom in a silicon crystal cannot attain more than 8 electrons, thus it is saturated.

Sometimes depending on the ambient temperature, the heat energy causes the atoms in the crystal to vibrate. This vibration might dislodge an electron from its valence orbit, offering it enough energy to go into a larger orbit. The loss of electron creates a vacancy in the valence orbit, called hole and the loss of electrons creates a positive ion. The higher the temperature the higher the tendency of electrons dislodgement, but these holes exist only for nanoseconds to microseconds. The existence of hole is the critical difference between conductors and semiconductors. In order to increase the conductivity of a semiconductor there is a procedure called doping.

Doping is the process during which impurity atoms are being added to a pure silicon crystal to alter its electrical conductivity. The goal is to either increase the number of free electrons or increase the number of holes. In order to increase the number of electrons, pentavalent atoms are added to the silicon, atoms which have 5 electrons in the valence orbit.

Examples of these are arsenic, antimony and phosphorus. The figure below shows how the silicon crystal appears with a pentavalent atom in the center. Since the neighboring atoms share an electron with the central atom and since it already has 5 electrons in its valence orbit, 1 electron is left over in a larger orbit, thus it is a free electron.

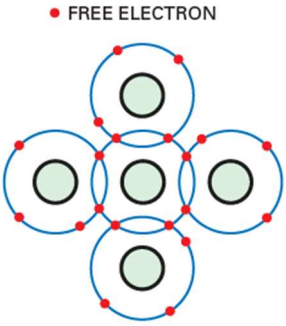

Figure 21: Pentavalent atom with a free electron.

On the other hand, adding a trivalent atom to the silicon, atoms which have 3 electrons in the valence orbit create a hole in the valence orbit. Examples include aluminum, boron and gallium. Since a trivalent atom has 3 electrons in its valence orbit and since the neighboring atoms share 1 electron with the central atom, only 7 electrons are in the valence orbit and thus a hole.

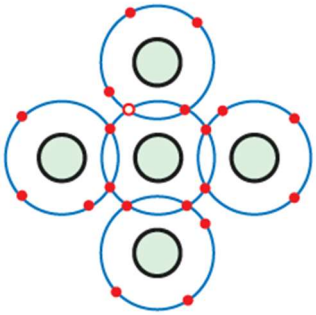

Figure 22: Trivalent atom with a hole in the valence zone.

Silicon that has been doped with a trivalent impurity is called p-type semiconductor, where the p stands for positive whereas doped silicon with a pentavalent impurity is called n-type semiconductor where n stands for negative. P- and n- type semiconductors alone are not useful but when a crystal's one half is p-type and the other half is n-type something very useful comes in existence. The border between the p-type and n-type is called the pn junction. This junction has led to all kinds of inventions, including diodes, transistors e.t.c.

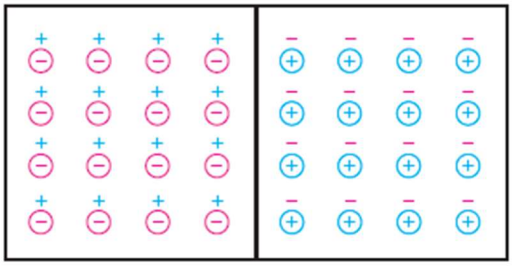

Figure 23: Pn junction.

The left side of the above figure consists of trivalent atoms which produce one hole and for this reason each atom can be visualized as a circled minus and its hole as a plus sign. Similarly, the right side consists of pentavalent atoms represented by a circled plus whereas the free electron is shown by a minus. Each piece of semiconductor is electrically neutral because the number of pluses and minuses is equal.

Because of the excess of electrons in the right side, they tend to diffuse in all directions. Some enter the p region and they recombine with a hole. By leaving the n side they create a pentavalent atom that is short one negative charge, this atom becomes a positive ion. On the other hand, when they fall into a hole in the left side, they create a negative ion.

The flow of electrons from the right to the left side create a pair of positive and negative ions at the junction, called a dipole. The number of dipoles builds up and the region near the junction is emptied of carriers (holes and free electrons). This charge-empty region is called the depletion layer. Each dipole has an electric field between the positive and negative ions. This electric field tires to push back the electrons trying to enter the depletion layer. The strength of the electric field increases with each crossing electron until equilibrium is reached. The electric field is equivalent to a difference of potential, called the barrier potential. For silicon diodes this is equal to 0.7V.

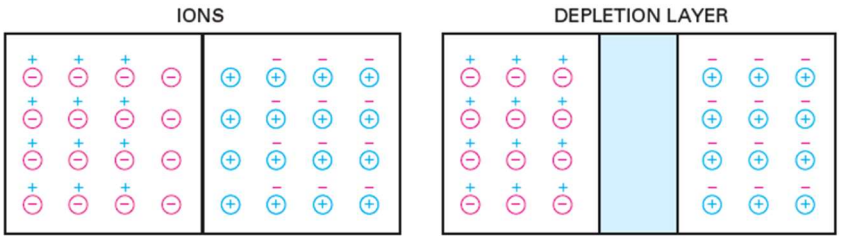

Figure 24: Depletion layer, emptied of carriers.

This barrier potential is of great importance. By connecting a voltage across the diode, its operating principle will be clear. In the figure below there is a battery connected where its positive end is connected to the left side and its negative end at the right side. The battery connected in that order pushes holes and free electrons toward the junction. When the free electrons enter the depletion layer, they are pushed back due to the barrier potential. However,

if the applied voltage is greater than that of the depletion layer the free electrons can bypass the depletion layer and recombine with the holes. Since the free electrons continuously enter the right end of the diode and holes are being continuously created at the left end, there is a constant flow of current through the diode. This is called the forward bias.

On the other hand, if the battery terminals are reversely connected, the negative terminals attract the holes and the positive attract the free electrons. Because of this, holes and free electrons flow away from the junction and this makes the depletion layer wider. The depletion layer keeps extending until its barrier potential is equal to the applied voltage. This is called the reverse bias. There is a limit to how much reverse voltage a diode can withstand before it is destroyed. For many diodes this is equal to at least 50V. The breakdown voltage is shown on the data sheet for the diode. Having briefly explained the working principle of a simple diode, it is time to introduce the Insulated-Gate Bipolar Transistor (IGBT), a three-terminal power semiconductor primarily used as an electronic switch, which offers high switching frequencies and high efficiency.

3.5.2 Insulated-Gate Bipolar Transistor (IGBT)

The IGBT is used in switching power supplies in high-power applications, in variable-frequency drives, in electric cars. Its ability to turn on and off rapidly offers the ability to create complex waveforms with pulse-width modulation.

IGBT as already mentioned is a three-terminal semiconductor, consisting of the Gate(G), the Emitter(E) and the Collector(C). Its typical symbol is being presented below. The Collector and the Emitter are the conduction terminals whereas the Gate is the control terminal with which the switching operation is controlled.

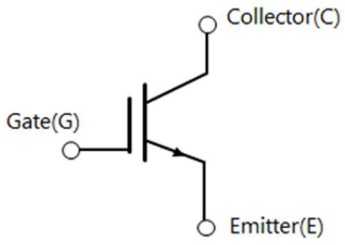

Figure 25: IGBT symbol.

The working principle of IGBT can be explained using the figure below. Each one of the three different terminals are attached to three different metal layers and the metal layer of the gate terminal is insulated from the semiconductors by a layer of silicon dioxide (SiO_2). IGBT is constructed with 4 layers of semiconductor sandwiched together. The layer closer to the collector is the p^+ substrate layer called also injection region, above that is the n^- layer, the drift region, another p layer is kept closer to the emitter, the body region and inside the p layer there are two n^+ layers. The n^+ symbolized a highly doped semiconductor with excess electrons,

whereas n^- a lowly doped semiconductor with less electrons. Similarly, the same applies to the p^+ and p^-.

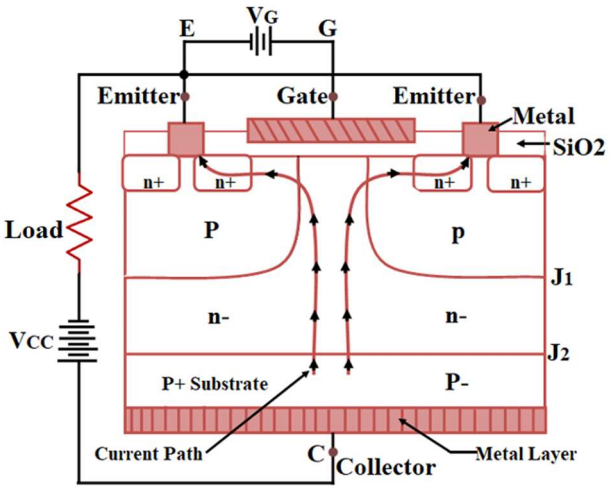

Figure 26: IGBT structure.

To understand the working principle, consider a voltage source V_G connected positively to the gate terminal with respect to the emitter. Also, consider another voltage source V_{CC} connected across the emitter and the collector, where collector is kept positive with respect to the emitter. Due to the voltage source the junction J_1 is forward biased whereas the junction J_2 will be reverse biased. Thus, the current cannot flow inside the IGBT, from the collector to the emitter.

By applying a voltage V_G positively to the gate terminal, it will attract the negative charge of the SiO_2 layer and consequently the positive charge will be close to the body region. Therefore, the positive charge will attract the negative charge of the p region and in this way a channel will be created between the J_2 junction which allows the flow of current from collector to the emitter. By increasing the gate voltage V_G, the current flow from the collector to the emitter is also increased.

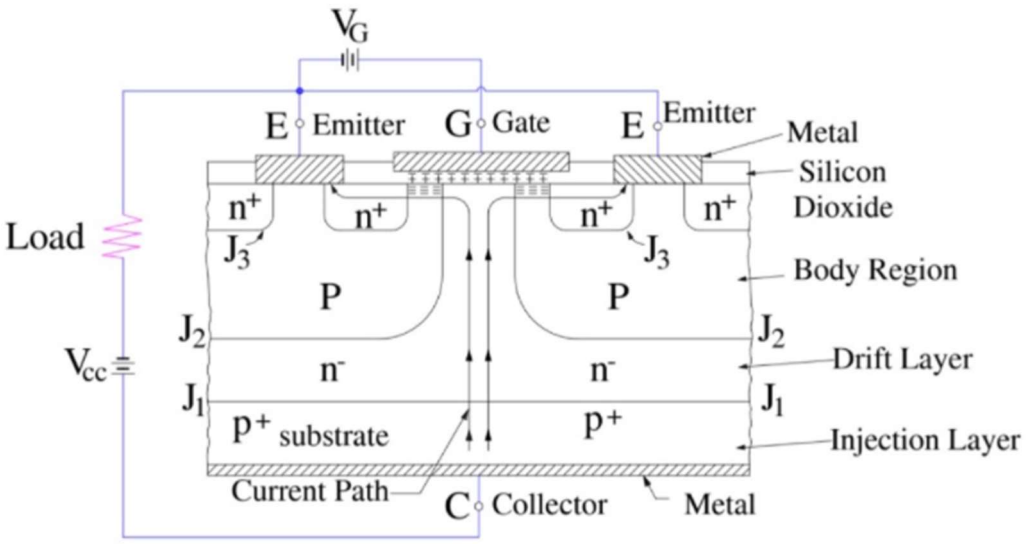

Figure 27: IGBT conducting state.

The input characteristics of the IGBT can be understood from the graph below. When no voltage V_G is applied the IGBT is in turn off condition and no current flows through the collector to the emitter. When the voltage V_G applied, exceeds the threshold voltage, the IGBT starts conducting and the collector current I_C starts to flow between the collect and emitter terminals.

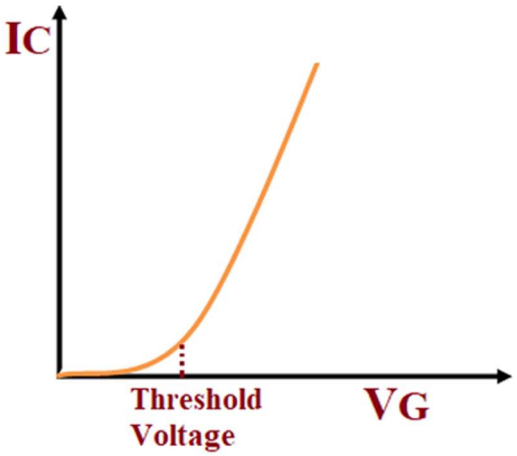

Figure 28: Collector current with respect to the applied gate voltage V_G.

The output characteristics of the IGBT have 3 stages, initially when the V_G voltage is 0 the device is in the off state, called cutoff region. When the V_G voltage starts increasing but it is less than the threshold voltage there is a small leakage current flowing through the device, but it will still be in the cutoff region. When the V_G increases above the threshold voltage, the IGBT goes into the active region and the current starts flowing through the device. The flow of current increases with an increase in the voltage V_G as shown in the graph below.

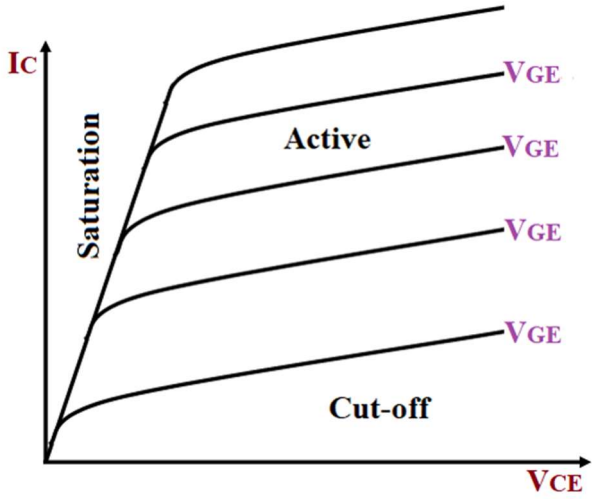

Figure 29: IGBT different active region with respect to applied gate voltage V_G.

3.5.3 Three-phase Inverter with hysteresis band

The three-phase inverter is used in order to transform the constant DC voltage source to an approximately three-phase AC voltage. The generated voltage is not a clear sine voltage but a sequence of variable width steps. This can be problematic for certain loads that need a smooth sine wave in order to operate properly, but for the case of the induction motor, since the load is mainly an inductive one, it contains a passive filter that smooths the current in the circuit. The schematic of a three-phase full bridge inverter is presented below.

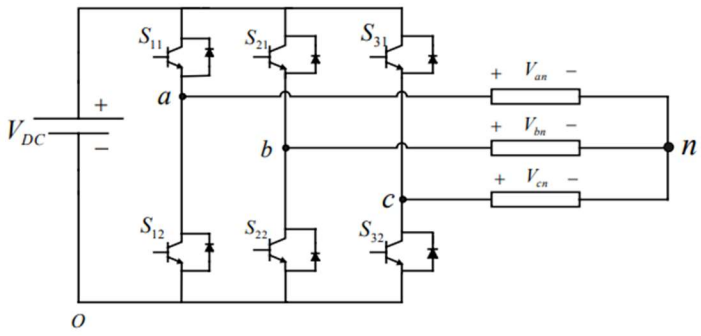

Figure 30: Three-phase full bridge inverter.

In the above figure it is clear that there are 6 switches. Each switch consists of an IGBT connected anti-parallel with a diode. When the load is inductive, as in the case of the induction motor, there are times when the current must continue its path even when the IGBT is OFF. For this reason, the diode offers a path to that current. The above inverter has 8 switch states given in the table below. It must be noted that both of the switches in the same leg cannot be turned ON simultaneously as the input voltage would be sort-circuited.

Table 4: Switching states in a three-phase inverter.

S_{11}	S_{12}	S_{31}	V_{ab}	V_{bc}	V_{ca}
0	0	0	0	0	0
0	0	1	0	$-V_{DC}$	V_{DC}
0	1	0	$-V_{DC}$	V_{DC}	0
0	1	1	$-V_{DC}$	0	$-V_{DC}$
1	0	0	V_{DC}	0	$-V_{DC}$
1	0	1	V_{DC}	$-V_{DC}$	0
1	1	0	0	V_{DC}	$-V_{DC}$
1	1	1	0	0	0

In the above table only the one of each pair switches are being presented. The reason for that is that by knowing the one switch state, one can find also the state of the other switch of the pair since they cannot be ON simultaneously because of a short-circuit of the voltage source. Thus, each switch pair must satisfy the following:

- $S_{11} + S_{12} = 1$
- $S_{21} + S_{22} = 1$
- $S_{31} + S_{32} = 1$

To control the switches a hysteresis controller is used. The hysteresis controller is fed from the reference currents $i_{a,ref}$, $i_{b,ref}$, $i_{c,ref}$ and the hysteresis band. The measured phase current i_a is compared to the reference current $i_{a,ref}$.

When the measured current i_a is bigger than the reference current $i_{a,ref}$ plus the band range, **($i_a > i_{a,ref} + Band$)** the switch S_{11} is turned OFF and S_{12} ON. This reduces the i_a current because the voltage to phase a becomes negative. On the other hand, when **($i_a < i_{a,ref} - Band$)**, the switch S_{11} is turned ON and the S_{12} OFF, which increases the current i_a because the phase voltage becomes positive. Below a graphical representation of this procedure is being presented:

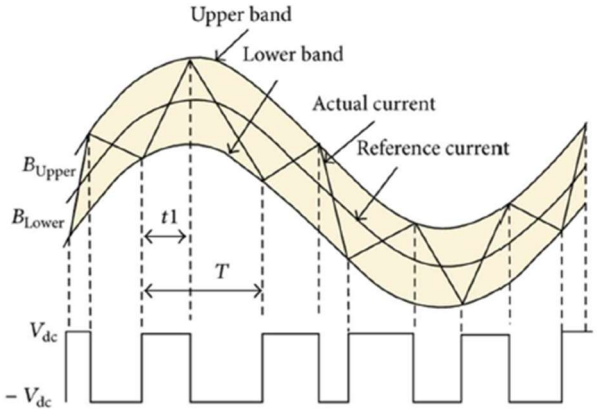

Figure 31: Reference current and actual in the hysteresis band.

The band range determines the current's fluctuation and consequently its harmonics. The lower the range, the lower the current's harmonics but with the expense of higher switching frequency and thus increased switching electrical losses.

4.0 Batteries

One of the more if not the most developed energy storage system is the battery. The principle of its operation is based on the conversion of chemical energy into electrical based on two electrochemical reactions, the loss of electrons called oxidation and the gain of electrons called reduction. A battery is nothing more than an arrangement of many electrochemical cells connected in series or parallel where each one contains:

- The cathode, which is the "positive" half of the battery cell which during the reduction accepts electrons flowing from the anode. The cathode is selected based on its voltage and chemical stability over time.
- The anode, which is the "negative" half of the battery cell which during the oxidation reaction releases electrons that flow to the cathode via an external circuit. The material for the anode is selected based on its efficiency, high specific capacity, ease of fabrication and low cost.
- The electrolyte which is the medium that offers a passage for the positive ions to flow between the anode and the cathode. The electrolyte can be either in liquid form, a salt, an acid or an alkaline solution or in the case of the dry cell a paste. It is chosen based on its high conductivity, non-reactivity with the electrode materials and temperature stability for a high range.
- The separator, which is a material placed between the anode and the cathode and its purpose is to prevent those two parts from creating a short circuit.

When the battery is discharged, chemical reactions initiate a flow of electrons from the anode to the cathode, which in fact is the electric current that flow in the external circuit. Simultaneously, positive charges (ions) flow from the anode to the cathode via the electrolyte and the separator which blocks the passage of other molecules. The electrical charge of ions is equal to that of the electrons based on the energy conservation principle.

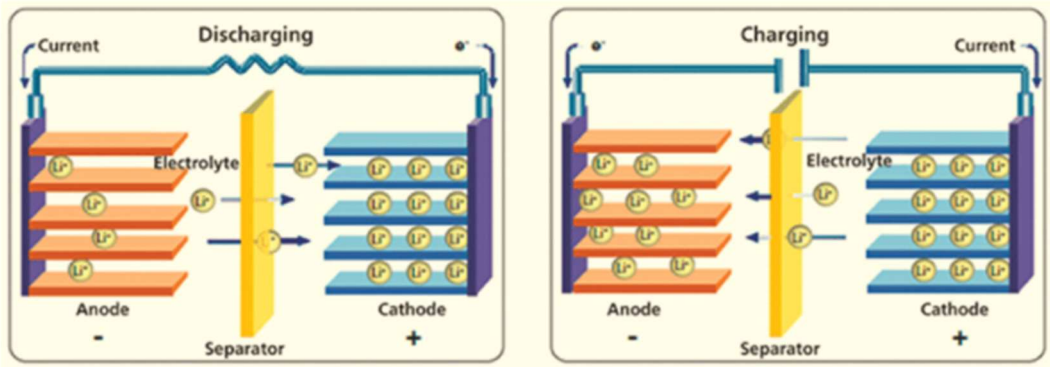

Figure 32: Principle of operation of a battery.

Batteries can be grouped into two major categories:

- Primary batteries: The chemical reactions eat away one of the electrodes, usually the negative one and thus the battery cannot be recharged. The process of discharge is therefore irreversible.
- Secondary batteries: In this case the electrodes and the electrolyte are altered by the chemical reaction that takes place when the battery delivers current. This type of battery can be recharged multiple times and the electrodes are made of different materials. Batteries used in marine applications are mainly rechargeable.

4.1 Battery Definitions

In order to be able to distinguish the main physical characteristics and the pros and cons between different battery technologies certain terminology must be introduced. The definitions presented below are taken from "A Guide to Understanding Battery Specifications", MIT Electric Vehicle Team, December 2008.

4.1.1 Battery Basics

- **Cell, modules and packs:** A cell is the smallest, packaged form a battery can take and it is generally on the order of one to six volts. A module consists of several cells connected in either in series or parallel. Then a battery pack can be made from several modules which in turn are connected again either in series or parallel.
- **Battery Classifications:** Batteries even those of same chemistry can differ a lot. The main trade-off that battery manufacturers face is between power and energy, batteries can be either high-power or high-energy, but not both simultaneously. Another classification between those two is the High Durability, the battery chemistry has been altered in order to provide higher battery life at the expense of power and energy.
- **C- and E- rates:** When describing batteries, it is useful to express the discharge current with respect to its nominal capacity. A C-rate is a measure of the rate at which a battery is discharged relative to its maximum capacity. A 1C rate means that the discharge current will discharge the battery completely in 1 hour. For instance, for a battery capacity of 100 A·hr, this equates to a discharge current of 100 Amps. A 5C equates to 500 Amps, this would discharge the battery in 12 mins and a C/2 rate equates to 50 Amps, with discharge duration of 2 hours. Similarly, an E-rate describes the discharge power, an 1E rate is the discharge power to discharge the battery in 1 hour.

4.1.2 Battery Conditions:

This section describes some of the variables used to describe the present condition of a battery.

- **State of Charge (SoC) (%):** This variable is an expression of the present battery capacity as a percentage of the maximum capacity. A fully charged battery has a SoC of 100% and a fully discharged of 0%. In order to calculate it, current integration with respect to time is necessary. However, the SoC is highly dependent of the temperature of the battery along with the terminal voltage of the battery. Also, the calculation must take into consideration the non-linear effects of different power levels and voltage or SOC ranges.
- **State of Health (SOH):** This variable is an indication of the general condition of the battery and its ability to deliver the specified performance compared to a new battery. As the battery is charged and discharged repeatedly the negative electrode accumulates less and less ions. This metric refers mainly to a reduction in the total amount of energy or total capacity.
- **Depth of Discharge (DOD) (%):** The percentage of the battery capacity that has been discharged expressed as a percentage of the maximum capacity. A discharge of 80% DOD is referred to as a deep discharge.
- **Terminal Voltage (V):** The voltage between the battery terminals with load applied. This differs from the nominal voltage and it is a function of SoC and discharge/charge current.
- **Open-circuit voltage (V):** The voltage between the battery terminals where no load is applied. It is highly dependent on battery state of charge, increasing with it.
- **Internal Resistance:** The resistance within the battery, generally differs for charging and discharging, also dependent on state of charge. As internal resistance increases, the battery efficiency decreases as more energy is converted into heat, increasing therefore the battery temperature and decreasing its thermal stability.

4.1.3 Battery Technical Specifications

This section explains the specifications on battery technical specifications sheets used to describe battery cells, modules and packs.

- **Nominal Voltage (V):** The reported or reference voltage of the battery, also thought of as the "normal" voltage of the battery.
- **Cut-off Voltage (V):** The minimum allowable voltage, in general describes the empty state of the battery.
- **Capacity or Nominal Capacity (A·h for a specific C-rate):** The coulometric capacity, the total Amp·hours available when the battery is discharged at a certain discharge current (specified as a C-rate) from 100 percent SoC to the cut-off voltage. Capacity is calculated by multiplying the discharge current (in Amps) by the discharge time (in hours) and decreases with increasing C-rate.
- **Capacity Fade:** Carbonaceous materials used in all Li-Ion batteries, have dominant effects in the capacity loss at high discharge currents. During the cell operation, non-reversible chemical reactions on the surface of graphite happen among lithium ions, solvents and electrons. The by-product of these reactions accumulates and form a surface film on the carbon electrode known as Solid Electrolyte Interface (SEI). A battery can stop performing when the lithium ions can no longer pass the SEI layer due to its thickness. Thus, lifetime and cyclability of a cell depends on its SEI layer. Capacity Fade has two components:
    1. **Calendar fade:** The reduction of capacity with the passage of time firstly due to the extension of direct interface between the electrode and the electrolyte and secondly because of the loss of active material.
    2. **Cycling fade:** The reduction of capacity due to the successive charge/discharge cycles which result in the alternation of electrode's structure and mechanical fatigue.

  Both of these effects are highly dependent on temperature. The higher the temperature the more rapidly the cell will degrade, with additional risks presented at low temperatures. Exposure to temperatures outside of the rated operating range can affect negatively the battery's lifespan.

- **Energy or Nominal Energy (W·h (for a specific C-rate)):** The "energy capacity" of the battery, the total Watt·hours available when the battery is discharged at a certain discharge current (specified at a C-rate) from 100 percent SoC to the cut-off voltage. Energy is calculated by multiplying the discharge power (in Watts) by the discharge time (in hours). Like capacity, energy decreases with increasing C-rate.

- **Cycle Life (number for a specific DOD):** The number of discharge-charge cycles the battery can experience before it fails to meet specific performance criteria. Cycle life is estimated for specific charge and discharge conditions. The actual operating life of the battery is affected by the rate and depth of cycles and by other conditions such as temperature and humidity. The higher the DOD, the lower the cycle life.
- **Specific Energy (W·h/kg):** The nominal battery energy per unit mass, sometimes referred to as the gravimetric energy density. Specific energy is a characteristic of the battery chemistry and packaging. Along with the energy consumption, it determines the required battery weight to achieve a given electric range.
- **Specific Power (W/kg):** The maximum available power per unit mass. It is also a characteristic of the battery chemistry and packaging. It determines the battery weight required to achieve a given performance target.
- **Energy Density (W·h/L):** Similar to the Specific Energy specification, it is the nominal battery energy per unit volume, sometimes referred to as the volumetric energy density. Energy density is a characteristic of battery chemistry and packaging. Along with the energy consumption, it determines the required battery size to achieve a given electric range.
- **Power Density (W/L):** The maximum available power per unit volume. It is also a characteristic of the battery chemistry and packaging. It determines the battery size required to achieve a given performance target.
- **Maximum Continuous Discharge Current:** The maximum current at which the battery can be discharged continuously. This limit is usually defined by the manufacturer in order to prevent excessive discharge rates that would damage the battery or reduce its capacity.
- **Maximum 30-sec Discharge Pulse Current:** The maximum current at which the battery can be discharged for pulses of up to 30 seconds. This limit is also defined by the manufacturer in order to prevent excessive discharge rates that would damage the battery or reduce its capacity.
- **Charge Voltage:** The voltage that the battery is charged to when charged to full capacity. Charging schemes generally consist of a constant current charging until the battery voltage reaches the charge voltage, then constant voltage charging, allowing the charge current to taper until it is very small.
- **Float Voltage:** The voltage at which the battery is maintained after being charged to 100% SoC, to maintain that capacity by compensating for self-discharge of the battery.

- **(Recommended) Charge Current:** The ideal current at which the battery is initially charged (to roughly 70% SoC) under constant charging scheme before transitioning into constant voltage charging.
- **(Maximum) Internal Resistance:** The resistance within the battery, usually different for charging and discharging.
- **Deep-cycle battery:** A battery which is designed to be regularly deep discharged using most of its capacity. It is also designed to produce steady power output over an extended period of time. On the contrary starter or 'cranking' automotive batteries are designed to deliver only a small part of their capacity in a short, high-current burst.
- **Memory Effect:** Occurs when the battery is repeatedly charged before all of its stored energy is depleted. This in turn will cause the battery to 'memorize' the decreased life cycle. Therefore, the capacity of the battery is decreased.
- **Self-discharge:** It is a phenomenon in battery where internal chemical reactions reduce the stored charge of the battery without any connection between the electrodes or any external circuit. Self-discharge decreases the shelf life of the battery and causes it to have less than a full charge when actually put to use.
- **Coulombic or Faradaic efficiency:** The ratio of the total charge extracted from the battery to the total charge put into the battery over a full cycle. It describes the charge efficiency by which electrons are transferred in batteries.
- **Cycle and Standby Use:** A battery is called to be in cyclic use when it is being used as a power source on a regular basis and it is being discharged and subsequently recharged. A battery in standby use is used as an emergency power source, therefore are kept fully charged so that they can provide energy immediately. In standby use the batteries have a design life of up to 5 years.

4.2 Battery types

The three main battery chemistries that have prevailed the market for different reasons are the Lead Acid, the Nickel based and the Lithium based batteries. In this section the main characteristics of these three different technologies will be analyzed, beginning with the Lead Acid battery.

4.2.1 Lead Acid batteries

The lead acid battery was the first rechargeable battery for commercial use and owns a considerable market share for more than a century. They are supplied by a large, well-established worldwide supplier base and have the largest market share for rechargeable batteries. The largest market is for automotive batteries with a turnover of $25BN and the second one for standby and motive power with a turnover of $10BN.

The grid structure of the lead acid battery is made from a lead alloy. Small quantities of other metals are added to get the required mechanical strength since pure lead is too soft and not able to support itself. This also improves electrical properties. The most common additives are antimony, calcium, tin and selenium. Antimony and tin can improve the deep cycling with the cost of increased water consumption. Calcium reduces self-discharge, but the positive lead-calcium plate has the side effect of growing due to grid oxidation when being over-charged. In modern designs doping agents such as selenium, cadmium, tin and arsenic are used to lower the antimony and calcium content.

A lead-acid battery has 3 life stages, the Formatting, the Peak and the Decline, as shown in the following Figure.

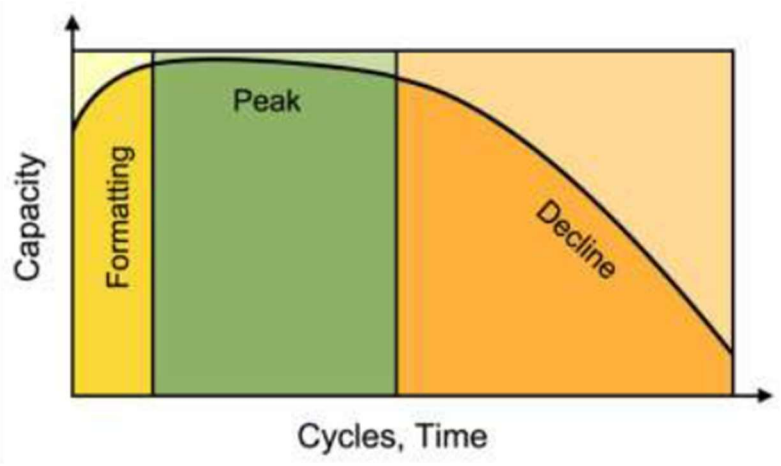

Figure 33: Lead acid battery life stages (Formatting, Peak and Decline).

The formatting stage is the most important and can be compared to a sponge (lead plates) surrounded by a liquid (electrolyte). Exercising the plates allows the absorption of electrolyte, much like squeezing and releasing a hardened sponge. As the electrodes activate, the capacity gradually increases. It is the most important phase for deep-cycle batteries and it requires 20-50 full cycles to reach peak capacity. In this life phase of the battery the load applied to the battery must mild.

A deep-cycle lead acid battery can offer 150-250 discharge/charge cycles before a gradual decline begins. Replacement should occur when the capacity drops to 70 or 80 percent. Some applications allow lower capacity thresholds but the time for retirement should never fall below 50 percent as aging may hasten once past the prime. Lead acid is less durable than nickel- and lithium-based systems when deep cycled. A full discharge causes strain and each discharge/charge cycle permanently robs the battery of a small amount of capacity. This loss is insignificant for the initial charge/discharge cycles but the fading increases once the performance drops to half the nominal capacity. The primary reasons for the relatively short deep cycle life of lead acid battery are the grid corrosion on the positive electrode, the depletion

of the active material and the expansion of the positive plates. Elevated temperatures and high discharge currents deteriorate those phenomena.

Charging of lead-acid batteries even simple, must be controlled. A high voltage limit can increase performance but forms grid corrosion on the positive plate, while a low voltage limit shelters the battery but decreases performance and causes a buildup of sulfation on the negative plate. Sulfation can be reversed if serviced in time, but corrosion is permanent.

Lead acid battery is not characterized by fast charging, full charge takes 14-16 hours. The battery must be always stored in full SoC. Low charge can cause sulfation which is the process of lead sulfate crystals building up on a battery cell. This can lead to longer charging times, excessive heat build-up and mainly shortening the battery's life. This can be treated by adding carbon on the negative electrode (anode) but this lowers the specific energy.

While lead acid has a small life span compared to other battery technologies, it has a very satisfactory self-discharging behavior. For instance, nickel-based systems lose approximately 40 percent of their stored energy in 3 months, while lead acid self-discharges the same amount in one year. Also, lead acid batteries work well at cold temperatures and are superior to lithium-ion ones when operating in subzero conditions.

Last but not least, it is important to mention the sustainability of lead acid batteries. Recycling of lead acid batteries has been an established practice since they were first used and is continuing to increase. Recycling rates approach 100% in Western countries while the production of batteries uses the 85% of lead worldwide production whereas the recycled lead represents 60% of that production. Almost complete recovery and re-use of lead acid battery materials can be achieved with a relatively low energy input, while lead emissions are maintained within the low limits required by environmental regulations. Scrap prices favors the recycling processes in contrast to Li-ion batteries where the recycling rates are much lower due to the low efficiency and the not favorable economics.

Table 5: Advantages and disadvantages of lead acid batteries.

Advantages	Disadvantages
Inexpensive and simple to manufacture	Limited cycle life (up to 300 cycles)
Good low and high temperature performance	Slow charge (14-16 hours)
Low self-discharge	Low specific energy (30-40 W·h/kg)
Sustainable with very high recycle rates	Must be stored in full SoC to avoid sulfation
Not affected by the memory effect	Hard to be manufactured in small sizes

4.2.2 Nickel-based batteries

Nickel-based batteries, including nickel-iron, nickel-cadmium, nickel-zinc, nickel-hydrogen and nickel-metal hydride, are similar in the way that nickel hydroxide electrodes are utilized as positive plates in these systems. As strong alkaline solutions are generally used as electrolyte for these systems, they are also called alkaline secondary batteries. Ni-based batteries have been and still are an important power source for a range of electronic devices.

4.2.2.1 Nickel-Cadmium (NiCd)

Invented by Waldemar Jungner in 1899, the nickel-cadmium battery offered several advantages over lead acid, the only rechargeable battery then. However, the necessary materials were expensive so the development of this battery was postponed until 1932 where advancements were made to deposit the active materials inside a porous nickel-plated electrode. In 1947 further improvements were made by absorbing the gases generated during charge, which led to the modern sealed NiCd battery.

For many years, NiCd was the preferred battery choice for two-way radios, emergency medical equipment, professional video cameras and power tools. In 1980 the ultra-high capacity NiCd, with capacities 60% more than the standard NiCd, due to the packing of more active material into the cell in the expense of higher internal resistance and reduced cycle count, was a breakthrough in the nickel-based batteries market.

The main disadvantage of the standard NiCd battery is the memory effect that causes loss of capacity if not given a periodic full discharge cycle. The battery has the tendency to remember the previous energy delivered and once a routine has been established it cannot offer more. Still it is one of the most rugged and forgiving batteries, extendedly used in in the airline industry and with proper care it can attain longevity.

Table 6: Advantages and disadvantages of Nickel-Cadmium batteries.

Advantages	Disadvantages
Rugged, high cycle count with proper maintenance	Lower specific energy compared to new systems
Only battery that can be ultra-fast charged with little stress	Memory effect, requires periodic full discharges to be rejuvenated
Good load performance, forgiving if abused	Cadmium is toxic, cannot be disposed in landfills
Good low-temperature performance	High self-discharge, needs recharging after storage
Economically priced, $400 per kWh	Low cell voltage of 1.2 V, requires many cells in series

4.2.2.2 Nickel-Metal-Hydride (NiMH)

Research on nickel-metal-hydride started in 1967, however instabilities with the metal-hydride led to the development of the nickel-hydrogen (NiH) instead. New hydride alloys discovered in the 1980s eventually improved the stability issues and today NiMH provides 40% higher specific energy than the standard NiCd.

NiMH has certain important drawbacks. First of all, the battery is more delicate and trickier to charge than NiCd and mainly it has 20% self-discharge the first 24 hours and 10% per month thereafter, classifying NiMH one of the most self-discharging batteries. This can be improved by modifying the hydride materials, which also reduces alloy corrosion, in the expense of lower specific energy.

Table 7: Advantages and disadvantages of Nickel-Metal-Hydride batteries.

Advantages	Disadvantages
30-40% higher capacity than a standard NiCd	Limited service life, deep discharge reduces it
Less prone to memory effects than NiCd	Requires complex charge algorithm, sensitive to overcharge
Environmentally friendly, contains only mild toxins	High self-discharge
Nickel content makes recycling profitable	Coulombic efficiency around 65% (Li-ion has 99%)
Wide temperature range	Generates heat during fast charge and high-load discharge

4.2.2.3 Nickel-Iron (NiFe)

After inventing NiCd in 1899, Waldemar Jungner tried to substitute cadmium for iron due to its lower price; however, poor charge efficiency and hydrogen formation (gassing) led him to abandon the project. In 1901, Thomas Edison continued the development of nickel-iron battery as an alternative to lead acid batteries for electric vehicles, claiming that nickel-iron, immersed in an alkaline electrolyte was “far superior to batteries using lead plates in sulfuric acid”. Edison counted on the emerging electric vehicle market and felt disappointed not only because the gasoline-powered cares took over but also because the industry used lead acid batteries for starter, lighting and ignition (SLI), instead of lead acid.

Nickel-iron uses an oxide-hydroxide cathode and an iron anode with potassium hydroxide electrolyte that produces a nominal cell voltage of 1.2V. NiFe is durable to overcharge and over-discharge and can last for more than 20 years in standby applications. It

has also high resistance to vibrations and high temperatures, that is why it was extendedly used for mining in Europe. NiFe's main drawback is the low specific energy of about 50 W·h/kg, the poor low-temperature performance and the high self-discharge of 20-40% per month.

After considerable improvements, NiFe technology has been improved and can be considered a viable alternative in off-grid power systems. Ni-Fe has become immune to over- and under-charging and can last for over 50 years, compared to the 12 years with deep cycle lead acids in cycling mode. Also, the NiFe costs about 4 times as much as lead acid and its price is comparable to that of Li-Ion.

Table 8: Advantages and disadvantages of Nickel-Iron batteries.

Advantages	Disadvantages
Iron is environmentally benign compared to cadmium	Higher cost, comparable to that of Li-Ion
Iron electrodes are electrically robust; high tolerance of abuse (overcharge, over-discharge)	Low cell voltage, requires a lot of cells in series to create a high voltage
Do not suffer from memory effect	Cannot supply sudden large power spikes
Long cycle life even after abusive usage (up to 2000 cycles with 80% DoD)	Requires ventilation due to considerate amount of hydrogen production
Relatively high specific energy (1.5-2 times compared to lead acid)	

4.2.2.4 Nickel-Zinc (NiZn)

Nickel-zinc is similar to nickel-cadmium as it uses an alkaline electrolyte and a nickel electrode but it differs in voltage; NiZn provides 1.65V/cell rather than 1.2V, which NiCd and NiMH deliver. The specific energy is about 100W·h/kg and can be cycled 200-300 times. Furthermore, it is environmentally friendly as it does not contain heavy toxic materials and can be easily recycled.

Thomas Edison patented NiZn as a rechargeable alternative system in 1901 and was installed in rail cars between 1932 and 1948. NiZn suffered from high self-discharge and short cycle life due to dendrite growth, which often led to electrical short-circuit. Improvements have been made in the electrolyte and nowadays NiZn can be considered again for commercial use. Its chemistry can be considered as an attractive one due to the low cost, the high-power output and the good temperature operating range.

Table 9: Advantages and disadvantages of Nickel-Zinc batteries.

Advantages	Disadvantages
Low cost	High self-discharge
High power output, high specific energy (60-70 W·h/kg)	Short cycle life
Good temperature operating range	Formulation of dendrites during discharge, can lead to short-circuit
Higher voltage/cell (1.65 compared to NiCd and NiMH)	
Environmentally friendly, recyclable	

4.2.3 Lithium-based batteries

Pioneering work on the lithium battery began in 1912 under G. N. Lewis, but it was until 1970s that the first non-rechargeable lithium batteries became commercially available. Attempts to develop rechargeable lithium batteries followed in the 1980s but due to instabilities of the anode material, metallic lithium, they failed.

Lithium is the lightest of all metals, has great electrochemical potential and provides the largest specific energy per weight. Rechargeable batteries with lithium metal as anode could provide very high energy densities, however, it was discovered in the 1980s that cycling produced dendrites on the anode which penetrated the separator and cause an electrical short. The cell temperature would rise quickly and approach the melting point of lithium causing thermal runaway. The inherent instability of lithium metal, shifted the research to a non-metallic solution using lithium ions. In 1991, Sony commercialized the first Li-ion and till these days this chemistry has become the most promising and fastest growing battery on the market. Even if it offers lower specific energy than lithium-metal, Li-ion is safe provided the voltage and current limits are being respected.

The key to superior specific energy is the high cell voltage of 3.6V which can directly power mobile phones, tablets offering simplifications and cost-reductions over multi-cell designs. Li-ion is a low-maintenance battery, which has no memory effect and does not need exercising (deliberate full discharge) to keep it in good shape. Furthermore, self-discharge is less than that of nickel-based batteries. The drawbacks are the high price and the need for protection circuits.

Lithium-ion uses a cathode (positive electrode), and anode (negative electrode) and electrolyte as conductor. (The anode of a discharging battery is negative and the cathode is positive). The cathode is metal oxide (Li metal oxide) and the anode consists of porous carbon. During discharge, the ions flow from the anode to the cathode through the electrolyte and separator; charge reverses the direction and the ions flow from the cathode to the anode.

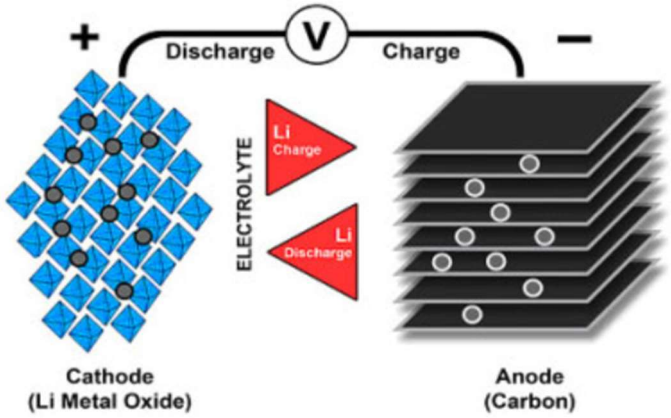

Figure 34: Ion flow in lithium-ion battery.

Original lithium-ion batteries consisted of coke as the anode however, in order to attain a flatter discharge curve, the material for the anode shifted to graphite. Graphite has the advantage of a flatter voltage discharge curve with respect to SoC%.

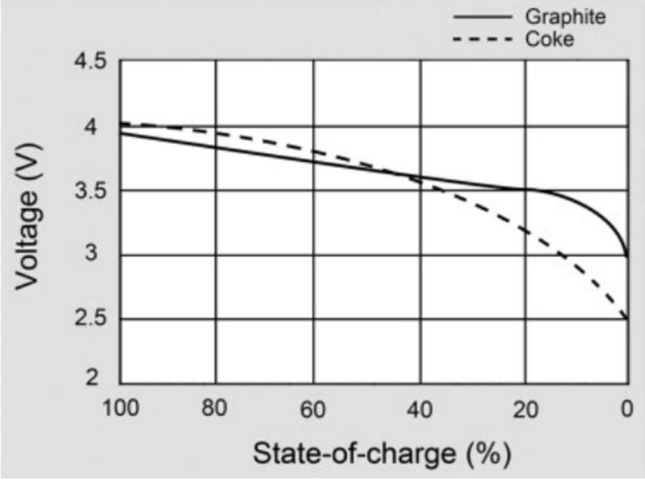

Figure 35: Voltage discharge curve of lithium-ion.

The 6 most common Li-ion-based systems will be discussed below. These consist of:

- Lithium Cobalt Oxide ($LiCoO_2$) – LCO
- Lithium Manganese Oxide ($LiMn_2O_4$) – LMO
- Lithium Nickel Manganese Cobalt Oxide ($LiNiMnCoO_2$) – NMC
- Lithium Iron Phosphate ($LiFePO_4$) – LFP

- Lithium Nickel Cobalt Aluminum Oxide ($LiNiCoAlO_2$) – NCA
- Lithium Titanate (Li_2TiO_3) -LTO

4.2.3.1 Lithium Cobalt Oxide ($LiCoO_2$) – LCO

The battery consists of a lithium cobalt oxide cathode and a graphite carbon anode. Its high specific energy makes it a popular choice for mobile phones, laptops and digital cameras. The main drawback is the limited load capabilities (low specific power). Also, LCO has a relatively short life span due to the graphite anode that limits the cycle life by a changing solid electrolyte interface (SEI), thickening on the anode and lithium plating while fast charging and charging at low temperature. Therefore, it is important to not charge and discharge at a rate higher than its C-rating. This means that for a cell with a capacity of 2400 mA·h the maximum charge and discharge current must not exceed 2400 mA. Manufacturers advice for a C-rate of 0.8 C or about 2000 mA.

A good graphical representation of the characteristics of Li-ion battery and all its types is the hexagonal spider graphic which summarizes the performance in terms of specific energy or capacity; specific power or the ability to deliver high current; safety; performance at hot and cold temperatures; life span reflecting cycle life and longevity and cost. From the figure below it is clear that LCO systems are superior concerning the capacity but fall short with respect to the cycle life and the discharge current.

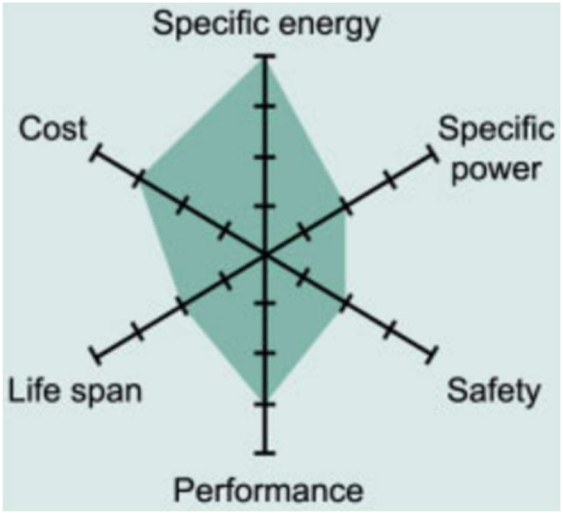

Figure 36: Li-cobalt battery performance.

4.2.3.2 Lithium Manganese Oxide ($LiMn_2O_4$) – LMO

LMO's three-dimensional spinel structure offers a significant improvement in ion flow on the electrode which results in lower internal resistance and improved current handling. A further advantage of spinel is the high thermal stability and enhanced safety, with the cost of decreased cycle and calendar life.

Low internal cell resistance enables fast charging and high-current discharging, for

instance an 18650 Li-manganese package can be discharged at currents of 20-30A with a moderate heat buildup. It is also possible to apply one-second load pulses of up to 50A but not continuous since it would heat the system; the cell temperature must not exceed 80° C.

Li-manganese has a capacity that is roughly one-third lower than Li-cobalt. Design flexibility allows manufacturers to maximize the battery for either longevity (cycle life), maximum load current (specific power) or high capacity (specific energy). The spider web of a typical Li-manganese system is presented below; the characteristics appear marginal but newer designs have improved in terms of specific power, safety and life span. Nowadays pure Li-manganese designs are no longer common, except for special applications.

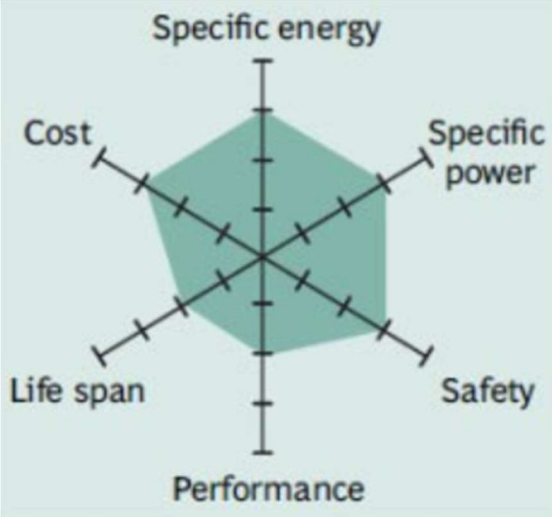

Figure 37: Li-manganese battery performance.

Blending LMO with lithium nickel manganese cobalt oxide (NMC) can improve the specific energy and prolong the cycle life; this combination brings out the best in each system and the LMO (NMC) system is used mainly for electric vehicles, since the LMO part, being 30 percent of the battery, offers high current boost for acceleration whereas the NMC part delivers the long driving range (capacity of specific energy). Some newer research attempts add a small amount of silicon to the anode which can increase the capacity of up to 25% however the intrinsic ability of silicon to grow and shrink with charge-discharge reduces the cycle life due to excessive mechanical stress. Thus, the main advantage of LMO battery is that it can flexibly attain very good performance with respect to either specific energy, specific power or longevity depending on the added active material.

4.2.3.3 Lithium Nickel Manganese Cobalt Oxide ($LiNiMnCoO_2$) – NMC

Combining nickel-manganese-cobalt (NMC) for cathode gave birth to one of the most successful Li-ion systems. Similar to the flexibility of Li-manganese these systems can either serve as energy cells (high capacity) or power cells (high current). For example, a NMC in an 18650 cell for moderate load condition has a capacity of about 2800 mA·h and can deliver 4A

to 5A whereas NMC in the same cell optimized for specific power has a capacity of only about 2000 mA·h but can deliver continuous discharge current around 20A. A silicon-based anode can go up to 4000 mA·h but with the drawback of reduced loading capacity and shorter cycle life due to the mechanical instability of silicon.

NMC advantages lie in combining nickel and manganese, nickel is known for its high specific energy but poor stability whereas manganese has the benefit of forming a spinel structure to achieve low internal resistance with the drawback of low specific energy. Combining these two enhances both specific energy and specific power (higher discharge current). NMC typically consists of one-third nickel, one-third manganese and one-third cobalt, also known as 1-1-1. Manufacturers tend to reduce cobalt content with some compromise in performance because cobalt stabilized nickel, a high energy active material. The flexibility of NMC-blended Li-ion system is based on the ability to modify the percentages of the three active materials of nickel, manganese and cobalt to suit a wide range of applications. The spider graphic of NMC below, shows that NMC excels in the specific energy while its performance on all the other characteristics is at least satisfactory.

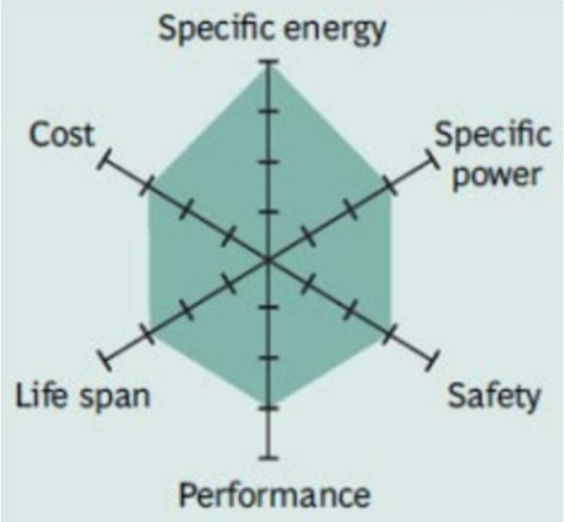

Figure 38: Nickel-manganese-cobalt battery performance.

4.2.3.4 Lithium Iron Phosphate ($LiFePO_4$) – LFP

In 1996, University of Texas discovered phosphate as cathode material for rechargeable lithium batteries. Li-phosphate offers good electrochemical performance along with low resistance. The key advantages are high current rating and long cycle life with good thermal stability, enhanced safety and tolerance if abused.

Li-phosphate has the ability to be more tolerant to full charge conditions and is less stressed than other lithium-ion systems if kept at high voltage for a prolonged time. As a trade-off its lower nominal voltage of 3.2V/cell reduces the specific energy below that of cobalt-blended lithium-ion. Furthermore, Li-phosphate battery suffers from higher self-discharge with

respect to other Li-ion batteries and has thermal issues since in low temperatures the performance is reduces and at elevated storage temperature its service life is shortened.

Li-phosphate is a good replacement to lead acid SLI battery since 4 cells in series can produce 12.8V, a similar voltage to six 2.0V lead acid batteries. Vehicles charge lead acid to 14.4V, (2.4V/cell) and maintain a topping charge in order to maintain full charge level and prevent sulfation on lead acid batteries. In the case of Li-phosphate batteries in series, each cell tops at 3.6V but contrary to the lead acid batteries the charge should be disconnected which does not happen while driving. Li-phosphate is tolerant to some over-charge however its durability is in question under the stress of constant over-charging. Therefore, the Li-phosphate alternative has the advantages of increased life span along with the high discharge current (specific power).

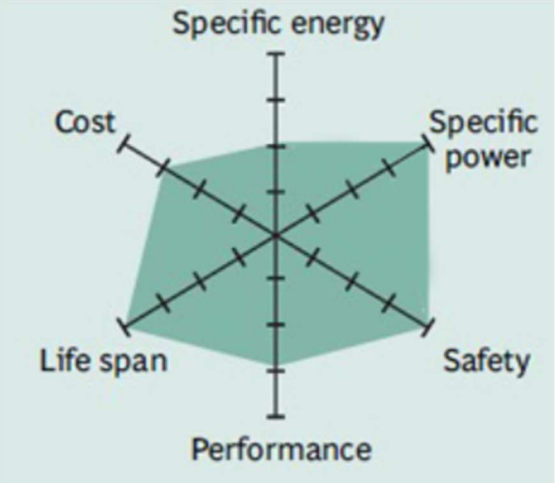

Figure 39: Lithium-Iron-Phosphate battery performance.

4.2.3.5 Lithium Nickel Cobalt Aluminum Oxide ($LiNiCoAlO_2$)

Lithium nickel cobalt aluminum oxide battery shares a lot of similarities with NMC, having high specific energy, reasonably good specific power along with a satisfactory life span. Its main drawbacks are safety and the higher cost. Its specific energy ranges from 200-260 W·h/kg with predictions to reach up to 300 W·h/kg in the imminent future. It can reach a life cycle of 500 cycles always with respect to the DoD along with the operating temperature. Its high specific energy along with the specific power makes this battery a good candidate for EVs since it can also offer a fast charge with certain cells modifications.

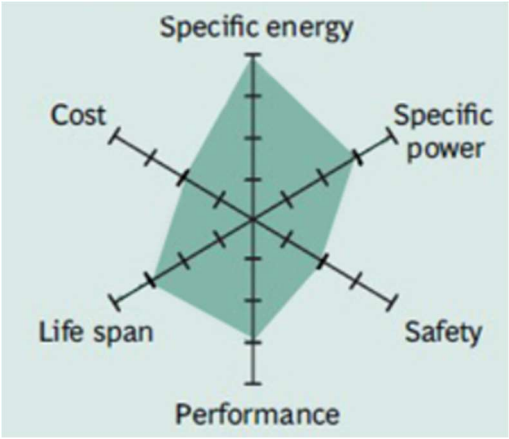

Figure 40: Lithium-Nickel-Cobalt-Aluminum-Oxide battery performance.

4.2.3.6 Lithium Titanate (Li_2TiO_3) – LTO

Li-titanate replaces the graphite in the anode of a typical lithium-ion battery and the material forms into a spinel structure offering good electrochemical performance with low resistance. Li-titanate has a nominal cell voltage of 2.4V which is lower with respect to the other lithium-based systems but can be extremely fast charged and can deliver a high discharge current of 10C, or 10 times the rated capacity. Li-titanate has very high safety standards, and a better cycle count than that of regular Li-ion. Also, it has excellent low-temperature discharge characteristics and can obtain a capacity of 80% at -30°C.

LTO has advantages over the conventional cobalt-blended Li-ion with graphite anode one of which is the no SEI film formation and no lithium plating when fast charging and charging at low temperature. Furthermore, thermal stability at high temperature is better than other Li-ion systems with the expense of the increased cost, at $1005 per kWh making it one of the most expensive Li-based batteries. The main drawback is the low specific energy at only 65 W·h/kg rivalling that of NiCd.

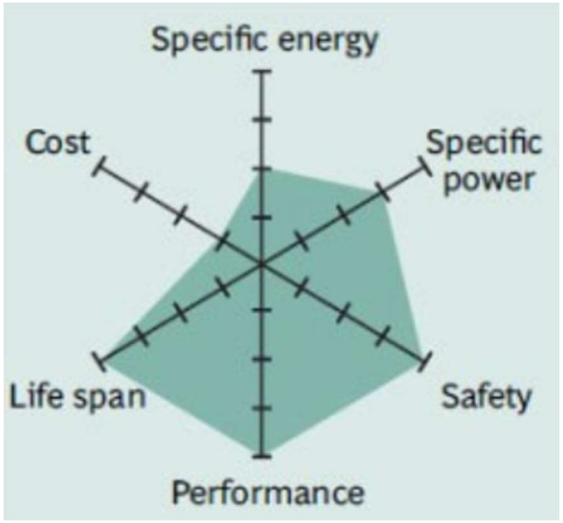

Figure 41: Li-titanate battery performance.

4.2.3.7 Lithium-polymer

Lithium-polymer is not a distinguished type of lithium-based batteries. It differs from other battery systems in terms of the type of electrolyte used. The original polymer design back in 1970s used a solid (dry) polymer electrolyte that resembled a plastic-like film. This insulator allows the exchange of ions (electrically positive charged atoms) and replaces the traditional porous separator that is soaked with electrolyte. Since the solid polymer has poor conductivity at room temperature it must be heated at least to 60ºC to enable current flow.

The modern Li-polymer systems in order to be operative at room temperature use also a gelled electrolyte and most Li-ion polymer batteries nowadays incorporate a micro porous separator with some moisture. Li-polymer can be built on many systems like Li-cobalt, NMC, Li-phosphate or Li-manganese and is not considered a unique battery system.

The main advantage of this technology is that Li-polymer cells come in a flexible foil-type case that resembles a food package while the standard Li-ion needs a rigid case to press the electrodes together. This thin film technology offers the possibility to create batteries of any shape, having extensive use in modern phones and tables. The light weight and consequently the high specific power make Li-polymer a very interesting alternative.

4.2.4 Comparison of different battery systems

Having analyzed the main lead-, nickel- and lithium-ion-based battery systems a brief comparison between their important characteristics is followed. First of all, an important characteristic mainly for nonstationary applications is the specific energy or capacity of the battery system. In the following figure the specific energy of lead-, nickel- and lithium-based batteries is being presented.

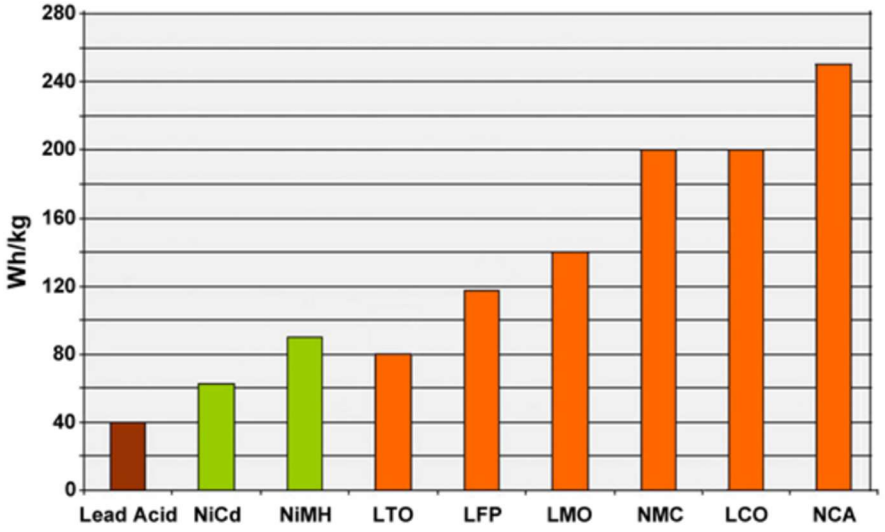

Figure 42: Typical specific energy of lead-, nickel- and lithium-based batteries.

It is clear that Lithium Nickel Cobalt Aluminum Oxide – NCA battery packs the most of energy among the other alternatives and that is the main reason that it has prevailed at the EVs market. On the other hand, in terms of specific power Li-manganese (LMO) and Li-phosphate (LFP) are superior.

A very important parameter when assessing battery performance is the cycle life. In the following figures the capacity (%), the internal resistance (mΩ) and the self-discharge (%) with respect to the number of cycles are being presented for the case of nickel-based batteries.

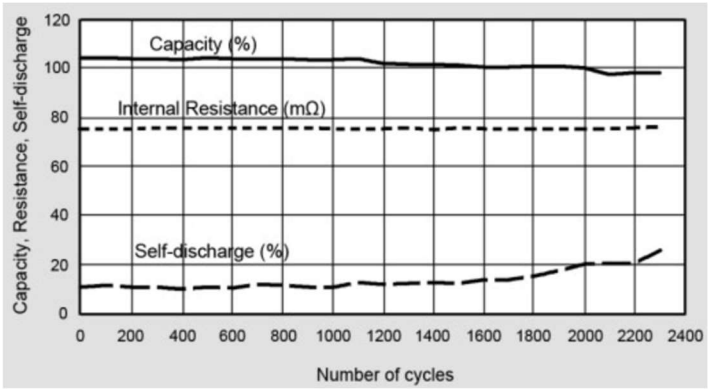

Figure 43: Performance of standard NiCd.

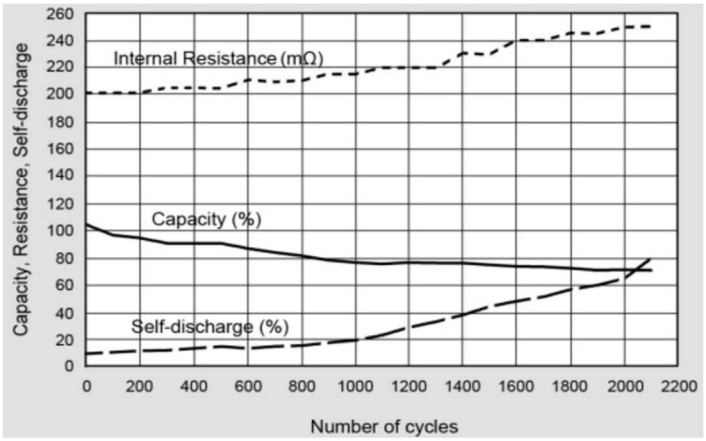

Figure 44: Performance of ultra-high-capacity NiCd.

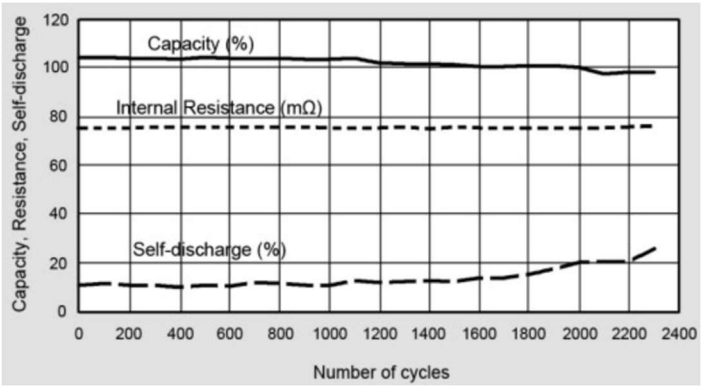

Figure 45: Performance of NiMH.

From the figures above, it is clear that the standard NiCd has a high durability after even 2000 cycles whereas the ultra-high capacity NiCd exhibits a significant capacity drop even after 200 cycles. Similar to the standard NiCd, NiMH also has a constant capacity till 1000 cycles and then diminishes a bit till 2000 cycles. However, NiCd does not operate well with partial charges-discharges since it suffers from memory effects so periodic full charge-discharge cycles must be given. Furthermore, its specific energy is low, at 45-80 W·h/kg compared to the 150-200 W·h/kg of a typical lithium-based battery. Therefore, nickel-based batteries are not suitable for mobile applications, like in case of marine propulsion, where the weight factor is important. Lithium-based batteries even if being in need of regular maintenance and proper care offer at least 3 times the specific energy compared to a typical nickel-based system therefore their selection is justified as a proper energy saving system.

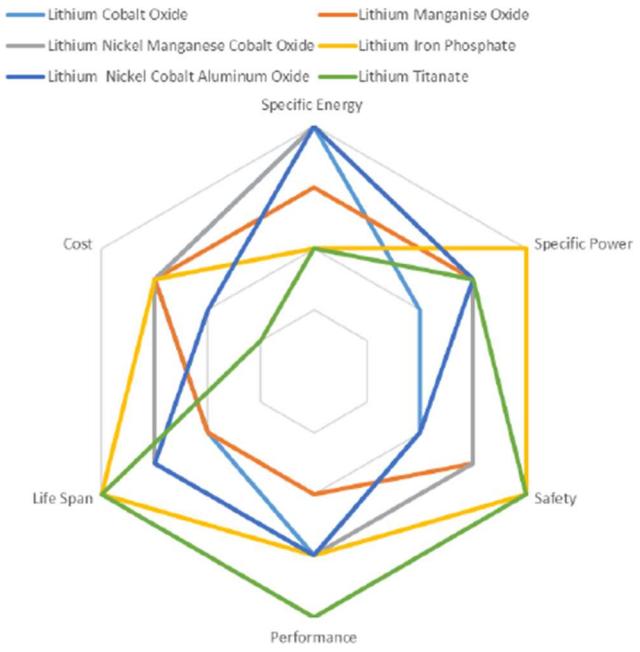

Figure 46: Lithium-based batteries characteristics.

Summarizing the main characteristics of lithium-based systems:

- Lithium Cobalt Oxide has a relatively high specific energy of 150-200 W·h/kg, a high 3.6V/cell and a satisfactory life cycle of 500-1000 cycles. As a main disadvantage it has low charging and discharging rate at 1C.
- Lithium Manganese Oxide has a moderate specific power, moderate specific energy and a moderate level of safety when compared to other types of lithium-ion batteries. The pros are the low cost and the high discharge current of 20-30A and the cons its low lifespan of 300-700 cycles.

- Lithium Nickel Manganese Cobalt Oxide has the advantage over the other lithium-based batteries of higher specific energy from 150-220 W·h/kg, a good life cycle of 1000-2000 cycles and the increased safety making it a good candidate for powering EVs. Also, it can be optimized either for high specific energy or high specific power.
- Lithium Iron Phosphate has the advantage of high life due to the increased life cycles of 1000-2000 compared to other lithium-based systems but suffers from lower voltage/cell at 3.2V/cell and considerably lower specific energy of 90-120 W·h/kg. However, it is one of the safest lithium-based batteries with high durability.
- Lithium Nickel Cobalt Aluminum Oxide can boast about the best specific energy performance among lithium-based systems at 200-260 W·h/kg, while having a reasonably good specific power and a moderate life span of 500 cycles. However, it is one of the lowest safe lithium-based system without fast charging or discharging capabilities (cannot exceed 1C).
- Lithium Titanate one of the most durable batteries in time, can reach up to 2000 life cycles, with fast charging abilities and wide operational temperature range. One of the safest Li-ion batteries but suffers from low capacity of 70-80 W·h/kg.

It is clear that the selection of the battery type is not an easy task since there are many parameters that must be taken into consideration. Concerning marine applications there are certain important parameters that can help with the battery selection. Weight is not a big issue, concerning it for instance with EVs where manufacturers try for light builds, specific power is also not so important since a vessel is not subjected to many accelerations therefore there is no need for high discharge currents. On the other hand, the energy demands of a vessel with electrical propulsion cannot be compared to that of an EV therefore it is important to select a battery system with high specific energy. Lithium Nickel Manganese Oxide system selection seems an optimal choice since it can pack a high capacity of 150-220 W·h/kg, with a high 3.6V/cell and a high life cycle of at least 1000 cycles. Also, its cost is moderate at $420 per kW·h and its market share is more and more increasing.

4.3 Types of battery cells

There are three main types of battery cells that have prevailed the market:

- The cylindrical cell,
- The prismatic cell and
- The pouch.

4.3.1 The cylindrical cell

One of the most widely used packaging styles for primary and secondary batteries, was developed in 1900 where the popular AA type was introduced in 1907. Its advantages are the easy of manufacture and the good mechanical stability. The tubular cylinder is able to withstand high internal pressures without deforming.

Many lithium- and nickel-based cylindrical cells include a positive thermal coefficient (PTC) switch which when exposed to excessive current, heats up and become resistive, stopping current flow and acting as a short circuit protection. Once the short is removed, the PTC cools down and returns to its conductive state. Furthermore, most cylindrical cells also feature a pressure relief mechanism, a membrane seal that ruptures under high pressure, which can come from the gases that lithium might emit, mainly CO_2 and CO, after a certain number of cycles. Below, a cross section of a lithium-ion cylindrical cell is being shown. The cylindrical cell has good cycling ability, offers a long calendar life and is economical however its higher weight along with the low packaging density due to space cavities make it unviable for compact applications.

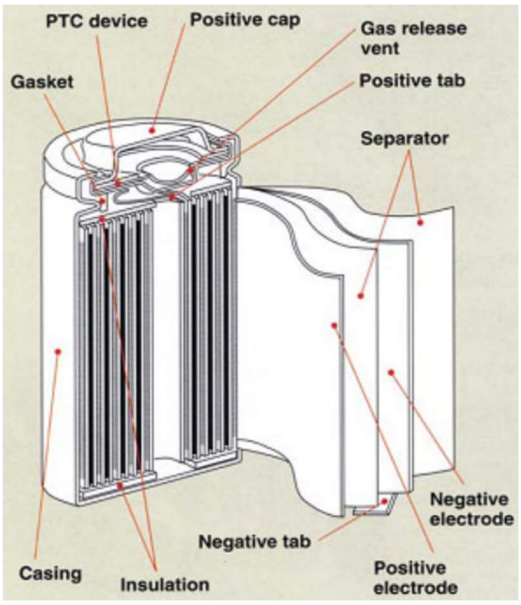

Figure 47: Cross section of a lithium-ion cylindrical cell.

The 18650 design remains one of the most popular cell packages nowadays since it can be formed in partial lengths, such as half and three-quarter formats. It offers one of the lowest costs per W·h and has good reliability records but over the last years consumers move to the flat designs for compact electronics applications and the demand would have fallen if not for Tesla electric vehicles that also use this cell format for the time being.

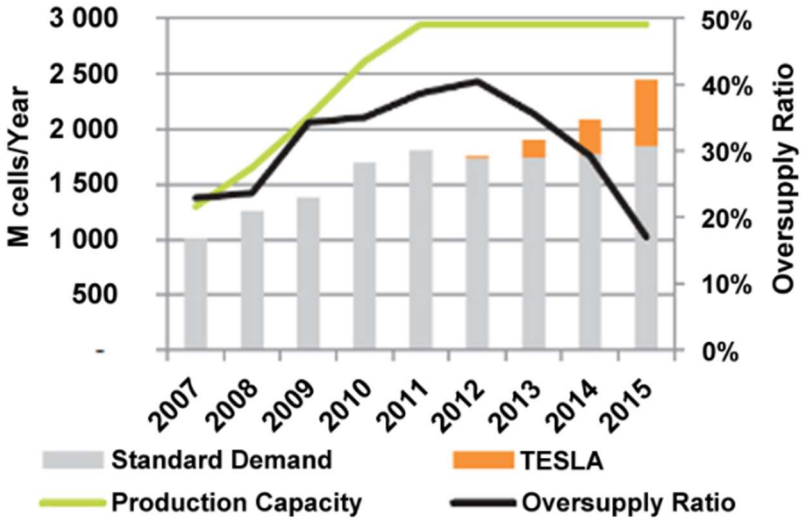

Figure 48: Demand and supply of 18650.

Even though the cylindrical cell does not fully utilize the space by creating air cavities its energy density is higher than that of a prismatic/pouch Li-ion cell, for instance the 3A·h 18650 delivers 248A·h/kg whereas the modern pouch cell has about 140 A·h/kg. The higher energy density of the cylindrical cell compensates for its less ideal stacking abilities and the empty space can always be utilized for cooling to improve the thermal management.
However, along with the rapid surge of consumer electronics production that utilize the pouch design the 18650 is expected to see a decline in the imminent future.

4.3.2 Prismatic cell

Introduced in 1900s, the modern prismatic cell satisfies the demand for thinner sizes for mobile phones, tablets and low-profile laptops ranging from 800mA·h to 4000mA·h. There is no a universal standard and each manufacturer design its own form. Prismatic cells can also be found in large formats, packaged in welded aluminum housings, the cell can deliver capacities of 20-50A·h and are primarily used for electric powertrains in electric vehicles.

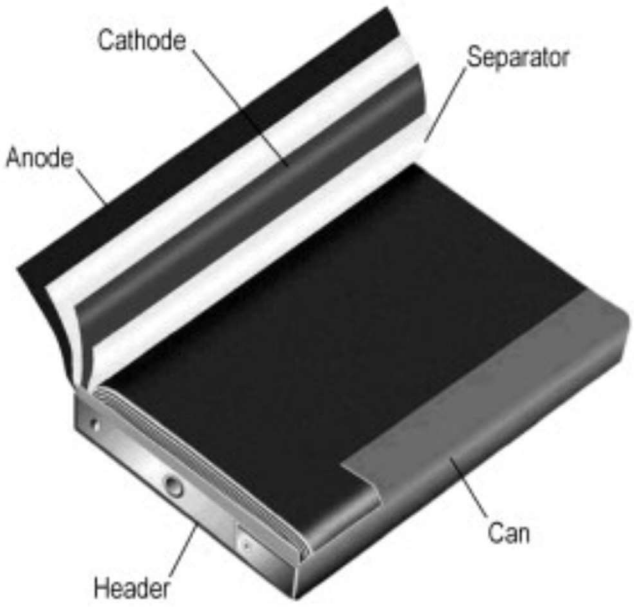

Figure 49: Prismatic cell cross section.

The pros of the prismatic cell are the improved space utilization along with its flexible design and the cons are its higher manufacture cost along with its inefficient thermal management which is the reason for its shorter life cycle. It is important to allow room for some growth due to swelling cause of gas buildup, for instance a 5mm cell can grow to 8 mm after 500 cycles, otherwise the swelling can damage electronics equipment.

4.3.3 Pouch cell

Pouch cell offers a simple flexible and lightweight solution to battery design based on the Li-polymer design. It makes the most efficient use of space and can achieve 90-95% packaging efficiency, the highest among battery packs. The elimination of the metal enclosure reduces weight, but cell support measures must be taken into consideration. Again, in this case there is not a standard and each manufacturer designs its own format.

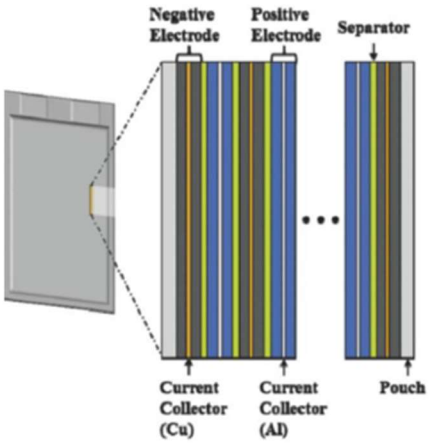

Figure 50: Pouch cell cross section.

Although easily stackable, measures must be taken for swelling. Smaller pouch packs can grow 8-10% over 500 cycles, large cells might expand to that size in 5000 cycles. Extreme swelling is a concern and users of pouch packs have reported up to 3% swelling on a poor batch run. The pressure can crack the battery open and destroy the display along with the electronic circuit boards.

A good method is to add a temporary "gasbag" during manufacturing on the side. During the first charge gases escape into the gasbag while forming the solid electrolyte interface (SEI), then that gasbag is cut off and the pack is resealed as part of the finishing process. The technology has matured and pouch cells have the potential for greater specific energy than the cylindrical format. Large flat packs serve electric powertrains with satisfactory results. The cost per kW·h in the pouch cell is still higher than that of 18650 cell, however there is a constant downward trend and flat-cell designs are becoming more and more cost competitive due to the increased market share and market demand.

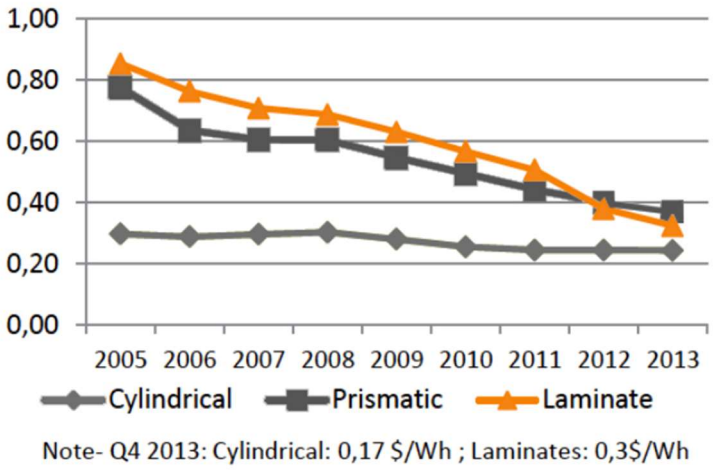

Figure 51: Price of Li-ion ($US/W·h).

4.3.4 Summary

Summarizing the pros and cons for each one of the three designs are:

- **Cylindrical cell,** has the highest of specific energy along the other 2 designs, high mechanical stability, high cycle life and the lowest cost but does not utilize the space well, having not ideal packaging density.
- **Prismatic cell,** is encased in aluminum or steel for stability, increasing its weight. It utilizes the space in a much more efficient way than the 18650 cell but can be costlier to manufacture and have less safety compared to the cylindrical cell.
- **Pouch cell,** uses the laminated architecture. The absence of casing makes it lighter, increasing its specific energy but its loss of mechanical stability must be taken into consideration. Requires a very careful manufacturing procedure and a swelling of 8-

10% must be expected after 500 cycles. Requires a careful management to not be stressed since due to the bad thermal management it can be highly stressed. Extensive research makes it one of the most promising battery types for the future and its specific energy is expected to increase.

4.4 Future batteries

In the modern era of EVs there is a constant need of batteries with higher qualities. These qualities can be analyzed in 8 main categories:

1. High specific energy offering a lot of ampere-hours (A·h),
2. High specific power providing high load capabilities usually with the cost of decreased specific energy,
3. Affordable price, since the materials, the refining processes and the manufacturing costs are still high,
4. Long life, meaning a high number of life cycles even for more than 80% DoD,
5. Safety, the main concern of lithium-based batteries which can be reactive and unstable,
6. Wide temperature operating range, high temperatures stress the battery and low temperatures slow the electrochemical reactions,
7. Toxicity, cadmium- and mercury-based batteries does not satisfy the sustainability criteria of the modern era,
8. Fast charging, where Lithium- and nickel-based batteries should be charged at 1C or slower, only NiCd accepts ultra-fast charge with minimal stress.

The above 8 basic requirements cover the main characteristics a battery must have. As already mentioned, these traits are self-conflicting meaning that in order to excel in one characteristic, for instance having high specific energy, there is always a cost on another one, in this case usually specific power. The so-called transition from internal combustion engines to electric motors stumbles upon the difficult to solve problem of energy storage. Batteries nowadays do not offer either the specific energy of gasoline at 13 kW·h/kg or the low refill time of gasoline powered cars. There is the necessity for a modern battery revolution and there are certain promising technologies that can be commercialized in the near future, which will be briefly analyzed below:

- The Lithium-air (Li-air),
- the Lithium-metal (Li-metal),
- the Solid-state Lithium,
- and the Lithium-sulfur (Li-S).

4.4.1 Lithium-air (Li-air)

Lithium-air is a very promising technology promising to store far more energy than what is possible with current Li-ion technologies. The battery uses a catalytic air cathode that supplies oxygen, an electrolyte and a lithium anode.

The theoretical specific energy of lithium-air is 13kW·h/kg and if this specific energy could indeed be delivered would be on par with gasoline's one. But even if the commercialized Li-air could offer the one-quarter of this energy, the electric's motor efficiency of 90% compared to the 25-30% of ICE's would make up for this lower capacity.

Li-air has a nominal cell voltage of 1.7-3.2V/cell but suffers from low specific power especially at cold temperatures. Furthermore, high air purity is required and there might be need of compressors, pumps and filters consuming around 30% of its produced energy for auxiliary support. Another problem is the sudden death syndrome, because of the lithium peroxide films that produce a barrier which prevents electron movement and limits the cycle life to around 50 cycles.

4.4.2 Lithium-metal (Li-metal)

Lithium-metal has long been seen as the future rechargeable battery because of its high specific energy and good loading capability. However, its main problem is the dendrite growth due to the uncontrolled lithium deposition that induces safety hazards by penetrating the separator and producing an electrical short.

After several failed attempts to commercialize rechargeable lithium-based batteries DBM Energy in 2010, claimed the installation of a 300W·h/kg battery in an experimental vehicle with a life cycle of 2500 cycles, short charging time and competitive pricing. Also, Audi experimented on this technology by implementing it in an Audi A2, claiming a mile range of 284 miles. Even if lithium-metal battery passed the stringent approval test, there were rumors for a laboratory fire cause of the battery. Nowadays, there are solid hopes for a solution to the instability of Li-metal batteries by adding nanodiamonds as an electrolyte additive. Tests have shown a stable cycling for 200 hours; not enough for consumer applications.

4.4.3 Solid-state lithium

Graphite anode being used in the current Li-ion reduces the specific energy. An alternative is to use pure lithium and substitute the liquid electrolyte soaked in a porous separator with a solid polymer or a ceramic separator. This technology shares similarities with lithium-metal and specially the dendrite formation even with dry polymer and ceramic separators. Furthermore, at low temperatures the polymer exhibits low conductivity and the cycle life of solid-state prototypes are said to only reach 100 cycles.

Solid-state batteries promise to deliver twice the energy compare to regular Li-ion however with the expense of low loading capabilities thus making them not suitable for

applications that require high currents. On the other side, they can offer fast charge times making them a suitable candidate for EVs. Research laboratories, including Bosch, claim that the solid-state battery might be implemented in cars by 2025. Labs also report high specific energy and superior safety compared to regular Li-ion but yet its viability to replace Li-ion is in question.

4.4.4 Lithium-Sulfur (Li-S)

Low atomic weight of lithium along with the moderate atomic weight of sulfur, lithium-sulfur batteries offer a very high specific energy of 550W·h/kg along with a respectable specific power of 2500W/kg. Li-S has a cell voltage of 2.10V, less than the regular Li-ion systems, but offers good cold temperature discharge characteristics and can be recharged at -60°C. Furthermore, it is a very sustainable alternative since sulfur is abundantly available.

A challenge of Li-S battery is the limited cycle life of only 40-50 cycles as sulfur is lost during cycling by shuttling away from the cathode and reacting with the lithium anode. Test labs report that with improvements they can reach 200 cycles. Other issues are the poor conductivity, the degradation of the sulfur cathode with time and the poor stability at higher temperatures.

4.4.5 Summary

In order to have a clear understanding of the pros and cons of each alternative lithium-based future battery technology, the main characteristics of the 4 prementioned systems are being presented below.

Table 10: Summary table of the Li-air, Li-metal, Solid-state-Li and Li-S batteries.

Chemistry	Lithium-air	Lithium-metal	Solid-state Lithium	Lithium-sulfur
Type	Air cathode with lithium anode	Lithium anode; graphite cathode	Lithium anode; polymer separator	Lithium anode; sulfur cathode
Voltage/cell	1.7-3.2V	3.6V	3.6V	2.1V
Specific energy	13kW·h/kg (theoretical)	300W·h/kg	300W·h/kg	500W·h/kg
Charging	Unknown	Rapid charge	Rapid charge	0.2C (5h)

Discharging (specific power)	Low power	High power	Poor conductivity when cold	High power (2500W/kg)
Cycle life	50 cycles	2500 cycles	100 cycles	50 cycles but questionable
Safety	Unknown	Needs improvement	Needs improvement	Protection circuit required

From the four prementioned alternatives Li-air is the most promising technology but stills requires a lot of research to be commercialized. Li-metal while packing a lot of specific energy still requires a lot of research in order to ensure high level of safety for commercial use. Solid-state-lithium suffers from the typical dendrite formation thus alike lithium-metal it also needs a lot of research to meets the required safety standards. Finally, Li-S battery seems a very interesting lithium-based alternative which not only packs a lot of energy, at 500W·h/kg but does not exhibits safety concerns. The main problem is the low cycle life of only 50 cycles which requires further investigation.

5.0 Tugboats

Tugboats are an integral part of the marine industry not only due to the problem of the restricted maneuverability of ships in harbors, rivers and canals but also due to numerous important tasks that they can take care of. Apart from the towing capabilities that they are designed to have, tugs can also have fire-fighting and anchor-handling capabilities but can also be designed for survey and research purposes. Tugs can be characterized as vessels with disproportional power compared to their size. This large power is used mainly for towing reasons and it is utilized for a short time of its operation. Tugboats do not follow certain design standards but they are based on owner's requirements without taking into account the hydrodynamics and the energy efficiency or environmental impacts. Tugs can be categorized into two main categories according to their propulsive arrangement or their function.

5.1 Propulsion Arrangement

Tugboats can be categorized into four main types concerning their propulsion configurations. These are the Conventional tugs, the Azimuth stern drive tugs (ASD), the Tractor tugs and the Voith tugs.

5.1.1 Conventional Tugs

Tugs of this type are used worldwide and can have various characteristics. They can be equipped with fixed single or twin-screw propellers and single rudders with fixed nozzles. Rudder nozzles are very efficient for speeds less than 10 knots, where tugs operate most of the time. New building can have steering or nozzles, controllable pitch propellers (CPP) and nose rudders. The main characteristics are:

- Manoeuvrable and effective for most work, but less manoeuvrable than Azimuth stern drive tugs (ASD) or tractor tugs.
- Good steering ability, especially as a forward pulling tug.
- Good sea-keeping ability.
- Good bollard-pull to power output.
- Towing point is usually situated just aft of amidships.
- Astern bollard-pull reduced by up to 50% of forward bollard pull.
- Increased risk of girting/girding when towing.

These tugs deliver the highest bollard pull in the forward direction. Being connected at the stern of the vessel being towed, they will be working in conventional mode, also refereed as "stern to stern".

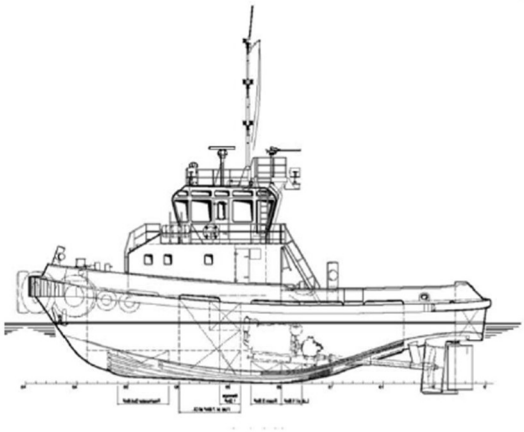

Figure 52: Conventional tugboat sketch.

5.1.2 Azimuth stern drive tugs (ASD)

This type is fitted with two azimuth thrusters in nozzles at the stern and with bow tunnel thrusters. Some are fitted with controllable pitch propellers (CPP). General characteristics are:

- Low relative draught.
- Good steering characteristics, except when going astern at higher speeds.
- Towing point is just forward or just aft of amidships.
- Underwater hull form improves the dynamic stability of the tug.
- Bollard pull going astern is reduced only by approximately 10%.
- Manoeuvrable and able to pull effectively over the stern or bow. Towing winches often fitted both fore and aft.
- Risk of girting/girding wen towing over the stern.
- Enhanced training of tug masters required when operating the forward winch.

This type of propulsion system offers high manoeuvrability mainly during transit sailing, with some limitations during the combination of thrust and direction resulting in a lower bollard pull.

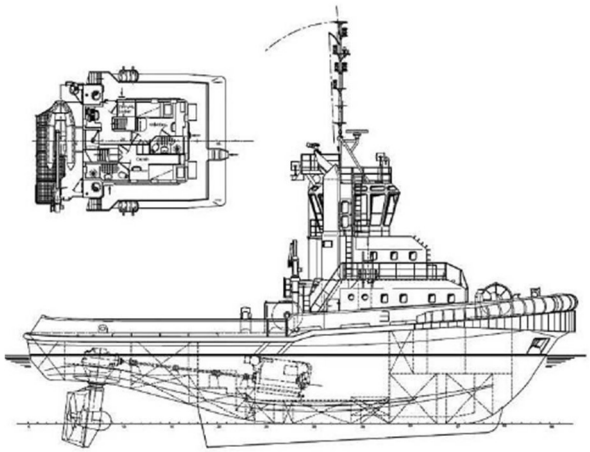

Figure 53: ASD tugboat sketch.

5.1.3 Tractor tugs

Tractor tugs are not similar to conventional tugs. The propulsion units are fully turning controllable pitch propellers (CPP), able to give thrust in any direction and act as steering units or azimuthing fixed or controllable pitched propellers. The propulsion units are placed far ahead of the towing point, close to the pivot thereby producing a large turning momentum. This potentially gives a poor steering performance, which is overcome by fitting a large centerline skeg. General characteristics are:

- Full power available in all directions.
- Quick response to engine movements.
- Very manoeuvrable, especially in tight sea space.
- Reduced risk of girting/girding.
- Reduced manoeuvrability if towing from forward at higher speeds.
- Reduced directional stability, particularly in open waters.
- Reduced bollard pull for kilowatt output.
- Relatively deeper in draught therefore increased risk of bottom damage from grounding.
- Increased training required for tug masters.

A further advancement of tractor tug is the rotor one. It uses a propulsion configuration consisting of three azimuth thrusters placed in a triangular configuration, called also as a triple Z drive. Two units are placed forward and one astern on the centerline of the tug. This arrangement enhances manoeuvrability and transverse bollard pull.

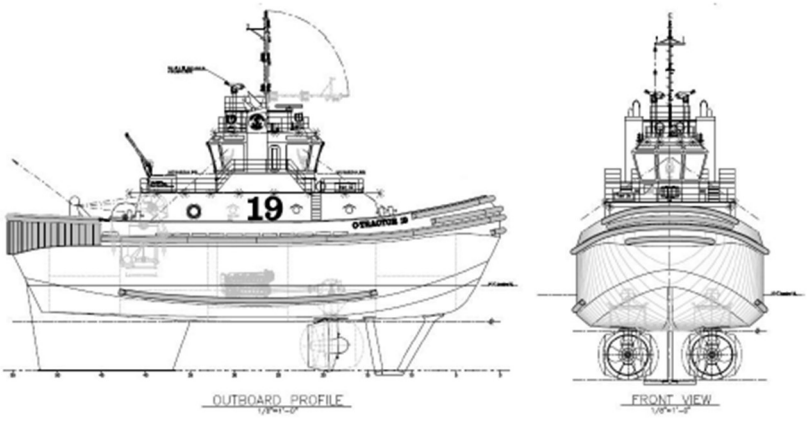

Figure 54: Tractor tugboat sketch.

5.1.4 Voith Tugs

These tugs are fitted with two cycloid propellers located at the bow (forward or midship). The Voith Schneider propeller consists of a circular plate, rotating around a vertical axis and a circular array of vertical blades (normally 5 of a hydrofoil cross section) protruding out of the bottom of the tug. Each blade can rotate itself around a vertical axis due to the internal gear that can change the angle of attack of each blade, synchronized with the rotation of the plate in order for each blade to provide thrust in any direction. Along with its high efficiency another advantage of the VSP system is that the rudder is no more necessary. Furthermore, they are characterized by the possibility to offer an almost instantaneous change of direction. Instead of a nozzle, VSPs are often fitted with a "thrust plate" or "propeller guard" which acts as a nozzle at low speeds, protecting the VSP from grounding.

Figure 55: Voith tugboat sketch.

5.2 Tugboat functions

Tugs are designed to perform one or more very specific functions which can be guidance in mooring operations, fire-fighting, oil spill response, icebreaking and pushing, pulling and directing large ships in docking and undocking. Most of the times tugs also tend to get used to perform more than one of these duties, becoming multi-purpose tugs. It is understandable that the more diverse the duties are the most compromised the design will be with respect to its ability to do a certain function very well. The main functions of tugboats will be analyzed below:

- Harbor tugs: One of the most conventional function, to assist the ships while entering or leaving a port and during berthing and unberthing operations. Large ships do not have control over the steering when operating at very low speeds thus, they are susceptible to the forces of the currents and the wind. The risk of a large ship self-

navigating in confined waters include the risk of collision or grounding with severe local mainly environmental consequences. Modern ship-assisted tugs are fitted with Z-drive or VSP propulsion where its length range from 20 to 32 m and their power from 2000 to 4000 kW.

- Escort tugs: One of the newest and most challenging tug designs. These tugs have the ability to provide emergency steering and braking functions mainly to tankers in sensitive or coastal areas. The Exxon Valdez incident in 1989, lead to the regulation that tankers withing specific waters must be “escorted” by tugboats. Escort tugs are different with respect to harbor tugs because the escorting takes place at higher speeds than harbor-assisting, generally from 7 to 10 knots. Escort tugs can generate forces for steering and braking a disabled tanker which are greater than the bollard pull of the propulsion system.
- Salvage/rescue tugs: A class of tugs that becomes more and more obsolete because hopefully there are fewer sinking incidents these days. They were typically large tugs with specialized winches and pumps which could be used to pull ships off a beach or prevent them from sinking.
- Coastal tugs: These tugs must be able to handle more weather than a harbor tug and also do not need the same degree of fendering. They have larger crews and hence more crew facilities. In general, these tugs have conventional propulsion with single or twin screws and a towing winch aft.
- Terminal tugs: A relatively new category of tugs used to provide ship-handling and other services at either offshore oil terminals or at LNG terminals situated in more exposed locales. Because they work in typically rougher waters, they tend to be larger and more powerful than normal ship-handling tugs and will frequently also have fire-fighting and anchor-handling capabilities. Some may also have some deck or bulk fuel or water cargo capacity.
- Anchor handling tugs: Tugs of this category are designed to deploy, relocate or retrieve the large anchors used in offshore drilling applications. Although typically this operation is done by larger AHTS (Anchor-Handling Tug/Supply vessels), tugs are very useful for working with smaller anchors. This operation requires a large roller at deck level aft, an open stern and a powerful winch, as well as typically wooden sheathing to protect the steel deck from the impact of anchors coming aboard.
- Fire-fighting tugs: In most ports in the world, the tug fleets are equipped with fire-fighting capabilities to provide a “first response” service as tugs are nearly always in the vicinity. The fire-fighting required mechanical power can be provided from the axis of one of the propeller’s after disengaging it.

5.3 Power systems for tugboats

The primary source of propeller power nowadays for tugboats is the conventional well-tested diesel engine. Tugboats engines produce power ranging from 500 – 2500 kW (680 – 3400 HP). The main issue with this set-up is that the selection of the Max Continuous Rating (MCR) and thus the sizing of the diesel engine is based on the full bollard pull operation. However, tugs only operate at this condition for 7-15% of the total time thus, leading to pool specific fuel consumption and increased emissions as well as engine wear. The flexibility that the electric propulsion offers, the ability to be operated efficiently at a high range of loads offers a very promising alternative to the conventional diesel propulsion. However, compared to the conventional diesel propulsion electrical one introduces additional conversion losses of 5-15% of the propulsive power in electrical components, such as generators, power converters, transformers and electric motors.

This trade-off between efficiency and the operational ability to a wide range of loads have led to several power architectures which can be categorized as:

- Mechanical propulsion
- Diesel-Electric propulsion
- Hybrid propulsion
- Electric propulsion with hybrid power supply
- Hybrid propulsion with hybrid power supply
- All electric propulsion

5.3.1 Mechanical propulsion

A typical mechanical propulsion architecture consists of the prime mover (diesel engine) with a reduction gear attached and the shaft transmitting the mechanical power to the propeller. Each one of the propellers of the tugboat either with fixed or controllable pitch are connected to each one of the diesel engines.

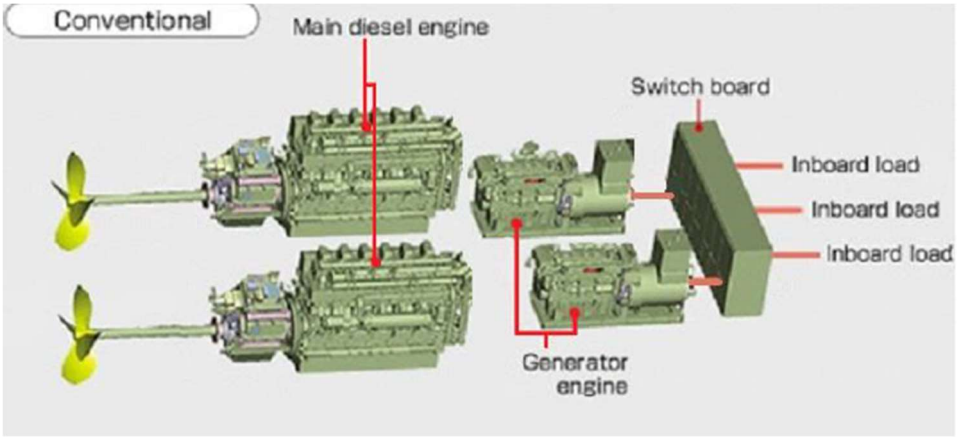

Figure 56: Conventional mechanical system.

The electric power required for auxiliary loads such as VSDs (variable speed drives), heating and ventilation along with air-conditioning (HVAC) and other systems is provided from diesel generators most of the time. A typical example of the engine room arrangement is provided in the next figure. Most of the times the generators are one deck above that of the main engine in order to have a certain degree of safety and operability even if the engine room gets flooded in case of a breach.

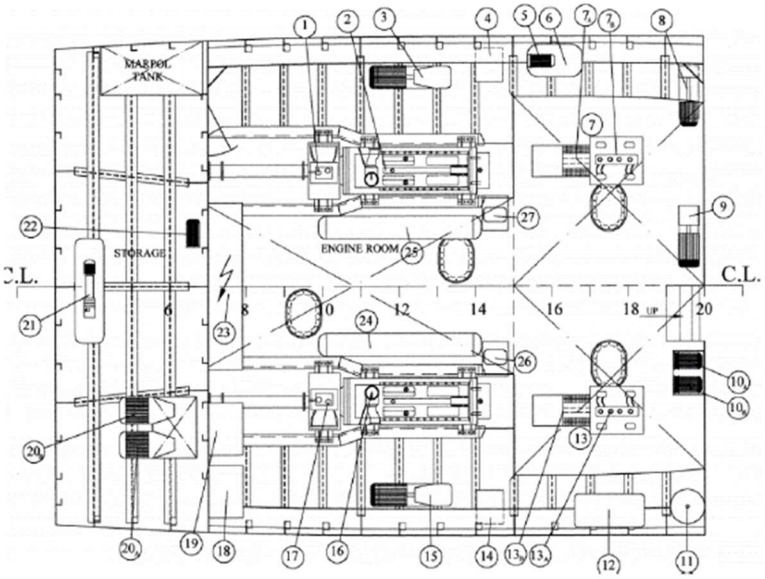

Figure 57: Typical engine room of conventional tugboat.

More than 50% tugs operating today consist of mechanical propulsion. It is well controllable, well understood and relatively efficient when operating at 80-100% of the maximum load. The low efficiency of internal combustion engines (below 40%) can be compensated with the low transmission losses due to the simplicity of the architecture. However, tugboats operate from 7-15% of their total time close to their design point therefore this architecture has poor specific fuel oil consumption (SFOC) and high emissions. Even so, this architecture has prevailed on the tugboat designs and even if it can be characterized as not an efficient one, the high SFOC and emissions are not that significant because tugboats engines are minor compared to a tanker or bulker's where their efficient operation is a prerequisite.

5.3.2 Diesel-Electric propulsion

Compared to mechanical propulsion the diesel-electric one is far more superior both in terms of technology and operation. For this reason, there is a growing transition to this architecture. Multiple diesel generators feed a fixed frequency high voltage electric bus, which in turn feeds the electrical propulsion motor drive along with the hotel loads via a transformer. The electric propulsion motor is being controlled with a power electronic converter which regulates the frequency and thus the rotational mechanical speed.

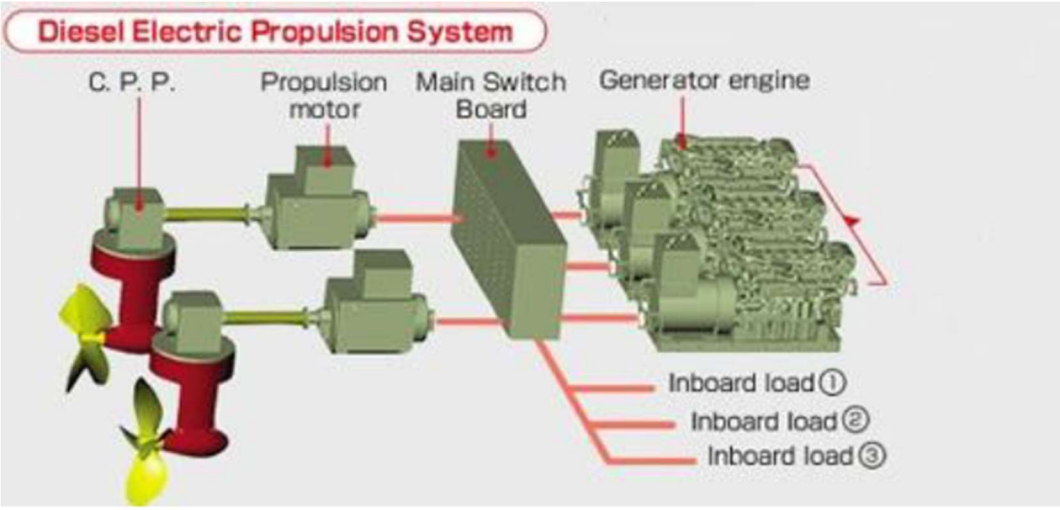

Figure 58: Diesel-Electric propulsion system.

Electrical propulsion architecture can be characterized as economical, environmentally friendly and reliable while offering considerable comfort in terms of operation and control, due to high manoeuvering and positioning capabilities, the low vibration and noise levels and importantly the best possible utilization of space, since there is no need for a length shaft line. The most frequent designs are the frequency-controlled AC motors and SCR controlled DC motors. Their application is limited to special purpose vessels that require a degree of low speed manoeuvering. These are harbor tugs and ferries and various other applications where the mechanical systems could not provide the required speed control and manoeuvrability.

Diesel-electrical propulsion is an efficient alternative when the required propulsion power is similar in magnitude with the required electrical power for other loads. Vessels of that category are cruise ships, icebreakers, ferries, shuttle tankers, chemical carriers and research vessels. Also, it is useful for vessels like drills ships where the main propulsion system is used in transit, otherwise the power is split between dynamic positioning (DP) and deck power consumption for equipment. The high efficiency at a wide range of propulsion loads can be justified by the fact that the generators are constantly operated close to their efficient range and the required propulsion power is controlled by the inverter. However, this comes along with the increased power losses mainly in the electronics.

5.3.3 Hybrid Propulsion

In hybrid propulsion, both a mechanical drive and an electrical motor are coupled on the same propeller's shaft trough a gearbox. During the high loads the mechanical engine provides the propulsion with high efficiency whereas, during the low loads the required propulsion power is provided from the electric motor. This is justified by the issue of the low efficiency of the mechanical engine at low speeds. Furthermore, this motor can also serve as a

generator where the mechanical power from the diesel engine provides both the propulsion power and the mechanical one to the motor/generator.

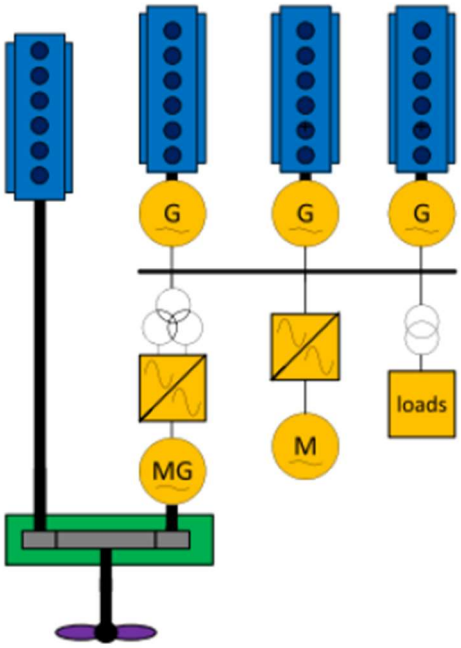

Figure 59: Hybrid propulsion system.

This architecture finds application mainly to towing vessels because it can be very efficient when the vessel's required propulsion power is at 20% of the maximum one for more than 90% of the operational time, a typical operational profile of that ship type. This is an economical alternative to the mechanical engine architecture but nowadays there are other more efficient and greener solutions.

5.3.4 Electrical propulsion with hybrid power supply

In the hybrid power supply electrical propulsion, the required power source can be derived from the following options:

- Generators which are supplied from the mechanical power of a combustion engine,
- Electrochemical power from fuel cells and
- Stored power supply from energy storage systems (ESS) such as batteries, flywheels or supercapacitors.

Fuel cells are mainly present in submarine applications whereas more sophisticated storage systems such as flywheels or supercapacitors are rarely used due to their disadvantages which are the low efficiency for the case of supercapacitors and the lower power density for the flywheels. The preferred energy storage system nowadays are batteries and especially Li-ion systems. The idea of the hybrid power supply was taken from the automotive industry which

used batteries in order to capture the braking energy instead of dissipating it as heat. Furthermore, the ability to switch off the main engine and use the batteries as primary energy source in low speeds is also applicable in the case of the vessel's propulsion.

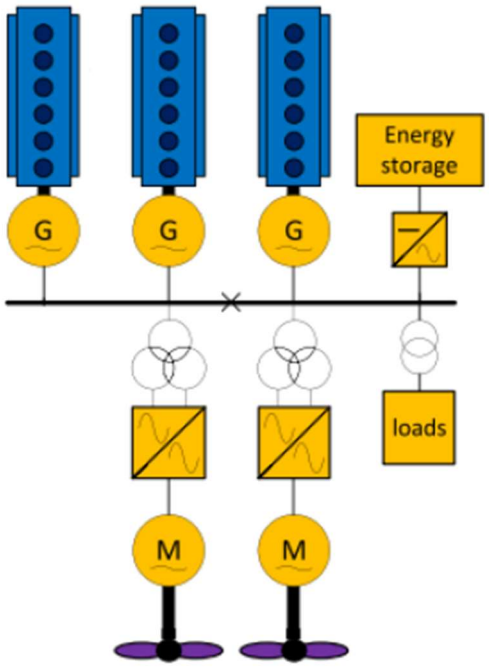

Figure 60: Electrical propulsion with hybrid supply system.

There is an increased tendency to utilize the hybrid supply system in maritime applications, but the real benefits are in doubt because the calculated fuel saving when the batteries are not recharged from the grid is marginal. However, there is need for further investigation to find whether or not this architecture is beneficial in terms of both fuel savings and economically.

5.3.5 Hybrid propulsion with hybrid power supply

This architecture provides the maximum efficiency of direct mechanical drive along with the flexibility of a combination of combustion power from prime movers and stored power from battery energy storage. Similar to hybrid propulsion at low propulsive power, the electric drive is available to propel the vessel and switch off the main engine whereas it can also be used as a generator fed from the combustion engine.

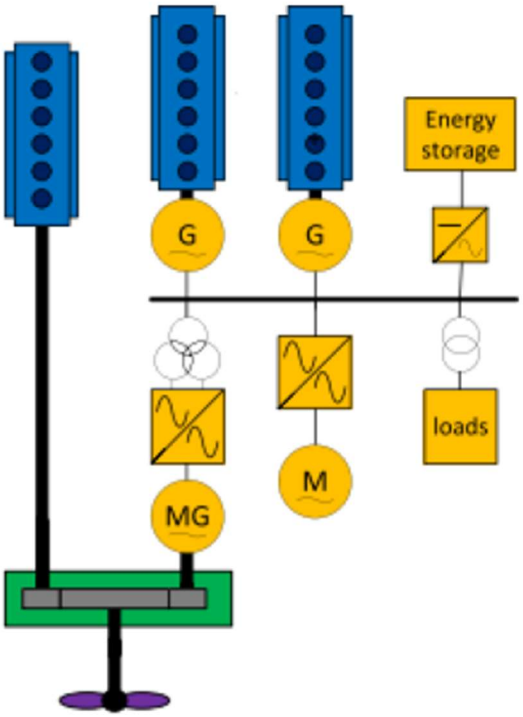

Figure 61: Hybrid propulsion with hybrid power supply.

The hybrid propulsion, hybrid supply system architecture has been extensively investigated for the case of harbor tugboats. Damen shipyards, the leader in this market, delivered the first tugboat with this architecture in 2014. Significant fuel savings in local emissions due to the utilization of batteries fed from the grid is a distinct advantage of this system. These savings can be achieved utilizing a heuristic rule-based approach. For the case of the harbor tugs, the control mode is determined from the operating mode of the vessel (high or low speed transit, towing or standby) and the battery SoC.

5.3.6 All-electric propulsion system

In all the architectures mentioned above the internal combustion engine was present. All-electric propulsion architecture utilized only electric motors which energy is delivered from energy storage systems such as supercapacitors, flywheels and mainly batteries. Currently for ship propulsion the main ESS is the Li-ion batteries due to their high specific energy along with the high efficiency and a relatively satisfying lifetime. This energy storage system provides both the required electrical and propulsive power to the ship, making the generators unnecessary along with the fuel tanks, the fuel processing equipment, the exhausts e.t.c. All these auxiliaries are being replaced by the necessary electronic modules such as the main switch boards, the inverters, the transformers which all already present in the diesel-electric ships.

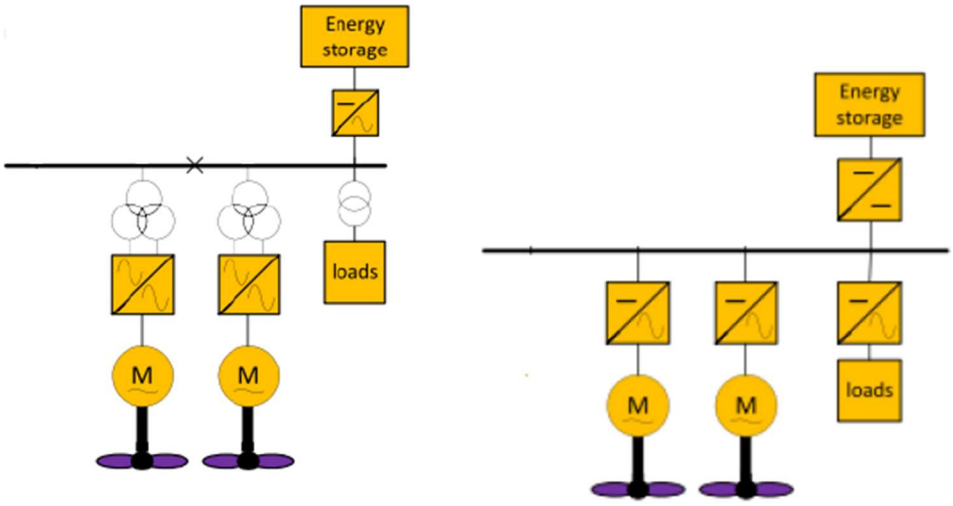

Figure 62: All-electric propulsion system with AC distribution system on the left and DC on the right.

The main drive for the all-electric propulsion is the decarbonization target for the marine industry. Apart from the transitional solutions of Liquified Natural Gas (LNG) the all-electric alternative offers complete detachment from carbon. Its total efficiency is far superior than that of internal combustion since the electric motor can achieve an efficiency of over 90% (even 97% depending on size) and by accounting a 10-15% losses due to the electronics and transmissions the all-electric alternative can reach a very conservative efficiency of at least 70%. The main limitation of this architecture is the low specific energy of the storage system (the 250W·h/kg cannot be compared with the specific energy of diesel which is around 12.5kW·h/kg). Thus, this drawback influences the operational performance of the vessel such as speed and mainly the range but also the port infrastructure since there is need for a high voltage recharging infrastructure.

For the above reasons it is understandable why the all-electric ship has not been implemented yet. The conservative way of thinking of maritime industry is also quite hesitant to investigate whether or not the all-electric alternative is viable. These days there are only a handful of all-electric ships that can pave the way for the adoption of this architecture.

NAVTEK Naval Technologies Inc., built the first all-electric tugboat called ZEETUG under the request for harbor tugs which can be characterized as lower in size but also in emissions. In this way they designed the ZEETUG-30 a harbor tugboat with 32 tonnes of bollard pull which draws its power from two 1450kW·h Li-ion battery packs.

Figure 63: ZEETUG figure.

ZEETUG can be custom built to provide from 5T BP up to 80T BP. The ZEETUG-30 is propelled from two electric motors of 925 kW with a design speed of 10 knots. It is also 10% smaller than similar tugboats and can be fully charged in less than an hour. The Smart Tug Energy Management System (STEMS) software has the objective of optimizing the electric power consumption and extending its driving range of operation cycles. Also, each ZEETUG can be adjusted in order to satisfy the constrains that arise according to the operational times and weather conditions at the region where it will operate.

Apart from ZEETUG there are several another all-electric projects some of which are currently operating. One of them is the ferry MV Ampere which operates at a 5.7 km crossing in Norway. It makes 34 trips a day, each one requiring 20 minutes apart from the 10 min of loading and unloading time for cars and passengers. It is an 80 m-long and 21 m-wide twin hull catamaran that can accommodate up to 120 cars and 360 passengers. Its hull is constructed from aluminum rather than steel in order to cut down the overall weight. The propulsion comes from two onboard 450kW electric motors, one of them driving the thrusters. The ESS consists of Li-ion batteries with an overall output of 1000 kW·h and a weight of 10 t.

Figure 64: MV Ampere figure.

Apart from the prementioned two cases which consisted mainly of ferries characterized with operation close to the coastline, with short routes and thus without the requirement for high energy autonomy another project which is in operation at the moment is the first all-electric cargo ship which was built in China by Guangzhou shipyard. It has an autonomy of up to 80 km, after a two-hour charge, with the ability to load a cargo of 2000 tonnes. The 70.5 m-long ship, 13.9 m-wide and with a draft of 3.3 m cargo ship uses two 160 kW electric propellers powered by an energy storage of 2.4 MW·h that is a mix of supercapacitors and Li-ion batteries.

Figure 65: First all-electric cargo ship.

In the following decades the diesel-built marine industry will have to follow a path towards decarbonization. Even if the current technology, mainly due to the low specific energy of battery systems, do not offer similar the energy density of fuel oil or LNG, all-electric ships can be a viable alternative for short route trips, mainly close to the coastline. It can be beneficial for the local area of their operation because due to their zero emissions and also another important factor which is usually forgotten, their much lower noise production they will gain an increasing market share in the following years.

6.0 Design Methodology

6.1 Retrofit Philosophy:

The tugboat being consider for the retrofit study is “CHRISTOS XL”. It is a conventional tugboat with main particulars:

Table 11: Main particulars of "CHRISTOS XL"

Main Particulars	
Length O.A. [m]	28.4
Length B.P. [m]	25.0
Breadth [m]	8.5
Depth [m]	4.2
Summer Draught [m]	3.25

The engine room consists of two main diesel engines coupled with a gearbox each of which drives a controllable pitch propeller (CPP), the STORK WERKSPOOR, 6FH240 that provide 670 kW at 1000 RPM. The reduction gears have a ratio of 4.045:1. Also, the vessel is equipped with three diesel generator sets, two of 70kVa and one of 14kVa, covering the electrical loads of the tugboat.

The goal of this retrofit is the complete electrification of the tugboat, meaning the total replacement of the main diesel engines and the generators by batteries. These batteries are going to cover both propulsion and electrical loads of the ship.

For the case study, the propulsion system up to the gearbox is assumed unchanged. This means that the angular velocity of the shaft as well the power output of the shaft after the reduction gear must be the same. For this reason, the main engines are being replaced from two electric induction motors of similar nominal power output and revolutions.

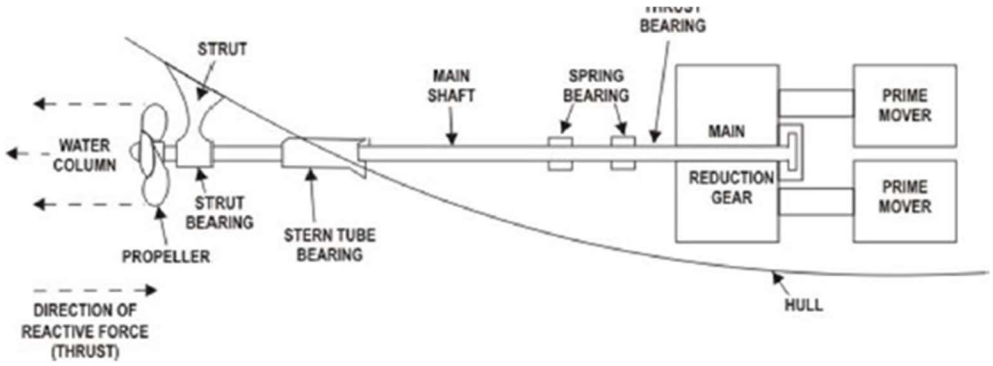

Figure 66: General principle of a geared ship propulsion.

The battery system is divided into two distinguished but similar battery packs each of which powers one of the motors as well as the hotel loads. The next figure offers a graphical representation of the architecture:

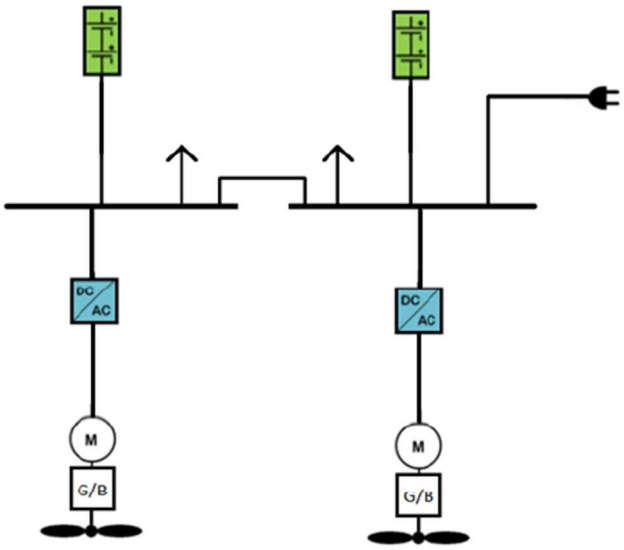

Figure 67: All-electric ship configuration with a DC distribution system.

- Two electric induction motors (M),
- Two gearboxes (G/B),
- Two battery packs and
- Two inverters (DC/AC), each one before the induction motor to convert the DC voltage to AC.

The most important part of this case study is the sizing and the placement of the battery packs. Battery packs will be the only power source of the vessel, for both its propulsion and electrical power needs. Thus, the battery sizing has to be sufficient for the intended operation of the vessel and to provide a certain power margin. On the other hand, the battery cost will be the highest expense for this retrofit and a golden rule must be found between the reliability and the economic viability. Moreover, the invariable weight of the battery system and its position along the vessel poses an additional challenge with respect to vessel's stability and trim. Last but not least, the lower specific energy of batteries with respect to fuel oil raises another one problem with respect to the available space for their installation. Thus, it is clear that the sizing of the batteries requires a lot of parameters to be taken into consideration in order to find an optimum solution.

Battery system's sizing mainly depend on its energy consumption along with the available time for charging during its shift. The most accurate way to calculate the ship energy needs with respect to its operational profile would be to perform CFD simulations and estimate

the required power with respect to speed. However, lack of CAD data, mainly the vessel's lines plan or a systematic series used for these vessels ruled out that possibility. For this reason, Noon Reports were provided for the certain vessel. Noon Reports provide information such as the trips the vessel did during the day, the average speed during a certain trip along with engine's information such as the rotational speed, its power and consumptions such as fuel oil, lubricating oil e.t.c. Knowing the required rotational speed and engine's power with respect to vessel's speed during certain operations, it is possible to perform a simulation for the case of the induction machine. This can be done based on the Field Oriented Control (FOC) which was analyzed in section 2. For each investigated scenario, the diesel engine's power and speed is provided, which will be the inputs for the FOC. The currents fed to the motor from the batteries along with the duration of the trip, that is determined from the vessel's speed which is already known, will result in the required A·h capacity the batteries must have.

6.2 Electric motor selection and control implementation in Simulink

The selection of the electric induction motor was based on the assumption that its nominal speed and power must be similar to the diesel one. In that order, after looking into manufacturer's catalogs and mainly at Valiadis Hellenic Motors, the Low Voltage 3-Phase Cast Iron K450-6-710kW induction motor was chosen. Its characteristics are presented below:

Table 12: K450-6-710kW Characteristics.

Valiadis K450-6-710kW characteristics			
Rated Power	710 kW/965 hp	Efficiency at 100% load, η	96.7%
Rated Speed	995 RPM	Full load current	1251 A/ 722.27 A
Voltage	400-Δ/690-Y	Nominal Torque	6814 N·m
Frequency	50 Hz	Locked rotor torque/Full load torque	1.40
Poles	6	Pull out torque/Full load torque	2.21
Moment of Inertia	48.6 kg·m^2	Locked rotor current/Full load current	5.7
Power factor at 100% load, S.F.	0.85	Weight	5100 kg

Its rated power at 710 kW is similar to the diesel's one at 670 kW and both motors have the same rated speed, which is favorable because there is no need to change the gearbox. In order to estimate the required battery capacity, the motor's energy consumption must be calculated. This can be done by simulating the motor's operation in a simulation software, one of which is MATLAB simulink. Simulink is a MATLAB-based graphical programming environment for modeling, simulating and analyzing multidomain dynamical systems. Its primary interface is a graphical block diagramming tool and a customizable set of block libraries. It offers tight integration with the rest of MATLAB environment and can either drive MATLAB or be scripted from it. Simulink is widely used in automatic control and digital signal processing for multidomain simulation and model-based design.

The simulation of the induction motor is based on its equivalent circuit. Therefore, it is necessary to either retrieve somehow or calculate the electric motor's parameters of the equivalent circuit. These are the stator windings' resistance R_s, the rotor's resistance R_r and the leakage inductances L_{lr}, L_{ls} and the mutual inductance L_m. These are not provided in data manufacturer's sheet and their estimation is difficult. In order to calculate them, ordinary values per unit (p.u.) were selected for an induction motor of typical structure. These are:

- r_s = 0.0106 p.u.,
- x_{ls} = 0.10601 p.u.,
- x_m = 2.65036 p.u.,
- x_{lr} = 0.08481 p.u. and
- r_r = 0.042408 p.u.

Since they are in per unit format the base impedance Z_b must be calculated:

$$P_{in} = \frac{P_{out}}{\eta} = \frac{710\ \text{kW}}{0.967} = 734.22\ \text{kW}$$

$$S = \frac{P_{in}}{\cos\varphi} = \frac{734.22}{0.85} = 863.78\ \text{kVa}$$

$$Z_b = \frac{V_b^2}{S_b} = \frac{690^2}{863.78 * 10^3} = 0.5512\ \Omega$$

Subsequently, the equivalent circuit's parameters are being calculated:

Stator windings' resistance:

$$R_s = Z_b \cdot r_s = 0.8346\ m\Omega$$

Stator's leakage inductance:

$$L_{ls} = \frac{x_{ls} \cdot Z_b}{2\pi f} = 0.0266\ mH$$

Mutual inductance:

$$L_m = \frac{x_m \cdot Z_b}{2\pi f} = 3.2068\ mH$$

Rotor's resistance:

$$R_r = r_r \cdot Z_b = 3.3392\ m\Omega$$

Rotor's leakage inductance:

$$L_{lr} = \frac{x_{lr} \cdot Z_b}{2\pi f} = 0.0213\ mH$$

The induction motor in Simulink can be represented from the Asynchronous Machine block.

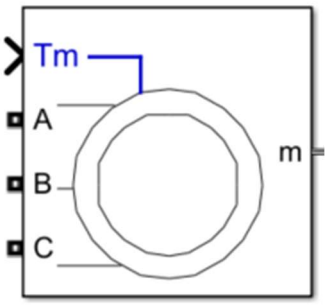

Figure 68: Asynchronous Machine block.

The Asynchronous Machine block uses as inputs the voltage from each one of the phases along with the mechanical torque at machine's shaft. The m output can provide numerous measurements as the stator's currents i_a, i_b, i_c, the rotor's speed, the electromagnetic torque T_e, even the dq currents for both the stator and the rotor. Before setting the parameters, mainly the equivalent circuit's and the initial conditions, the Squirrel-cage rotor type must be selected. Furthermore, the Reference frame can be selected as the Synchronous one, this only affects the output currents i_d and i_q.

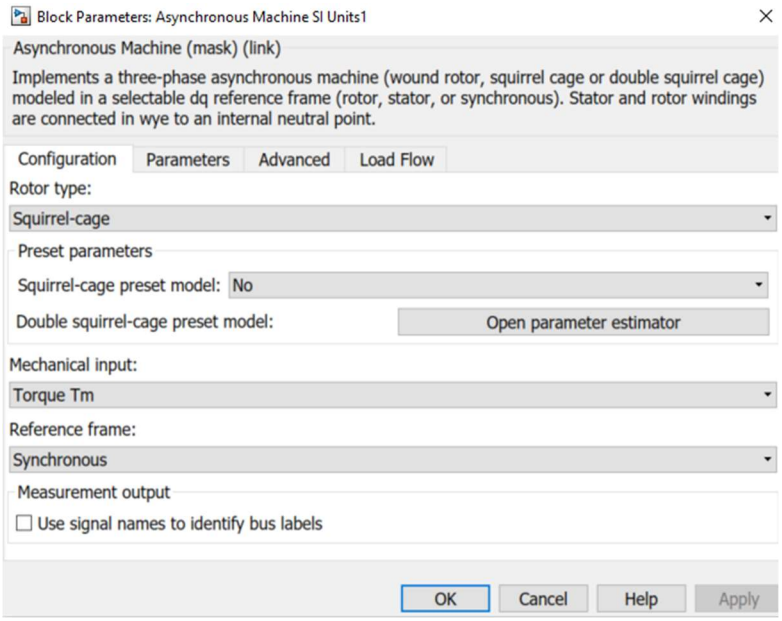

Figure 69: Asynchronous motor configuration.

Consequently, the parameters of the equivalent circuit and the initial conditions can be set. The stator's and rotor's resistances and inductances are being implemented in Simulink's workspace along with the rotor's inertia. The friction factor was selected equal to 0.05658 N·m·s a typical value for this case of motors. Below the configuration of these parameters is being presented along with their definition in Simulink's workspace.

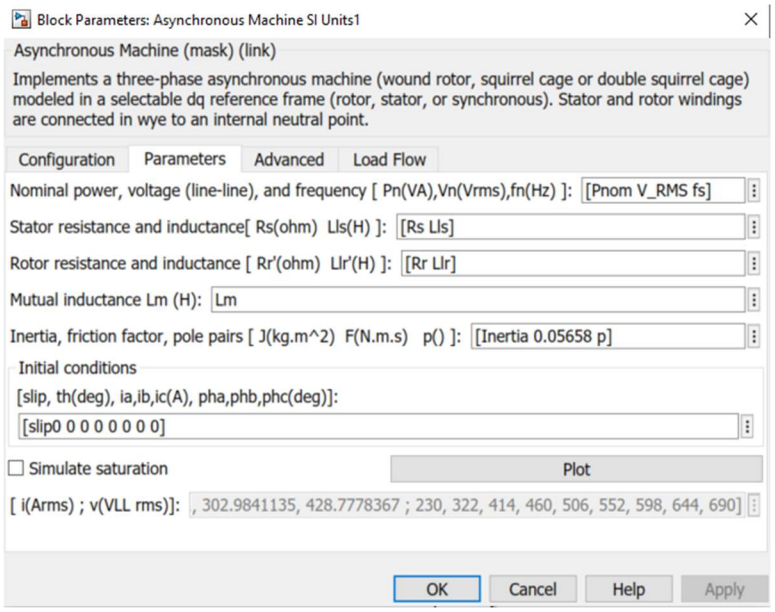

Figure 70: Asynchronous Machine Parameters configuration.

```
fixed_step = 1e-5; %Step size

h = 0.967; %Efficiency at 100% Load
PF = 0.85; %Power factor at 100% Load
Pout = 710*10^3; %Watt
Pnom = Pout/(PF*h); %Va
Nominal_Speed = 995; %RPM
Nominal_Torque = 6814; %N*m
fs = 50; %Supply frequency
V_RMS = 690; %Voltage RMS value Phase to Phase for wye
p = 3; %Pole pairs
slip0 = 1; %Initial slip for stationary rotor

%Per unit values
rs = 0.0015142; %p.u.
xls = 0.0151442; %p.u.
xm = 1.8278344; %p.u.
xlr = 0.0121157; %p.u.
```

```
xlr = 0.0121157; %p.u.
rr = 0.0060583; %p.u.

%Calculate the base impedance
Zb = V_RMS^2/Pnom;

%Induction motor impedances
Llr = xlr*Zb/(2*pi*fs);
Lls = xls*Zb/(2*pi*fs);
Lm = xm*Zb/(2*pi*fs);
Ls = Lm + Lls;
Lr = Lm + Llr;
Rr = Zb*rr;
Rs = Zb*rs;
Tr = Lr/Rr;
Inertia = 48.6; %kg/m2

Rated_flux = 1.779; %We
```

Figure 71: Parameters definition in Simulink environment.

The control of the induction motor will be based on the Field Oriented Control, FOC. The goal is to calculate the reference currents $i_{a,ref}$, $i_{b,ref}$ and $i_{c,ref}$ which will result from the inverse Clarke and Park transformations of $i_{d,ref}$ and $i_{q,ref}$ of the stator. The $i_{d,ref}$ will be calculated from 3.4.26, assuming that the rotor's d axis flux, rotor's flux since the dq reference frame is aligned to that flux, is equal to the rated one, $\lambda_{r,net,nom.}$ The goal therefore is to calculate the rated rotor's flux. This can be done by simulating the motor, with zero input torque and with the rated three-phase voltage. Below the model schematics are being presented, each one of the subsystems will be analyzed.

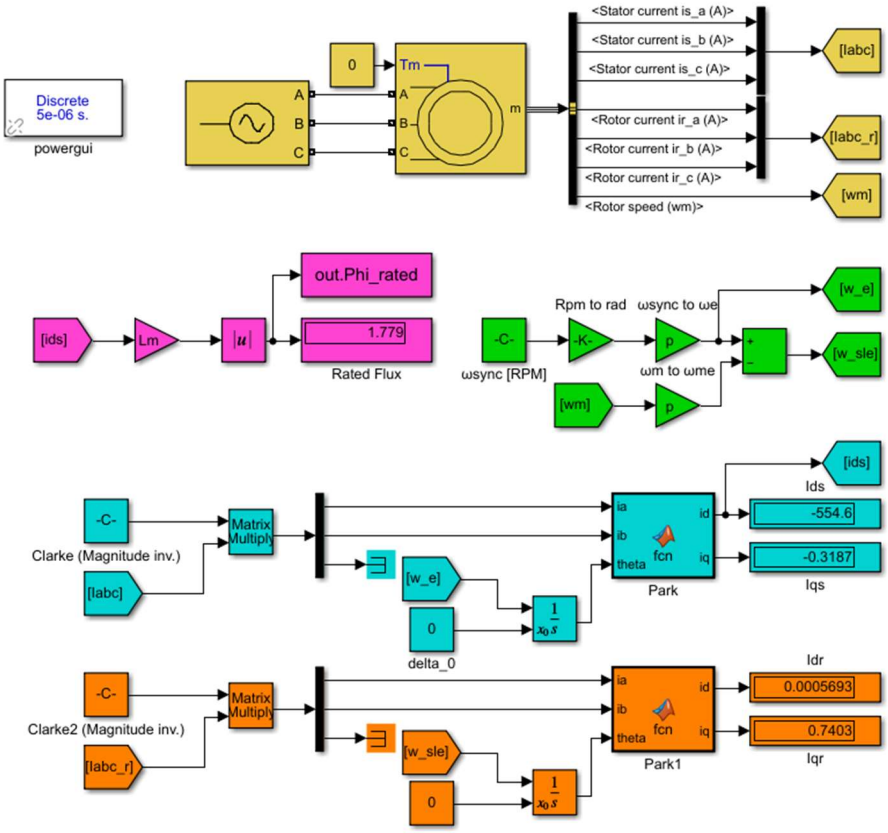

Figure 72: Simulink model calculation of rotor's rated flux.

The timestep of the simulation was selected equal to $1 \cdot e^{-5}$ sec. Beginning with the input voltages, a three-phase voltage source, was used, connected in wye to the stator's circuits. The V_{RMS} was set equal to 690 V, which is the rated stator's voltage for wye connection and the frequency equal to 50 Hz. The torque input was set equal to 0 and the measured outputs are the stator's currents i_{s_a}, i_{s_b}, i_{s_c}, the rotor's currents i_{r_a}, i_{r_b} and i_{r_c} and the rotor's rotational speed w_m.

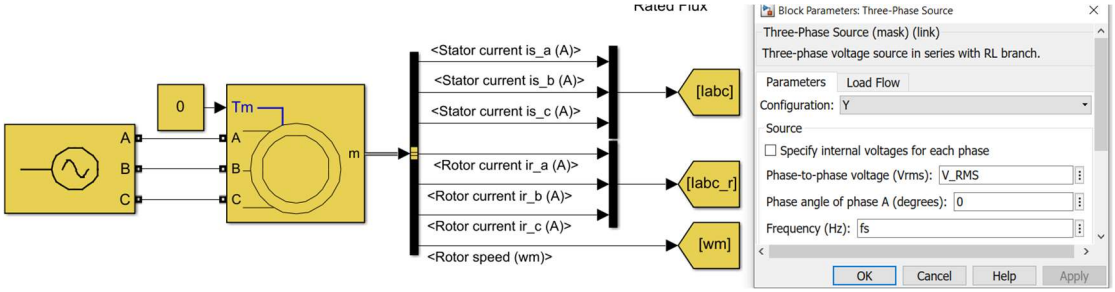

Figure 73: Voltage source and motor's measured quantities.

The calculated currents both for the stator and the rotor must be transformed to the equivalent dq currents. Therefore, both the stator's and the rotor's currents are transformed initially to the αβ reference frame, using the magnitude invariant Clarke transformation (3.4.2). Consequently, the stationary αβ reference frame must be transformed to the dq rotating reference frame, based on the formula 3.4.3. The main issue that arises is that for the case of the stator and the rotor the angle δ is not equal. For the stator's currents the angle δ will be calculated by integrating the synchronous electrical rotational speed ω_{se} from the formula 3.4.4, where ω_{sync} was calculated based on 3.1.2 and p is the number of pole pairs, equal to 3. For the case of the rotor the angle δ will be calculated by integrating the slip electrical speed of the rotor's currents, ω_{sle} which can be calculated by the difference between the ω_e and ω_{me}. Similar to the synchronous electrical speed ω_e the electrical mechanical speed ω_{me} can be calculated based on the formula 3.4.5.

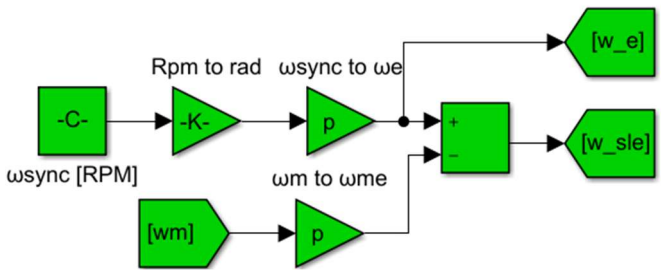

Figure 74: Calculation of ω_e and ω_{sle}.

In order to have the rotor's flux aligned with the d axis of the rotating reference frame, the initial angle δ_0 must be calculated. This was set equal to 0 in the initial conditions (Figure 70).

Thus, by performing Park transformation based on the measured angular velocities ω_{me} and $\omega_{sl,e}$ the dq currents of the stator and the rotor can be calculated.

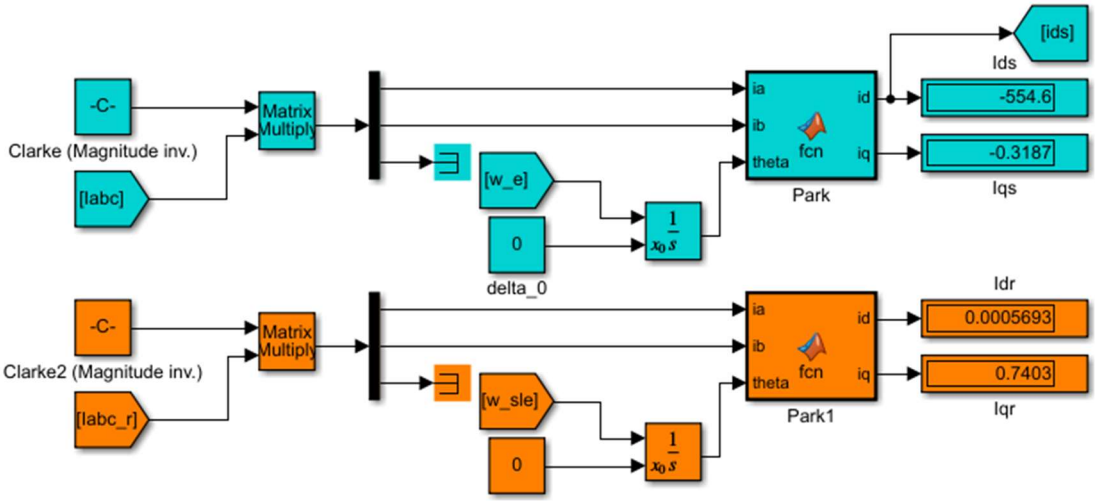

Figure 75: Calculation of dq currents of the stator and the rotor.

It must be noted that the current of the rotor along the d axis, i_{dr}, is approaching 0 as expected since the rotor's flux along q axis is equal to 0, having aligned the dq frame with the rotor's flux, based on the formula 3.4.15. Therefore, the rotor's rated flux can be calculated based on the formula 3.4.23, which is equal to 1.779 We. The reference rotor's flux will be independent of the rotor's angular speed or the mechanical torque the machine must provide. This is based on the fact that the machine is built in order to operate constantly on the rated flux, in order to avoid magnetic saturation, which will increase the losses. Thus, the i_{ds} reference current will be calculated from the rated flux based on the formula 3.4.26.

Apart from the i_{ds} reference current, in order to obtain the $i_{a,ref}$, $i_{b,ref}$ and $i_{c,ref}$ currents of the stator, the i_{qs} reference current must be also calculated. This will be calculated from the formula 3.4.27. In order to have a closed loop control of the motor both with respect to torque and speed, a PID controller will be implemented. The input of the PID controller will be the error between the reference and the actual rotating speed and the output will be the reference torque T_{ref}. When the reference speed increases, the rotor accelerates therefore the reference torque is positive, $T_{ref} > 0$, whereas when the reference speed decreases the reference torque is negative, $T_{ref} < 0$. Also, at the output of the PID a saturation block must be implemented in order to suppress reference torques higher than the pull-out one since it does not represent the actual physics of the system.

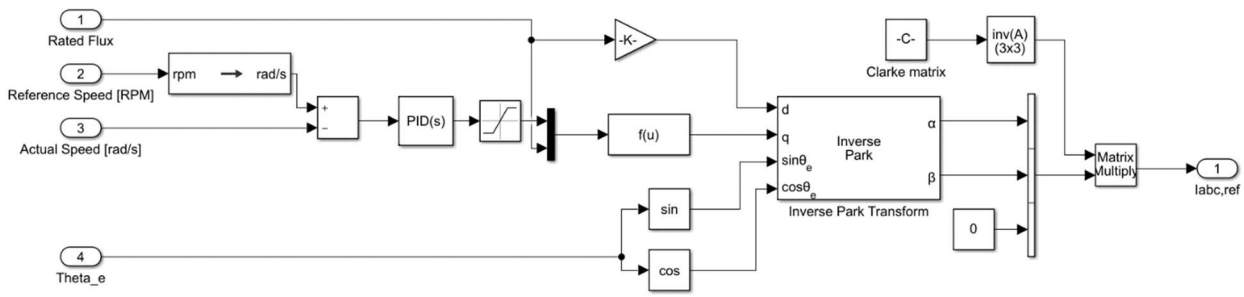

Figure 76: Reference currents calculation.

The parameters of the PID controller were calculated based on a trial and error procedure, using a step function as input and trying different K_P, K_I and K_D values in order to obtain the desirable output, both in terms of responsiveness and oscillating behavior. These parameters are presented below:

Table 13: PID parameters.

PID Controller parameters	
K_P	350
K_I	50
K_D	5

Having calculated the dq reference currents it is necessary to obtain the abc reference currents by utilizing the inverse Park and Clarke transformations. The necessary θ_e angle will be calculated based on the actual abc currents.

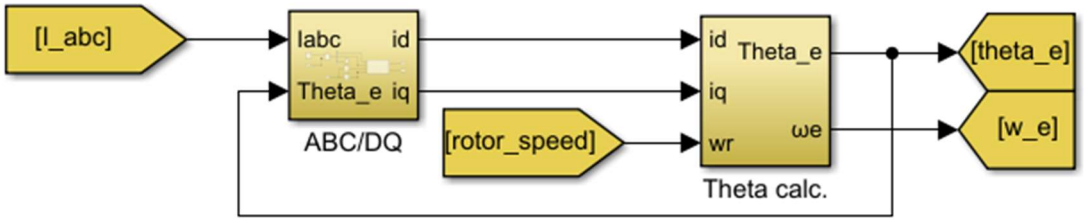

Figure 77: Theta electrical angle calculation.

The measured abc currents of the stator are transformed into dq currents from the Clarke and Park transformations. The θ_e angle is calculated based on a recursive procedure. The dq currents along with the rotor's angular speed ω_m are the input in the Theta calc. block. The θ_e angle will be calculated by integrating the synchronous electrical velocity ω_{se}. This velocity can be found based on the formula 3.4.34. The flux along the d axis, λ_{dr}, will be calculated from 3.4.19 since during the simulation there are transient phenomena therefore it is not possible to assume that

the derivative of flux is equal to 0. By performing Laplace transformation, the following transfer function is derived for the calculation of rotor flux along the d axis.

$$\boldsymbol{\lambda_{dr} = \frac{L_m}{p \cdot \frac{L_r}{R_r} + 1}}$$

This flux cannot exceed the rated one, so for this case also a saturation block is implemented with an upper bound of the rated flux and a lower bound of $1e^{-3}$ for mathematical stability issues that were observed during the initialization of the simulation. The ω_{me} was calculated from the rotor's angular speed from 3.4.5.

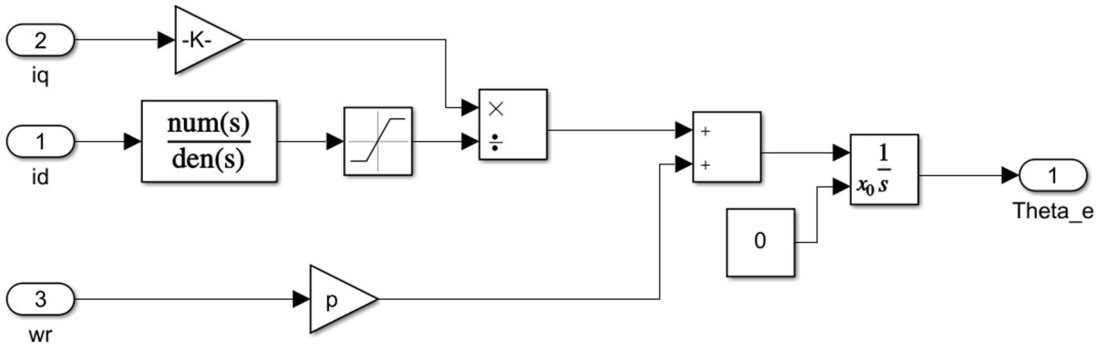

Figure 78: Theta calc. block expansion.

In order to control the voltages for the induction machine a Current Source Inverter (CSI) was implemented. The goal was to control the stator's voltages in order that the stator's measured currents abc would be placed between the limits (I_{ref} – Band, I_{ref} + Band), according to Figure 31. Three different band values are examined, 1, 5 and 10% of the reference current. The switching states S_{ii} were defined from the output of the Current Controller block.

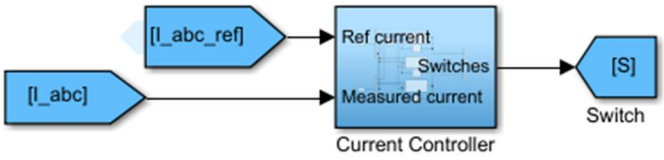

Figure 79: Current Controller block.

The inverter was designed based on the schematics of Figure 30. The inverter block receives as inputs the three switching states S_{11}, S_{21} and S_{31} and the input voltage DC source. The selected IGBTs have an internal resistance of $1e^{-3}$ Ω and a forward voltage of 1V.

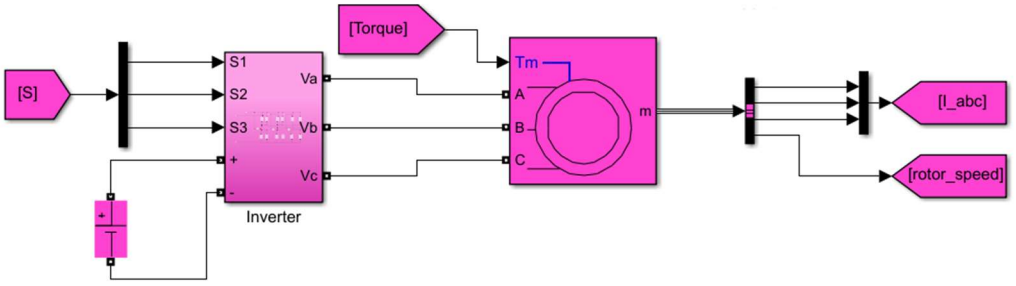

Figure 80: Inverter - Induction motor.

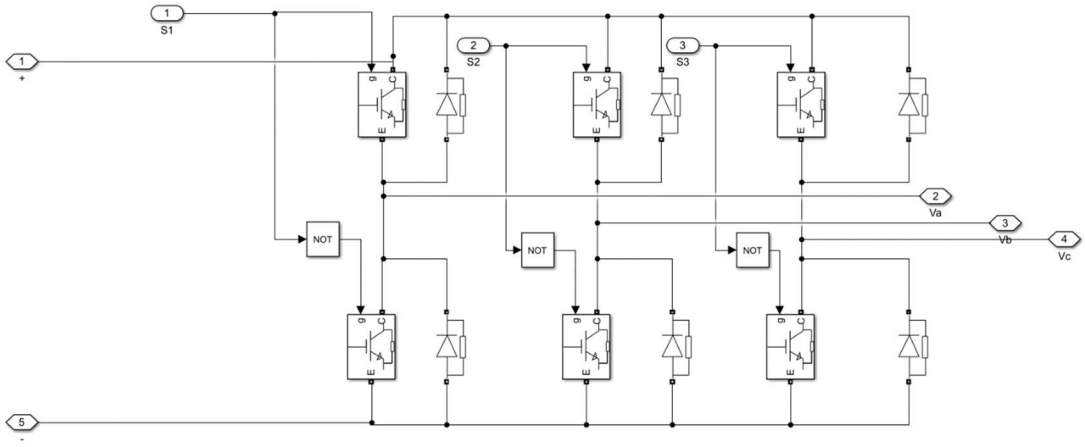

Figure 81: Inverter block expansion.

The schematics of the whole control system are presented below:

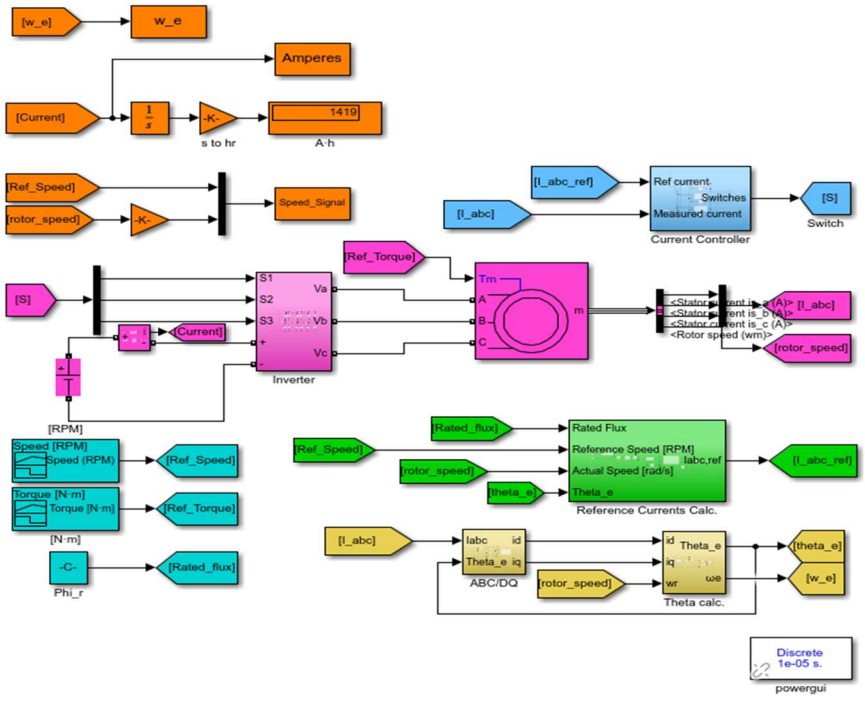

Figure 82: Control system schematics.

The main goal of the simulation is the battery sizing which will result from the calculation of the current that the DC voltage source provides. The battery capacity will be calculated by integrating that current, for a time period dependent on the operating profile of the tugboat. The operating profile will be defined in the next section. In order to calculate that current, a current measurement block was implemented in the voltage source.

6.3 Case study

The purpose of this study is the investigation of the technological viability of the replacement of the main and auxiliary engines with a battery pack in a harbor tugboat. As previously stated, the tugboat chosen for this preliminary study is the vessel "CHRISTOS XL", a conventional tugboat with two diesel main engines coupled with a gearbox each of which drives a CPP propeller, along with three gensets to cover the electrical loads of the tugboat.

The tugboat will operate inside and close to the port of Piraeus in a very narrow and tight environment. Its range will be a maximum of 5 to 10 nautical miles outside the port. The operational profile of the tug is based on a 12-hour daily operation, 360 days per year, based on a similar study found on the paper "Raptures: Resolving the Tugboat Energy Equation".

The operational profile is divided into three different periods:

- Harbor Duty: During this period the tugboat is primarily engaged in ship berthing/unberthing in a harbor environment, where transits are short. On harbor duty the tugboat spends a significant amount of time idling and transiting on low speeds mixed in with short periods of high BP operations.
- Ship Assist Duty: In this period the tug is tasked with accompanying ships entering or leaving the harbor over a greater distance for light escort operations, where the tugboat spends more time at higher transit speeds and less time at operations involving high static thrust compared to harbor duty.
- Port Stay: This is the time in-between missions where the tugboat is berthed and completely idle. This is the time window in which a battery powered tugboat can recharge its batteries.

Every mission takes three hours to complete and it is divided into two parts, the first one consists of the time period in which the tugboat departs from the port and assists the ship entering the harbor, described as "Ship Assist Duty" mode and takes approximately 2 hours to complete. The second part consists of the time period in which the tugboat is engaged in berthing the ship and arrives back to its station. This part is described by the "Harbor Duty" mode and takes approximately 1 hour to complete. In-between missions the tugboat is idling for approximately 1.5 hours. In total the tugboat is going to take part in three missions during its 12-hour shift.

As mentioned in the previous section, in order to perform the sizing of the battery system it is necessary to calculate the total A·h the two asynchronous motors consume based on an operational profile. The operational profile as described, consists of free running and towing operations. For the selected tugboat the main operational data provided were the Noon Reports for a free running and a towing scenario. Based on these data it is possible to estimate the required power with respect to engine's rotational speed, based on the propeller's law and the curve that describes the relationship between the vessel's and engine's speed:

$$P = C_p \cdot V^3 \qquad 6.3.1$$

$$V = k \cdot n \qquad 6.3.2$$

Thus, the coefficients C_p and k will be calculated for both the free running and the towing scenarios.

Table 14: Calculation of C_p and k of Power - Vessel's Speed and Vessel's Speed - Engine's RPM curves.

	Power (kW)	Speed [RPM]	Speed [knots]	C_p [kW/knots^3]	k [knots/RPM]
Towing	1072	800	5.66	5.912	0.007075
Free running	1072	800	9.0	1.476	0.01125

The operational conditions of the Ship Assist and Harbor Duty as a percentage of the total time of each period are presented below.

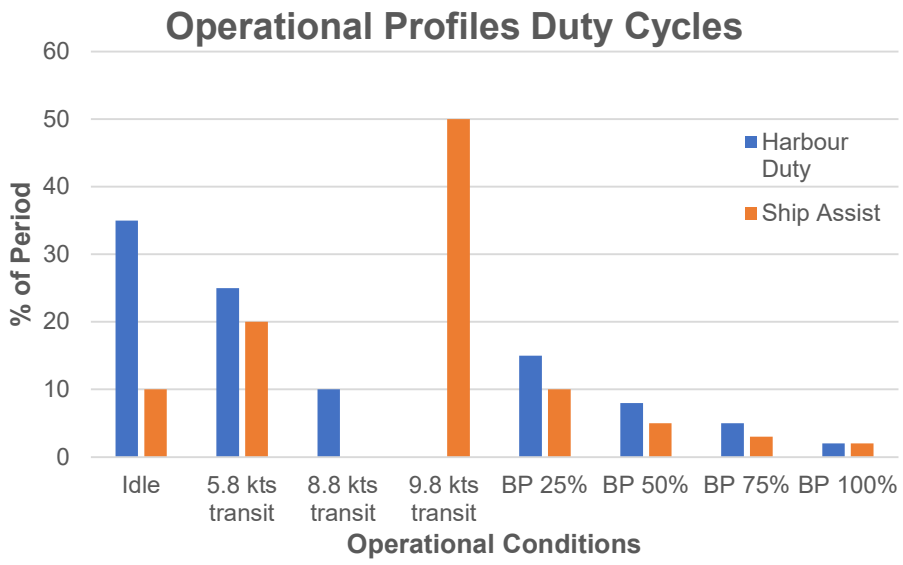

Figure 83: Duty cycles of Harbor and Ship Assist periods.

To estimate the required battery capacity, it is necessary first of all to calculate the electric motors energy needs based on the operational profiles described above. The Bollard Pull and Idle scenarios are described as a percentage of the total installed propulsion power. By utilizing the Figure 83 and the formulas 6.3.1-6.3.2 it is possible to calculate the reference torque and speed for the electric motors for one mission. The simulation of the motor based on the reference torque and speed values will be carried out for one out of the three missions, assuming that all three of them are identical. In the following table the reference motor's speed and torque are calculated based on the operational condition.

Table 15: Calculation of motor's reference torque and speed.

	Harbor Duty								Ship Assist							
	Idle	Transit [kts]			Bollard Pull [%·P_{nom}]				Idle	Transit [kts]			Bollard Pull [%·P_{nom}]			
	-	5.8	8.8	9.8	25	50	75	100	-	5.8	8.8	9.8	25	50	75	100
Period of mode of each operation [%]	35	25	10	0	15	8	5	2	10	20	0	50	10	5	3	2
Time cruising on each mode [min]	21	15	6	0	9	4.8	3	1.2	12	24	0	60	12	6	3.6	2.4
Total Power [kW]	71	288	1006	-	355	710	1065	1420	71	288	-	1389	355	710	1065	1420
Torque [N·m] (per motor)	-	2667	6140	-	3062	4861	6370	7717	-	2667	-	7614	3062	4861	6370	7717
Speed [RPM]	-	516	782	-	553	697	798	879	-	516	-	871	553	697	798	879

In order to create the reference curves for torque and speed it will be assumed that the Ship Assist operation is split into two one-hour operations where in-between there is the Harbor Duty one.

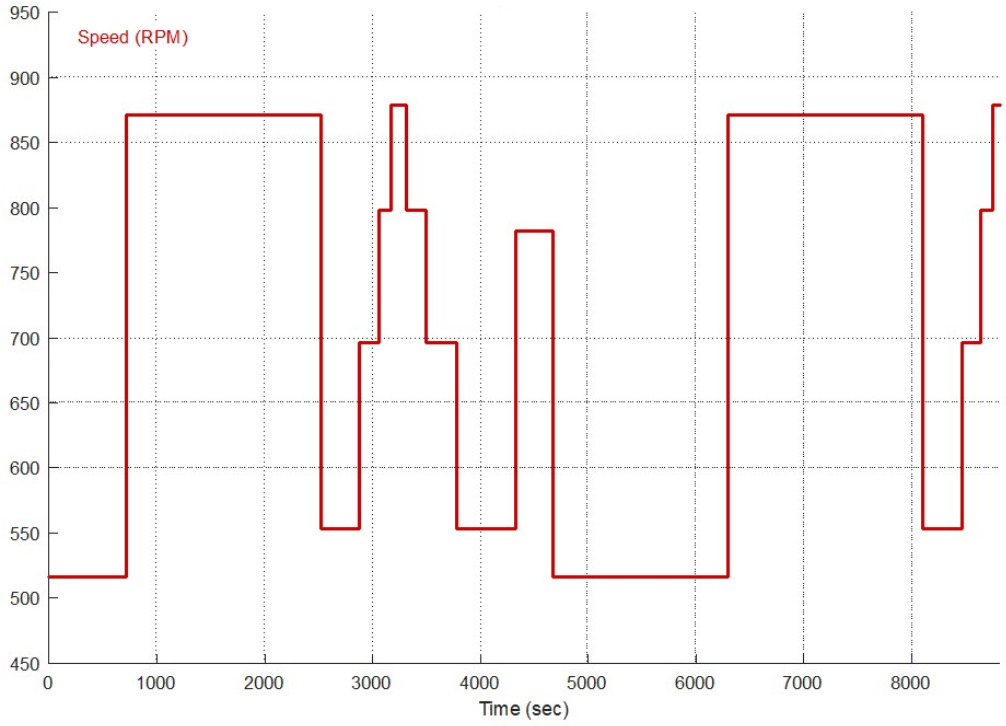

Figure 84: Motor's reference speed [RPM].

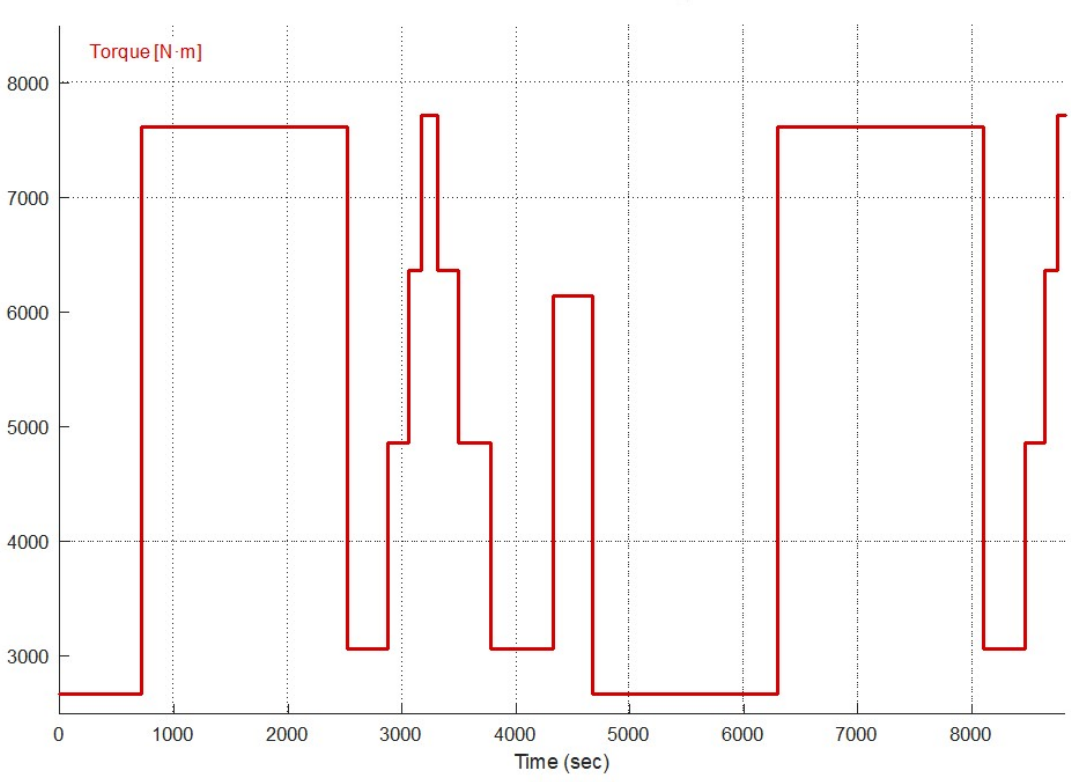

Figure 85: Motor's reference torque [N·m].

Irrespectively with the total required battery capacity, the motor's nominal phase to phase for wye connection voltage is 690 V. Therefore, before initializing the simulation, the total battery modules in series must be calculated based on the following formula:

$$N_{series} = \frac{V_{system}}{V_{module}}$$

The selected battery modules used in this retrofit are manufactured by Valence and the specific model is going to be the U-Charge U27-36XP of the XP series. U-Charge® is a range of 12, 18, 24 and 36 V Lithium Iron Magnesium Phosphate battery modules, offering intrinsic safety with twice the run-time and 70% weight compared to similarly sized sealed lead-acid batteries. They are also characterized by long cycle life and suitable for marine applications.

Table 16: U-Charge U27-36XP specifications.

Voltage (nominal)	38.4 V	Rec. Charge CCCV	≤ 25 A to 43.8 V
Capacity @ C/5	50 A·h	Specific Energy	102 W·h/kg
Energy	1.92 kW·h	Energy Density	162 W·h/l
Discharge Cont./Peak (30 sec)	100 A/150 A	Height/Width/Length	225/172/306 mm
Cutoff Voltage	30 V	Weight	18.7 ± 0.1 kg
Rec. Charge Voltage	43.8 V	IP Rating	IP56

The Voltage – DoD performance curves based on the C – rates are presented below. It is clear that after a DoD of 80% the battery voltage diminishes sharply, so it is important to keep the SoC higher than 20% on a regular basis. The battery technology is based on the Lithium Iron Phosphate therefore it offers very high safety standards, a long lifespan (more than 4000 cycles at 80% DoD) and a very high specific power since it can provide continuously current equal to 100 A.

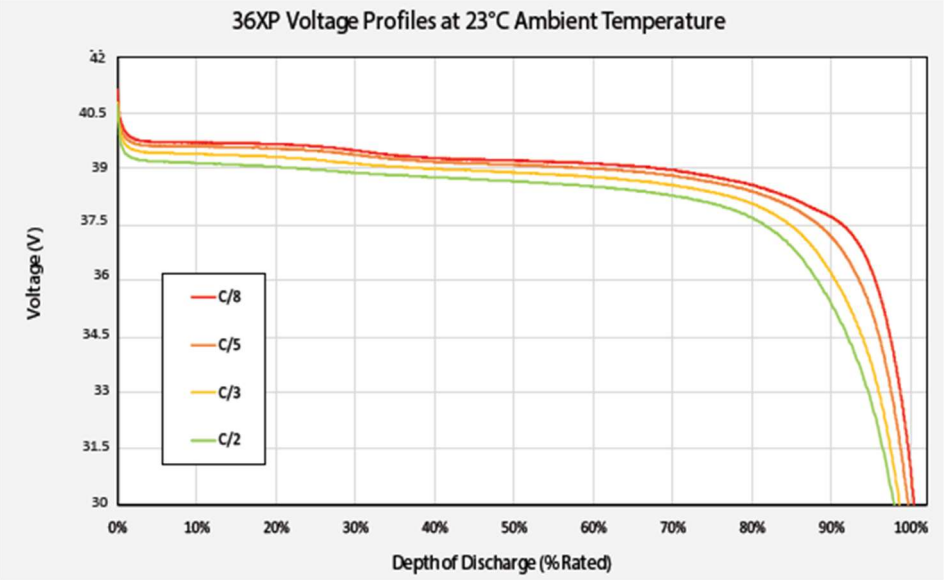

Figure 86: Depth of Discharge (DoD%) versus Voltage for U27-36XP.

Since the selected battery module has a nominal voltage of 36V, the total required modules in series are:

$$N_{series} = \frac{V_{system}}{V_{module}} = \frac{690}{36} = 19.16 \Rightarrow N_{series} = 20$$

Therefore for 20 modules in series the input voltage will be equal to:

$$V_{system} = 20 \cdot 36 = 720V$$

Both the Harbor Duty and Ship Assist periods consists of a time window that the vessel is idle. During that time the electric motor's do not operate therefore the energy consumption must be calculated in another way. It is assumed that in Idle operation the power needs are equal to 5% of the nominal propulsive power installed, 71 kW. Therefore, the energy needs in A·h can be calculated by taking into consideration the total time per mission, the vessel is idling.

Table 17: Energy consumption during idling.

	Time [min]	Power [kW]	Energy [kW·h]	Consumption [A·h]
Harbor Duty	35	71	41.4	57.5
Ship Assist	10	71	11.8	16.4

Therefore, the total A·h consumed per-mission for the Idle period of the tugboat are equal to:

$$C_{idle} = 73.9\ A \cdot h$$

The total A·h consumed based on the three-hour motor operation based on the torque and speed profiles, depicted in Figures 84 and 85 after running the simulation are equal to:

$$C_{motor} = 1419\ A \cdot h$$

The total consumption on auxiliary and hotel loads for the idle and transit periods based on the data from the Appendix A is equal to:

$$C_{aux,hot} = 6.4 + 50.37 = 56.77\ A \cdot h$$

The total consumption per mission is equal to:

$$C_{mission} = 2 \cdot C_{motor} + C_{idle} + C_{aux,hot} = 2968.7\ A \cdot h$$

It is assumed that the battery packs will be charged up to 90% SoC and discharged up to 20%, having thus a Depth of Discharge (DoD) equal to 70%. In that order the required battery capacity to cover the energy needs per missions, based on the assumed operational profiles are:

$$Capacity = \frac{C_{mission}}{0.7} = 4241\ A \cdot h$$

This capacity will be covered from two battery packs, each one will feed one electric motor. Therefore, the capacity per battery pack will be equal to 2120.5 A·h. Each battery module in series provide 50 A·h, to cover that need a total number of 43 parallel modules of 20 batteries are needed per battery system.

Table 18: Battery system sizing.

Number of modules in series	20
Number of parallel battery strings	86
Total number of batteries	1720
Total capacity of the two battery systems [A·h]	4300
Total weight [kg]	32164
Total Volume [m^3]	20.370

These battery packs each one of 10.185 m^3 can be fitted in the diesel oil tanks no 12&13 with the following dimensions, as depicted also in the General Arrangement's Lower and Profile views.

Table 19: Diesel oil tanks dimensions, for the housing of the battery systems.

Conventional Tug CHRISTOS XL: Diesel oil tanks				
Diesel Oil tanks (no 2)	Length [m]	3	Total Volume [m^3]	39.75
	Width [m]	2.65		
	Height [m]	2.5		

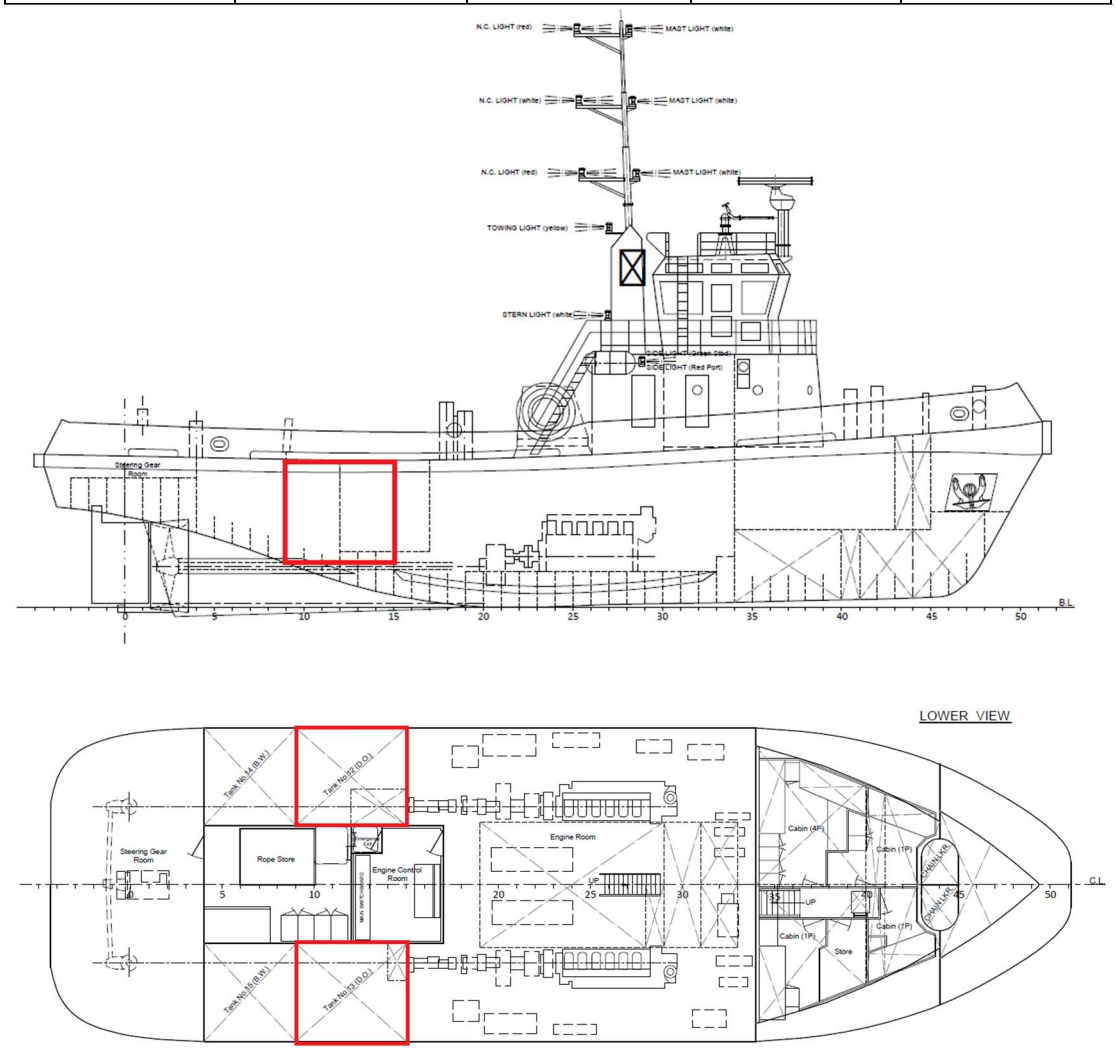

Figure 87: Available spaces found acceptable for housing the battery systems.

After each mission there is a time window of 1.50 hours to recharge the battery system. Assuming that the time needed to plug in/off to the grid can vary from 5 to 30 minutes the remaining time is selected equal to 75 minutes. In that time window the battery pack must be recharged to 90% SoC meaning that there is the need to replenish 2970 A·h, the 70% of the battery capacity that was consumed during the mission. The recommended charge CCCV (Continuous Current, Continuous Voltage) of one battery must be above 25 A and 43.8 V. Therefore, the charging voltage will be equal to:

$$V_{charging} = 43.8 \cdot 20 = 876 \approx 880\ V$$

and the charging current for each battery pack will be equal to 30 A in order to not stress the battery with high charge currents and simultaneously keep it above the recommended level.

Therefore, the charging current for the whole battery system will be equal to:

$$I_{charging} = 30 \cdot 86 = 2580 \text{ A}$$

In that order the required charging duration is equal to:

$$t_{charging} = \frac{2970}{2580} = 1.15 \text{ hr},$$

which is even less than the available charging time of 75 minutes.

The total required power supplied to the battery pack during the charge is equal to:

$$E_{charge} = I_{charging} \cdot V_{charging} = 2270.4 \text{ kW}$$

This power is supplied from the onshore bus at 6.6kV therefore it must be stepped down to 880 V with a use of a transformer. This transformer is generally large and bulky, but can be installed into the engine room or any other suitable location onboard.

The daily cycles considered for the estimation of battery system's life expectancy are:

$$\text{Cycles} = \frac{t_{charging} \cdot (N_{missions} - 1)}{DoD \cdot t_{0-100}} + 1$$

where:

- $t_{charging}$ is the total amount of time available to charge the batteries in-between missions,
- $t_{0\text{-}100}$ is the amount of time needed to recharge the batteries from 0-100% at nominal charging current.

Therefore, the daily cycles are equal to:

$$\text{Cycles} = 2.65 \text{ per day}$$

The Life Expectancy of the battery pack can be calculated from the following formula, where $Cycles_{nominal}$ are the nominal number of cycles if the system is operated at nominal values, where according to manufacturer for an 80% DoD the battery has a lifetime of more than 4000 cycles.

$$\text{Life Expectancy} = \frac{Cycles_{nominal}}{\text{Cycles}} = 4.19 \text{ years}$$

As already mentioned, the battery system will be split into two battery packs in order to ensure redundancy and safety, since there is always a slight possibility that one battery pack might fail. In that order the maximum range of the ship will be calculated assuming that it can return to port, with one battery pack and with a remaining capacity equal to 20%. The maximum DoD for that emergency scenario will be selected equal to 95% and it must be noted that the voltage is assumed constant, since there is no knowledge about the voltage – DoD relationship of the Figure 86. Moreover, a nominal return speed will be selected, taking into consideration that the power consumption is increased exponentially which is also depicted in the following figure.

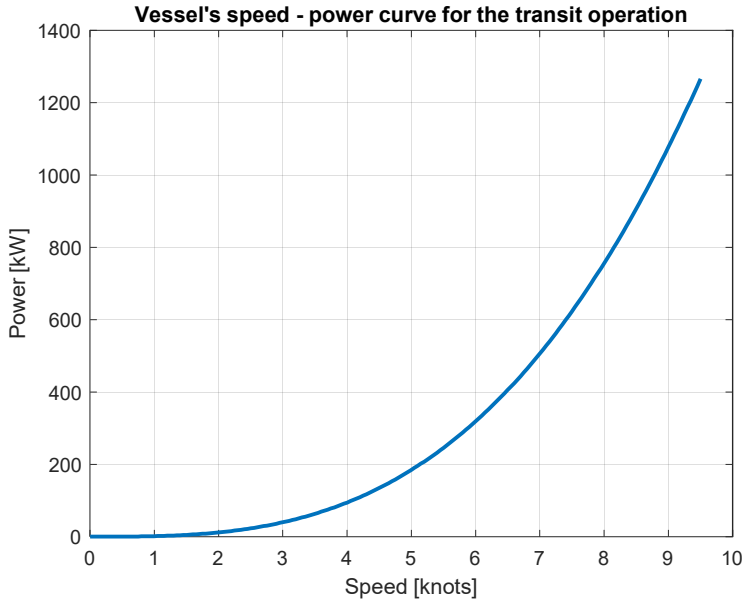

Figure 88: Speed - Power curve for the transit operation.

In that order the nominal emergency speed will be selected equal to 5 knots which is also an acceptable speed for operations close to ports. Thus, the reference Torque and Speed values can be calculated for that operational emergency profile, based on 6.3.1 and 6.3.2.

$$T_{emergency} = 1984\ N \cdot m\ per\ motor$$

$$N_{emergency} = 444\ RPM$$

The initial value of battery capacity for the simulation of the emergency return will be equal to 20% of the capacity of one battery pack or 80% DoD, whereas in the end of the trip the maximum DoD was selected equal to 95% therefore the available capacity for the emergency operation is equal to:

$$C_{emergency} = 0.15 \cdot 2150 = 322.5\ A \cdot h$$

The maximum range of the vessel in free running condition with a speed of 5 knots for the emergency return scenario will be calculated by integrating the current the battery provides based on the prementioned torque and speed references along with the electrical loads for the transit operation (neglecting the towing winch load). The simulation will stop once the total Ampere·hours reach the $C_{emergency}$ value. The simulation stopped at t = 6300 sec therefore the maximum range can be calculated as:

$$S_{emergency} = 5 \cdot \frac{6300}{3600} = 8.75 \text{ nautical miles}$$

Apart from the sizing of the battery system and the selection of an appropriate space for their housing, it is necessary to perform certain measurements for the evaluation of the whole system's operation. Based on the selected batteries, the continuous discharge current must be below 100 A. During the simulation, the current the DC source (battery system) provided was measured with a current measurement block. Since the operation of the inverter and the hysteresis band creates an oscillating current waveform, the average values were measured in-between intervals of constant speed/torque.

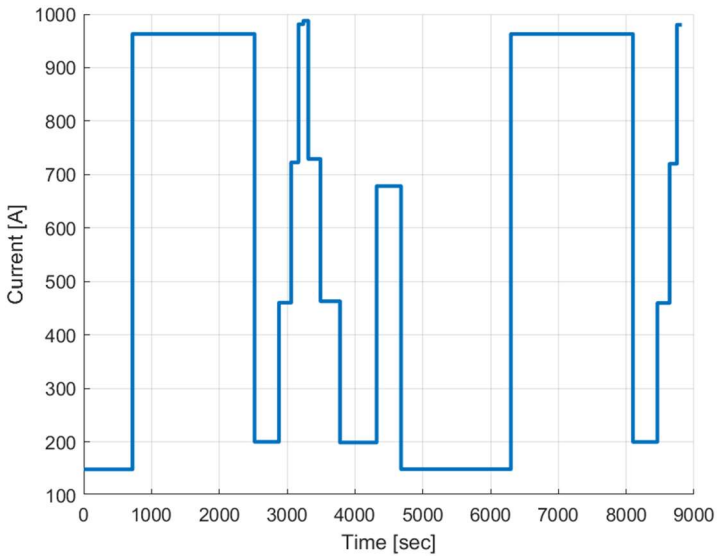

Figure 89: Average current of the battery pack.

Since each battery pack consists of 43 parallel strings it can be assumed that the output current is divided equally to each one of them. Therefore, the average current each string provides is presented in the figure below:

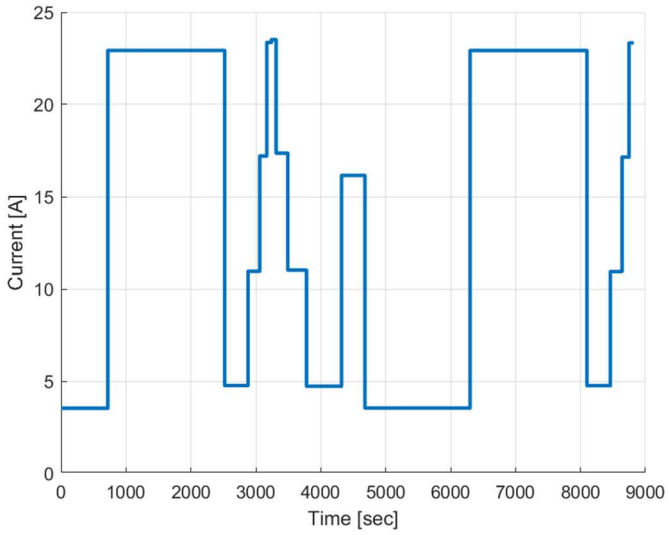

Figure 90: Average current per battery string.

It is clear that the average current of each battery string is at least 4 times less compared to the continuous discharge current threshold of the battery. Therefore, based on the assumed operational profile the battery's strain is minimal.

An important metric of the power quality in the system is the Total Harmonic Distortion (THD), which is defined as the ratio of the equivalent root mean square (RMS) of all the harmonic frequencies (from the 2nd harmonic on) over the RMS of the fundamental frequency. Harmonics higher than the 25th order are usually negligible so harmonic components up to 25th are taken for the calculation. The THD will be calculated for the stator's A-phase current.

$$\mathrm{THD} = \frac{\sqrt{\sum_{2}^{25} \mathrm{I}_{\mathrm{n,rms}}^{2}}}{\mathrm{I}_{\mathrm{fund,rms}}}$$

Usually the output signal controlled from an inverter based on an algorithm, which in this case is the hysteresis band algorithm, contains a number of higher order harmonic components. These components have frequencies integer multiples of the fundamental. The fundamental frequency f_e can be calculated from the ω_e angular speed which was the output of the block calculating the θ_e, Figure 77.

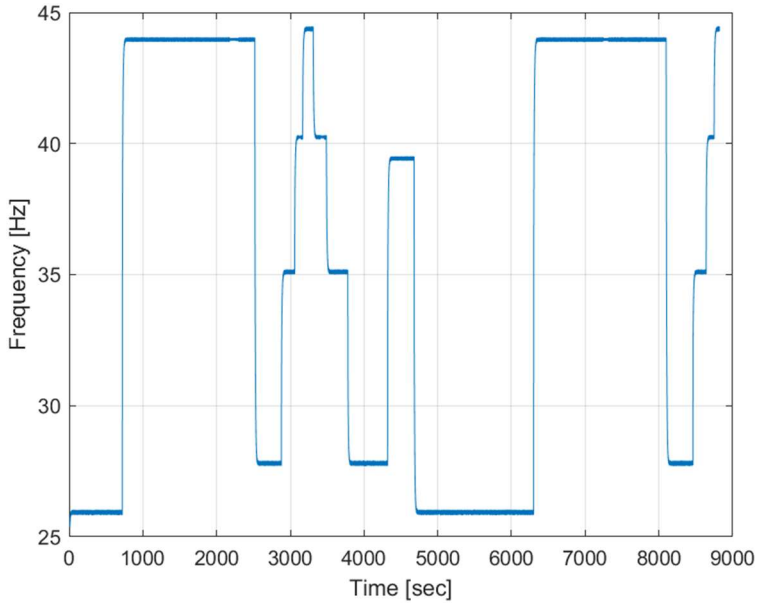

Figure 91: Fundamental frequency during the simulation.

The total harmonic distortion content will be calculated based on the fundamental frequency for several intervals of constant frequency, as depicted in the figure above. The THD will be calculated from the powergui block of MATLAB Simulink's environment. The settings for the calculations are presented below:

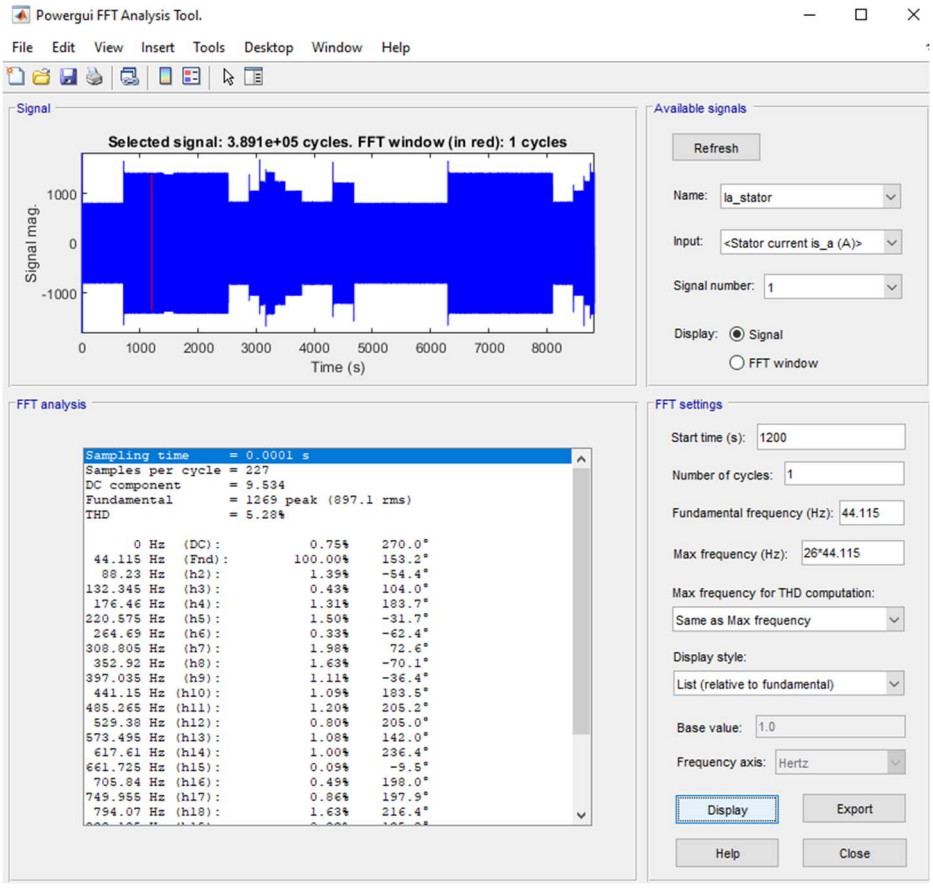

Figure 92: THD calculation parameters.

The following parameters are presented in the above figure:

- Start time (s): It is the starting time of the interval of the signal that will be used for the THD calculation.
- Number of cycles: It is the number of cycles that the FFT is going to analyze. By using a value equal to 1, the tool calculates the higher integer order harmonics of the fundamental frequency.
- Fundamental frequency: It is the fundamental frequency of the signal, the 1st order.
- Max frequency: The maximum frequency that will be taken into consideration. Since the THD will be calculated till the 25th order this will be equal to 26 times the fundamental.
- Max frequency for THD computation: Can select between the Max frequency and the Nyquist. The Nyquist frequency is equal to one half of the sampling rate which is equal to 10 kHz.

For the three different bands (1, 5 and 10% of the reference current) the THD values for various fundamental frequencies (depending on the reference angular speed) are being presented:

Figure 93: Total Harmonic Distortion (THD%) for 1, 5 and 10% band.

Total Harmonic Distortion for hysteresis band equal to 1% of the reference current					
Fundamental frequency f_e [Hz]	25.95	27.82	35.1	40.25	44.35
THD [%]	6.46	6.73	6.55	4.56	4.36
Total Harmonic Distortion for hysteresis band equal to 5% of the reference current					
Fundamental frequency f_e [Hz]	25.95	27.82	35.1	40.25	44.35
THD [%]	11.29	11.84	8.41	5.28	5.41
Total Harmonic Distortion for hysteresis band equal to 10% of the reference current					
Fundamental frequency f_e [Hz]	25.95	27.82	35.1	40.25	44.35
THD [%]	13.48	14.34	5.84	5.40	5.91

As expected, the lower THD values are being observed for the narrower band. Furthermore, another interesting fact is that the THD is decreased as the fundamental frequency increases. On the other hand, a very small band apart from the THD reduction comes with the disadvantage of increased switching losses, which are not investigated in the current thesis but must be taken into consideration when choosing an optimum hysteresis band.

7.0 Discussion

7.1 Conclusions:

From the results presented above the following conclusions can be made:

- The all-electric retrofit is technologically viable for the operational profile of the selected tugboat.
- The electric motor is flexible to provide the necessary power for a plethora of operating conditions.
- The closed loop control of the induction motor offers the possibility for implementation in future autonomous ships.
- The Total Harmonic Distortion (THD%) is minimal for a hysteresis band equal to 1% of the reference current and without significant variations for different fundamental frequencies.
- The selected Li – Ion battery system can be easily fitted into the tugboat and specifically into the fuel oil tanks, reducing also the total weight of the ship.
- The reduced weight of the battery system with respect to the fuel oil tank, can improve energy consumption whereas the negative effects such as the propeller emergence can be fixed with trim optimization.
- The safe return of the vessel to its station is secured in case of one battery pack failing.
- The strain on the batteries during their operation and charge is minimum.
- The charging duration is acceptable considering the idle period in-between the vessel's missions.
- On the other hand, the battery system's lifecycle of 4.2 years must be taken into consideration for an economic feasibility analysis.
- There is necessity for the creation of high voltage charging stations, which must be also taken into consideration for a technoeconomic analysis.

7.2 Further Research

The current thesis focused on the simulation of the induction motor based on closed loop control and the Field Oriented Control (FOC). Initially, several improvements can be suggested with respect to the simulation. Concerning the equivalent circuit parameters, the inductances were calculated based on the nominal frequency, however the motor operates at a wide range of frequencies therefore it would be more accurate if those parameters were modified each time based on the fundamental frequency. Furthermore, the FOC algorithm can create torque ripples that are not acceptable and can stress the electric motor. A suggestion would be to investigate more developed control algorithms that can face this problem. A more

accurate simulation would also include the dynamic circuit of the battery in order to capture the non - linear effects and the variation of the source's voltage which is dependent on the State of Charge (SoC%), since in the current thesis the battery pack's voltage was assumed constant.

Apart from the electric motor simulation's related parameters, the speed – power characteristics of the tugboat were calculated based on Noon Reports. A more thorough investigation would include to perform CFD simulations on a certain 3D tug model in order to assess the resistance curve based on various bollard pulls and the free towing scenarios, since the derivation of a speed – power curve from noon reports comes with a level of uncertainty. The harbor tugboat that was investigated was characterized also by insignificant hotel loads with respect to propulsive energy needs therefore future feasibility studies must also include vessels with higher electric loads such as firefighters or anchor handling ships.

All-electric ships are starting to emerge and late trends show that there is an increasing number of vessels adopting this technology. Therefore, there is a necessity for appropriate infrastructure to be installed in ports to be able to accommodate these ships.

Finally, the all-electric ship is the first step for the autonomous ship concept. A future research could also be focused on the investigation of a tugboat digital twin and implement the dynamics of the system along with the control of the electric motor.

8.0 References

Rong-Ching Wu, Yuan-Wei Tseng, Cheng-Yi Chen (2018), "Estimating Parameters of the Induction Machine by the Polynomial Regression ".

Model of Three-Phase Inverter, [Online] Available at: https://www.tntech.edu/engineering/pdf/cesr/ojo/asuri/Chapter4.pdf

M. H. Haque (2008), "Determination of NEMA Design Induction Motor Parameters from Manufacturer Data".

Zhen Guo et al. (2016), "Indirect Field Oriented Control of Three-Phase Induction Motor Based on Current-Source Inverter".

Sinisa Jurkovic, "Induction Motor Parameters Extraction".

Keun Lee et al., "Estimation of Induction Motor Equivalent Circuit Parameters from Nameplate Data".

Rahmatul Hidayah Salimin et al. (2013), "Parameter Identification of Three-Phase Induction Motor using MATLAB-Simulink".

Νέλα Αλέξανδρος, Πάσχος Βασίλειος (2015), "Μελέτη Επαγωγικού Κινητήρα Βραχυκυκλωμένου Δρομέα Ισχύος 45kW".

Bakirzoglou Christos (2017), "Techno-economical feasibility study on the retrofit of double-ended Ro/Pax ferries into battery-powered ones".

Alexandratos Ioannis (2018), "Techno-economic feasibility study on the retrofit of a conventional harbor tugboat into a battery powered one".

J. S. Thongam et al. (2013), "All-Electric Ships – A review of the Present State of the Art".

"Vince den Hertog et al., "Raptures: Resolving the Tugboat Energy Equation", [Online] Available at: https://ral.ca/wp-content/uploads/2016/05/D1P3-RAptures-Resolving-the-Tugboat-Energy-Equation.pdf

Jaroslaw Artyszuk (2013), "Types and Power of Harbour Tugs – The Latest Trends".

Rajesh Ingale (2014), "Harmonic Analysis Using FFT and STFT".

Καμνιτσάς Κωνσταντίνος (2010), "Μοντελοποίηση Ελέγχου Σύγχρονου και Ασύγχρονου Κινητήρα".

Άννα Μαρία Κοτρίκλα (2015), "Ναυτιλία και Περιβάλλον".

MAN B&W Diesel (2004), "Emission Control: MAN B&W Two Stroke Diesel Engines".

Dr Zabi Bazari (2020), "MARPOL Annex VI – Prevention of Air Pollution from Ships".

MIT Electric Vehicle Team (2008), "A guide to understanding battery specifications", MIT, December 2008.

Balakirshnan. P, Sasi. S (2006), "Technological and Economic Advancements of Tug Boats", Journal of Mechanical and Civil Engineering 2016, p 87-96.

Robert Allan Ltd (2012), "Tug and workboat design guide", [Online] Available at: http://ral.ca/wp-content/uploads/2016/01/BCSN-May-12-Tug-Design-Guide.pdf.

Indian Register of Shipping, IRCLASS, “Implementing Energy Efficiency Design Index (EEDI)”, [Online] Available at: https://www.irclass.org/media/1393/energy-efficiency-design-index.pdf

Deval L. Patrick, Richard K. Sullivan jr. (2018), “Health & Environmental Effects of Air Pollution”.

Web Sites:

Ship Technology: https://www.ship-technology.com/

Components 101: https://components101.com/

Electrical Posts: https://electricalposts.com/

Power Electronics: https://www.powerelectronics.com/

International Maritime Organization (IMO): https://www.imo.org/en

UC RIVERSIDE: https://pollution.ucr.edu/

U.S. Environmental Protection Agency (EPA): https://www.epa.gov/

Marine Insight: https://www.marineinsight.com/

Dieselnet: https://dieselnet.com/

Det Norske Veritas (DNV): https://www.dnv.com/

Transport & Environment: https://www.transportenvironment.org/

TransportPolicy.net: https://www.transportpolicy.net/

Seatrade maritime News: https://www.seatrade-maritime.com/

Battery University: https://batteryuniversity.com/

Sealed Performance Batteries: https://www.sealedperformance.com.au/

Energy Education: https://energyeducation.ca/encyclopedia/Main_Page

PowerSonic: https://www.power-sonic.com/

Rainbow Power Company: https://www.rpc.com.au/

Appendix A: Electrical Load Balance Sheet

This is the electrical load balance sheet as provided by the tugboat's operator. The load factors have been modified for the retrofit, all the diesel engines related auxiliary have load factor equal to 0.

	Equipment	Efficiency Factor	No. Installed	Installed Power			Idling			Transit		
				$P_{ον.αποδ}$ [kW]	$P_{ον.απορ}$ [kW]	$P_{εγκατ}$ [kW]	No. in Use	Load Factor	Power [kW]	No. in Use	Load Factor	Power [kW]
Engine Room Auxiliary Systems												
1	Fuel Oil transfer pump	0.850	1	6.375	7.500	7.500	0	0.200	0.000	0	0.100	0.750
2	Fire pump	0.850	2	23.000	27.050	54.100	0	0.000	0	0	0.000	0
3	General service pump	0.850	1	3.400	4.000	4.000	1	0.900	3.600	1	0.200	0.800
4	Portable water pump	0.850	2	1.275	1.500	3.000	2	0.500	1.500	2	0.500	1.500
5	Sanitary pump	0.850	1	1.275	1.500	1.500	1	0.400	0.600	1	0.400	0.600
6	Water Heater	1.000	1	6.000	6.000	6.000	1	0.500	3.000	1	0.100	0.600
7	Main engine cooling fan	0.850	2	2.550	3.000	6.000	2	0.200	1.200	2	0.850	5.100
8	Engine Room lighting	1.000	20	0.018	0.018	0.360	20	1.000	0.360	20	1.000	0.360
9	Engine Room ventilator	0.850	2	2.20	2.60	5.200	2	0.850	4.420	2	0.850	4.420
								Σ	14.680		**Σ**	13.380
Ship Auxiliary Systems												
1	Towing winch	0.850	1	38.250	45.000	45.000	0	0.000	0.000	1	0.235	10.575
2	Anchor windlass	0.850	1	4.675	5.500	5.500	0	0.000	0.000	0	0.000	0.000
3	Store room lighting	1.000	6	0.018	0.018	0.108	6	1.000	0.108	6	1.000	0.108
4	Deck lighting 1	1.000	18	0.018	0.018	0.324	18	1.000	0.324	18	1.000	0.324
	Deck lighting 2	1.000	2	0.100	0.100	0.200	2	1.000	0.200	2	1.000	0.200
	Deck lighting 3	1.000	2	0.100	0.100	0.200	2	1.000	0.200	2	1.000	0.200
	Deck lighting 4	1.000	3	1.000	1.000	3.000	3	1.000	3.000	3	1.000	3.000
	Deck lighting 5	1.000	1	1.000	1.000	1.000	1	1.000	1.000	1	1.000	1.000
5	Bridge lighting	1.000	8	0.018	0.018	0.144	8	1.000	0.144	8	1.000	0.144
6	Air compressor	0.850	1	1.573	1.850	1.850	1	0.200	0.370	1	0.200	0.370
7	Steering gear pump	0.850	2	3.825	4.500	9.000	0	0.100	0.000	2	0.200	1.800
8	Hydro oil pump	0.850	2	5.500	6.500	13.000	0	0.100	0.000	2	0.200	2.600
9	MARPOL pump	0.850	1	0.289	0.340	0.340	0	0.200	0.000	0	0.000	0.000
								Σ	5.346		**Σ**	25.667
Accommodation Quarters Auxiliary Systems												
1	Accommodation Lighting 1	1.000	26	0.018	0.018	0.468	26	1.000	0.468	26	1.000	0.468
	Accommodation Lighting 2	1.000	6	0.015	0.015	0.090	6	1.000	0.090	6	1.000	0.090
2	A/C unit	1.000	1	4.500	4.500	4.500	1	0.750	3.375	1	0.750	3.375
3	Accommodation quarters ventilation	0.850	1	0.030	0.035	0.035	1	0.850	0.030	1	0.850	0.030
4	WC ventilation	0.850	1	0.017	0.020	0.020	1	0.850	0.017	1	0.850	0.017
5	Fridge	0.850	1	0.425	0.500	0.500	1	1.000	0.500	1	1.000	0.500
6	Electric hob	1.000	1	3.000	3.000	3.000	1	0.200	0.600	1	0.200	0.600
7	TV	0.850	1	0.374	0.440	0.440	1	0.000	0.000	1	0.500	0.220
8	Public addressor	0.850	1	0.255	0.300	0.300	1	0.100	0.030	1	0.100	0.030
								Σ	5.110		**Σ**	5.360
								Total	25.136		**Total**	44.407